Investigation of Vanillin-Derived Bio-Based Epoxy as a High-Performance Composite Matrix Material

Master of Science Thesis

Bhuvesh Kaushik

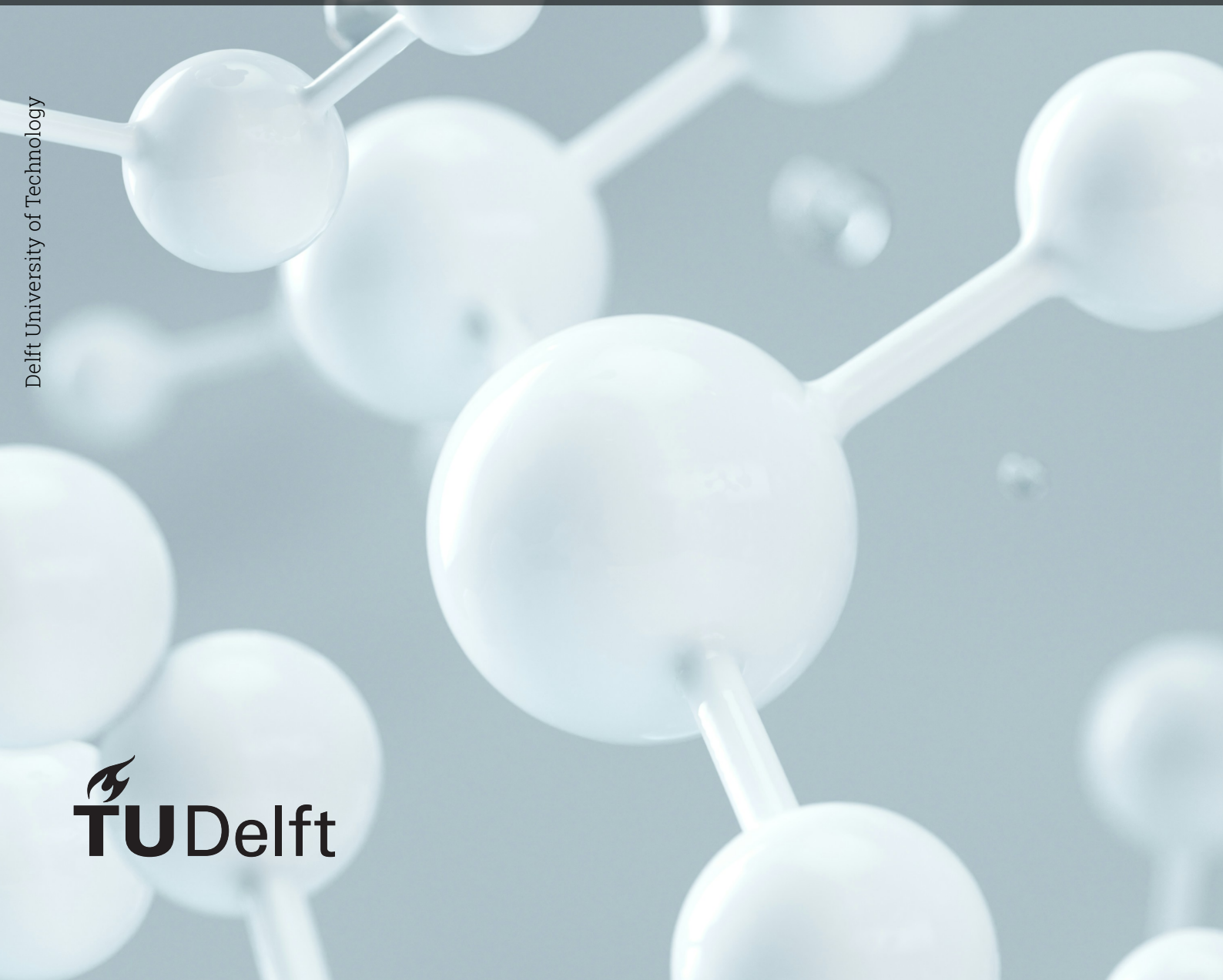

Delft University of Technology

TU Delft

Investigation of Vanillin-Derived Bio-Based Epoxy as a High-Performance Composite Matrix Material

Master Thesis Report

by

Bhuvesh Kaushik

to obtain the degree of Master of Science
at Delft University of Technology
to be defended publicly on October 18, 2024 at 14:00

Thesis committee:

Chair:	Dr. Otto Bergsma
Supervisors:	Dr. Baris Kumru
	William E. Dyer
External Examiner:	Dr. Yinglu Tang
Place:	Faculty of Aerospace Engineering, Delft
Project Duration:	15/03/2024 - 18/10/2024
Student number:	5722713

An electronic version of this thesis is available at http://repository.tudelft.nl/.

Cover: 3D rendering of molecules by D koi

Faculty of Aerospace Engineering · Delft University of Technology

Acknowledgements

The words written here mark the conclusion of my master's study at TU Delft and as such they carry a certain emotional weight. These past two years have been a challenging yet transformative period, filled with both personal and academic growth. The journey has not been without its setbacks, including a previous thesis project that I had to stop midway. While it was a difficult decision at the time, the experience ultimately shaped the direction of this thesis and helped me learn more about myself.

Though this thesis bears my name, it is the product of many people's contributions and support. The list of people to thank is long and I apologize in advance if I forget to mention someone. I am deeply grateful to my supervisor Dr. Baris Kumru, a cool person in general, for guiding me through both the difficulties of the earlier project and into the fascinating world of bio-based epoxies. Your support has been invaluable. I would also like to thank William Dyer for his assistance with both theoretical and experimental aspects of my work, and for patiently answering my stupid questions. I owe gratitude to Niklas Lorenz for explaining the very basics of cure kinetics and helping me during the experimental work. I would be remiss to not mention the rest of the research group- Daniel, Dimitrios and Pranshul, for their thought-provoking discussions and collaboration.

A special thanks to the lab technicians Victor, Chantal, Dave, Caitlin and Roy for helping me perform the experiments in the lab and for always providing me with insightful knowledge. A huge shoutout to Aditya Murali for helping me make the pleats during vacuum bagging because I could never get them right. Finally, my friends in the Msc workspace- Aakash, Harsha and Karan thank you for your presence and for making the most mundane of days a little more exciting.

I owe a profound debt of gratitude to my family, whose support and encouragement carried me through the most challenging moments of this journey and I am truly fortunate to have them by my side. From the bottom of my heart, thank you. And thank you for always believing in me, even when I didn't.

Bhuvesh Kaushik
Delft, October 2024

Abstract

The aerospace sector continues to drive innovations in high-performance materials. These materials however, tend to have energy intensive and emission heavy manufacturing processes. One of the most commonly used materials in aircrafts today are polymer matrix composites consisting of reinforcement fibers and a matrix. While the fibers provide the most strength to the composite, the matrix holds the fibers together and transfers the loads to them. The most commonly used matrix material today is made of BADGE (Bisphenol A Diglycidyl Ether), a material which is toxic to humans and comes from fossil-based products.

This thesis investigates the viability of a vanillin-derived bio-based alternative, VDE (Vanillyl Alcohol Diglycidyl Ether), to be used in high-performance composites for aerospace applications. VDE monomer is derived from vanillin, which is obtained from lignin, a material present in 35% of woody plants. The VDE-DDS resin system, when cured, exhibited comparable thermal and physical properties, such as glass transition temperature and heat deflection temperature, to traditional aerospace resins like BADGE-DDS. Mechanical testing, including tensile, flexural, and fracture toughness, demonstrated promising results, with VDE-DDS showing higher strength and modulus than BADGE-DDS. The flexural strength was considerably higher in particular. However, its hydrophilic nature led to higher water absorption, a challenge for long-term durability. For further testing, composite specimens were prepared using an autoclave.

Composite specimens reinforced with VDE-DDS displayed greater stiffness and strength under mechanical testing compared to BADGE-DDS in tests of in-plane shear strength, compression and inter-laminar shear strength tests, though BADGE-DDS composites outperformed in low-velocity impact resistance. The impact tetsing also revealed that BADGE-DDS samples had a higher damage initiation energy while VDE-DDS samples had a higher bending stiffness. Overall, VDE-DDS offers comparable, if not better, thermal and mechanical characteristics to BADGE-DDS. VDE, in summary, presents a compelling case as a potential bio-based alternative for structural aerospace applications.

Contents

Nomenclature

List of Abbreviations

AFM	Atomic Force Microscopy
BADGE	Bisphenol A Diglycidyl Ether
BPA	Bisphenol A
CAN	Covalent Adaptable Network
CF	Carbon Fibre
CFRP	Carbon-Fiber Reinforced Plastic
CNSL	Cashew Nut Shell Liquid
CTE	Coefficient of Thermal Expansion
DDM	4,4'-Diaminodiphenylmethane
DDS	4,4'-Diaminodiphenylsulfone
DGEM	Diglycidyl Ether of Magnolol
DGEVA	Diglycidyl Ether of Vanillyl Alcohol
DICY	Dicyandiamide
DMA	Dynamic Mechanical Analysis
DSC	Differential Scanning Calorimetry
EEW	Epoxy Equivalent Weight
EoL	End-of-Life
FEP	Fluorinated Ethylene Propylene
GF	Glass Fibre
HDT	Heat Deflection Temperature
IFSS	Inter Facial Shear Strength
ILSS	Inter-Laminar Shear Strength
IPDA	Isophorone Diamine
IPSS	In-Plane Shear Strength
LCA	Life Cycle Assessment
MMC	Metal Matrix Composite
PE	Polyethylene
PEEK	Poly Ether Ether Ketone
PHTE	Phloroglucinol Triglycidyl Ether
PLA	Polylactic Acid
PMC	Polymer Matrix Composite
PP	Polypropylene
RTM	Resin Transfer Moulding
TGA	Thermogravimetric Analysis
TMA	Thermo-Mechanical Analysis

List of Symbols

T_g	Glass Transition Temperature
K_{IC}	Critical Stress Intensity Factor
E'	Storage Modulus
E"	Loss Modulus

List of Figures

List of Tables

Part I

Introduction

1

Introduction to Problem Statement

Due to growing environmental concerns, the aerospace sector has come under immense scrutiny for its blatant use of resources and greenhouse gas emissions. To reduce this, several strategies are underway within the aviation industry. The biggest efforts are underway in sustainable aviation fuels and creating lighter structures so that fuel usage is reduced. Another area is the usage of sustainable materials and to create circularity within them.

Since the evolution of composites, their usage has grown rapidly, particularly within the aerospace industry. Whilst composites are used in primary load-bearing structures of aircraft, secondary and tertiary structures utilize materials with less efficient structural properties. The composites mainly used in the aerospace industry are PMCs (Polymer matrix composites). These contain reinforcement fibers and a polymer matrix. Composites contain high stiffness and specific strength. They also offer better fatigue and chemical resistance. This is primarily why composites are utilized in industry as well because they are so resistant to environmental degradation. PMCs offer greater mechanical rigidity and easier processing compared to metal matrix composites (MMC). PMCs also offer good damping characteristics to avoid resonance, high instant temperature resistance and ablation resistance making it suitable for a variety of applications [1].

Major aircraft manufacturers today utilize composites upto 50% by weight in their aircrafts [2]. In fact, the very first composite material used in aircrafts was glass fibers used in the fuselage skin of Vultee BT-15 trainer plane in 1944 [3]. As can be seen in Figure 1.1, the difference in usage of composites between two generations of aircraft of Boeing 777 and 787 which were manufactured in 1990 and 2007 shows their increasing prominence.

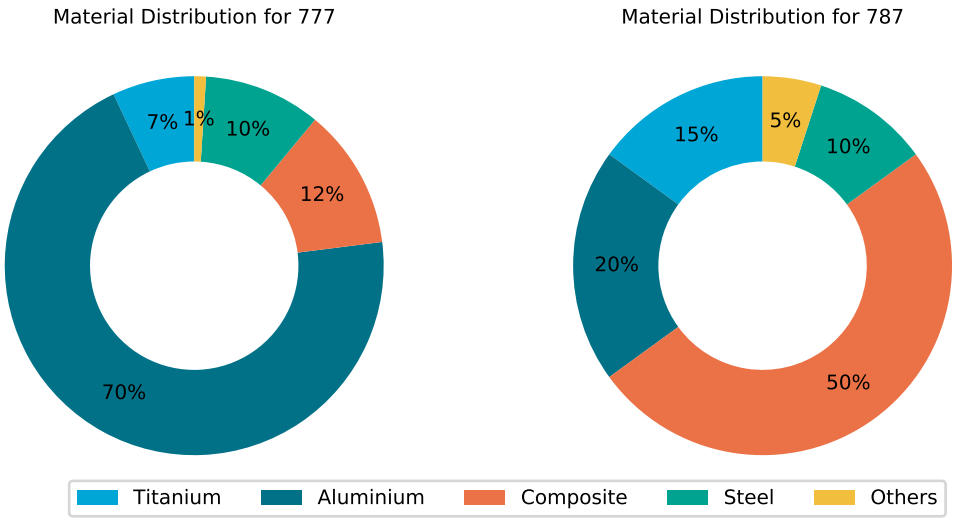

Figure 1.1: Material Composition of Boeing 777 and 787 (Data taken from [4])

It is theorized that more than 10,000 commercial, private and military aircrafts will reach their end-of-life

(EoL) till 2035 [5, 6]. Knowledge about EoL solutions for aircrafts is very limited in the current material landscape [5]. There is a clear need that a new approach of design for environment and design for disassembly be implemented. A review performed by Lunetto et al. [7] also suggested that the sustainability of composite parts should be done based on the entire life cycle including raw material production and EoL options.

The aircraft manufacturing sector required 69.5 TWh of energy emitting 18.1 Mt CO_2 eq, while the total material demand was 630 kt/yr [8]. Within the manufacturing phase of an aircraft, the wings and engines contribute the most to emissions, 63%, because of their use of composites over metals like aluminium and titanium [9]. Aluminium demand is the highest in the aviation sector, being around 59%; steel despite being second biggest by mass, uses the least amount of energy [8]. CFRP while being only 10% by mass is responsible for 45% of the emissions during manufacturing [9].

Composite manufacturing is a resource intensive process due to long curing times with some processes like autoclave curing generating nitrogen oxide, a gas responsible for ozone layer depletion [1]. The curing process is done to ensure crosslinking occurs within thermoset matrices which holds the fibers together in a composite. Most of the thermosets used in composites are based on fossil-fuel sources [10] .

This work aims to find the viability of a bio-based alternative to conventional thermoset epoxies used in aerospace structures.

1.1. Thesis Outline

The thesis is divided into three parts: Introduction, Methodology and Outcomes. Introduction consists of the problem statement and literature review performed to identify research gaps. This is followed by the research questions of the thesis.

Part II is divided into four main chapters to answer the research questions. These chapters are thermal and physical characterization of resin followed by its mechanical characterization. These characterization techniques included the cure kinetics of the resin, glass transition and degradation temperature, and tensile and flexural tests among others. Composite manufacturing and mechanical testing of the composite is discussed further on. The composites were tested for their in-plane shear strength, compression and inter-laminar shear strength along with some low-velocity impact tests.

Following this, Part III discusses and compares the characterization tests performed earlier with some of the commercial epoxies used in the aerospace sector to understand the place of the bio-based resin in terms of its applicability. A conclusion to the report is provided in Chapter 8 with recommendations provided for future work provided in the next chapter.

2

Literature Review

2.1. Composite Matrices

In a composite, the role of the matrix includes keeping the reinforcement intact, preventing mechanical and chemical deterioration. They also transfer load to the fibers, distribute the loads evenly, carry inter-laminar shear and prevent the fibers from coming in direct contact with the environment [3]. One of the major problems associated with PMCs is the cost and density of polymers' availability since they are petroleum-based. Generation of hazardous waste is a major cause of environmental impact generated by polymers [1].

The type of matrices are generally divided into two categories: thermoplastics and thermosets.

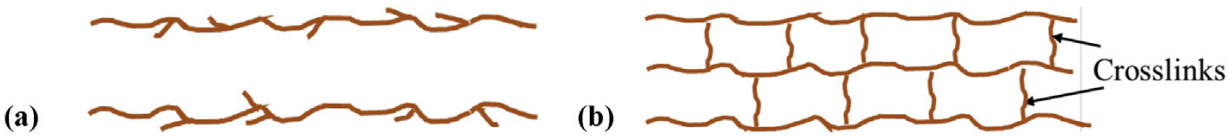

Figure 2.1: Network of Thermoplastics and Thermosets [3]

The most widely used thermoplastics in composites are: PE (Polyethylene), PP (Polypropylene), PEEK (Polyether Etherketone) [3]. Thermoplastics are advantageous in terms of recyclability as they can be remoulded and present high fracture toughness properties. However, they usually don't have high enough mechanical properties compared to thermosets.

Thermosets are network forming polymeric materials usually containing a highly cross-linked structure after curing reaction. Thermosets are used in coatings, adhesives, composites and electronic packaging. Majority of thermosets are based on BPA (Bisphenol A), acrylic acid and styrene leading to fossil depletion and environmental concerns [11].

2.1.1. Role of Fibers and Matrix in Composite

A composite consists of three main regions namely: reinforcement (usually long continuous fibers), matrix and interface, which is the region present in-between the reinforcement and matrix material shown in Figure 2.2. The role of fibers in composite include: carrying most of the tensile and compressive loads, bridging the cracks in the matrix and mitigating growth of cracks [3]. Higher strength and modulus fibers would convey more stiffness to the composite in these loading directions. Aside from fiber properties, the mechanical properties of the composite are also affected by the orientation of the fibers compared to the loading direction.

The load transfer in fiber-reinforced composites occurs through the following mechanism: deformation within the matrix generates shear stress at the fiber-matrix interface. This shear stress causes tensile stress within the fibers, allowing the fibers to carry the majority of the applied load. Due to the matrix's lower fracture strain relative to the fibers, micro-cracks first initiate within the matrix. Crack propagation ensues when the strain energy at the crack tip exceeds the energy required to form a new surface. In instances where fibers bridge the crack, the stress previously borne by the matrix is transferred to the

fibers through the interface. As the applied stress continues to increase, failure ultimately occurs either at the interface or within the fibers themselves.

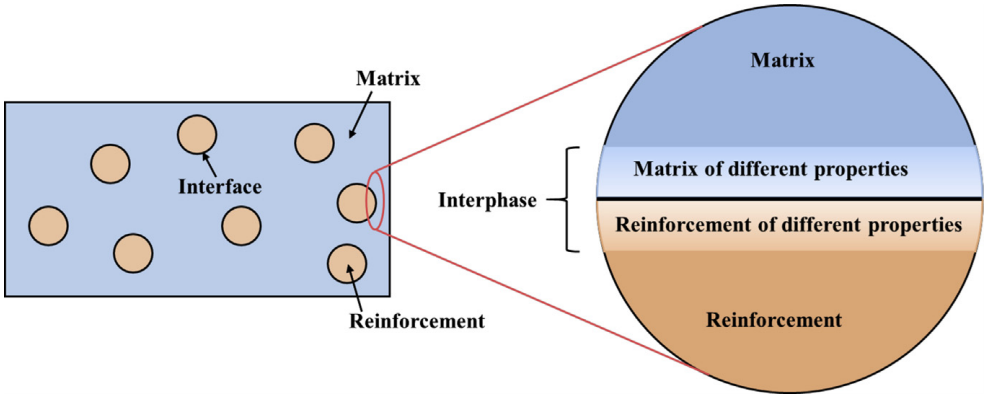

Figure 2.2: Layout Schematic of Composite Showing Reinforcement, Matrix and Interface [3]

Li et al. [12] found that the elastic modulus of the matrix has the greatest influence on the compressive strength of CFRPs (carbon fiber reinforced plastic). The same study found that plastic deformation properties of the matrix are also important since they affect the final strength of the composite.

Minty et al. [13] discussed the relation between the interfacial shear strength (IFSS) and properties of the matrix like its glass transition temperature and storage modulus. It was found that the hardener-epoxy ratio plays a big role for each property and changes in the final composite can be traced back to the thermomechanical properties of the matrix. The sizing applied on glass fibres usually involves chemicals which contain unreacted amine and epoxy groups to ensure adhesion between the fibre and matrix. The IFSS showed an increase with increasing glass transition temperature of the matrix. There was a noticeable drop-off in the properties when excess epoxy or amine were used in the resin systems which ultimately affected the composite [13].

The lower compressive strength of CFRP compared to its tensile strength hinders its widespread usability. Results by Li et al. [12] found that shear stress was an important factor in compressive failure process. Fiber misalignment is also a cause for compressive failure.

Composites are made to ensure that the load bearing member should be the fibers, however in certain situations, the matrix has to carry the load as well. Using tests that focused on these properties, it was determined which matrix material gave better properties to the composite as will be discussed in Chapter 6.

2.2. Thermosets

Different types of thermosets are used as composite matrices for their varying properties. These include epoxies, benzoxazines and cyanate esters among others [10].

Thermosets are desirable because of their manufacturing processibility as well. Common composite manufacturing techniques include autoclave, RTM and vacuum infusion. Ideal viscosity for vacuum infusion should be below $0.25\ Pa \cdot s$ [14]. Resin formulators face problems from certification side because of having desirable processing characteristics among viscosity profile, minimum viscosity and gel point for better impregnation.

Benzoxazine resins offer high temperature performance, have low water uptake, offer good flame characteristics and have the potential to be stored under ambient temperatures. Processes have been developed for their use in RTM and vacuum assisted RTM. Li et al. [14] showed that 6 month storage of a benzoxazine resin in ambient conditions did not affect infusion its characteristics, showing it to be better than bismaleimide resins.

Toughness is a characteristic which favours thermosplastics over thermosets. Commercial epoxy resins suffer from intrinsic brittleness and low toughness [15]. A study found that the type and amount of curing agent are by far the most important factor determining fracture toughness in thermosets [16]. The downside

of high toughness resin systems is that it generally results in higher viscosities leading to processibility issues [14].

Epoxy thermosets are preferred due to their dimensional stability, chemical resistance and thermomechanical properties [17]. Thermosets, in particular epoxy resins, are researched more due to their high mechanical properties, good adhesiveness, heat resistance, chemical resistance and dielectric properties [15]. More-highly cross-linked epoxy networks shrink less after post-curing and thus contain more free volume [16]. Due to the random orientation of the polymer network, thermosets can be considered to be isotropic in nature. Haba et al. [18] used AFM (atomic force microscopy) to determine that epoxy thermoset networks are homogeneous in nature, hence proving their isotropic nature. The study found that the previous claim of inhomogeneity arose due to observations of nanometer-scale nodular morphology on differently prepared surfaces.

Some drawbacks of thermosets include: source material is petro-based and non-renewable, cross-linked molecular structure hinders recycling and repairing [17]. Therefore, Liu et al. [11] mentioned that a sustainable thermoset should have the following characteristics: renewable feedstock, satisfactory performance and long service life or degradability.

New research has started to focus on optimizing degradation conditions and introduction of dynamic covalent bonds within thermoset networks [11]. These are also known as covalent adaptable networks (CANs). CANs lie somewhere in the middle of thermosets and thermoplastics since they can change their topology and turn into dynamic networks under certain conditions. This is done by thermally activated bond-exchange processes. CANs can be classified into associative and dissociative types. Associative CANs are known as vitrimers, meaning that they undergo exchange reaction while maintaining their cross-linking density. Dissociative CANs have their bonds cleaved and reformed through the exchange process, leading to a drop in viscosity during reprocessing [17].

Other strategies to create recyclable thermosets include: using acid or anhydride hardener, using raw materials with special functional groups (aldehyde, polyhydroxy, furan ring). Bio-based unsaturated polyesters are recyclable under extreme conditions but suffer from having bad thermal properties [11]. Similarly, Genua et al. [17] reported low T_g for their vitrimeric systems developed from different bio-based resin systems. Overall, vitrimers currently don't have the required performance characteristics to be used in aircraft structures. They are also not certified for use in the industry currently.

2.3. Epoxies

Epoxies are used in aircrafts because of their good thermomechanical properties, chemical resistance due to the chemical bonds present in its molecular structure [10].

Curing of epoxies is done through functional groups such as amines and anhydrides. These reactions are known as polyaddition reactions. Chemical structure of the hardener determines the cure kinetics of the reaction. Epoxies don't produce volatile byproducts while curing and offer low cure shrinkage, a property important for composites as carbon fibers (CF) have negative CTEs(coefficient of thermal expansion). Cure schedules can affect the possible chemical reactions during cure and also the rate of reaction [19]. Aromatic amines provide slow curing while linear ones provide fast curing. Epoxy systems have been developed for over six decades within the aerospace industry, however they involve toxic chemicals and petroleum-based sources. Phenolic resin's aromatic nature gives them high char yield. Epichlorohydrin is a major reagent used to create epoxy monomers within the aerospace industry [10]. Gelation and vitrification have been known to affect the morphology of the final product [19]. Industrially produced resins also include reactive diluents and accelerators to optimize the viscosity and curing time and temperature [20].

Commercial epoxies are overwhelmingly BADGE (Bisphenol A Diglycidyl Ether)-based (Figure 2.3) which is derived by reaction between BPA and epichlorohydrin [20]. BPA is hazardous, causing severe environmental issues and health concerns [11]. More than 90% of all epoxy resins are made of BADGE [21]. While epichlorohydrin can be produced from bio-based glycerol, BADGE remains petro-sourced. BPA is classified as an endocrine disruptor and a reprotoxic R2 substance posing a grave threat to human health [22].

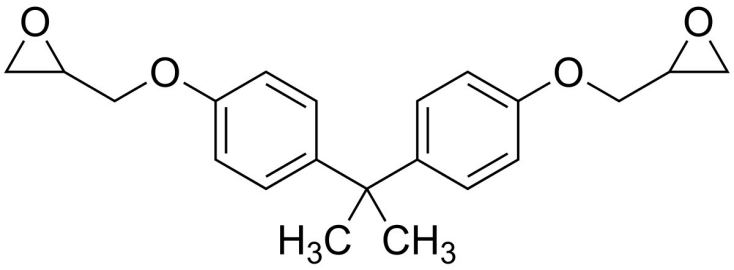

Figure 2.3: BADGE Chemical Structure [23]

2.4. Bio-Based Composites / Fibers

Bio-based composites offer a sustainable approach in material production. However, they are not currently used because of their shortcomings in mechanical characteristics and flammability. Bio-based materials are more prone to fungal attacks and are sensitive to moisture [24]. Bio-based materials could be used in furnishings and secondary structures, however secondary structures like interior panels in aircraft require good fire properties, currently satisfied by glass fibre reinforced by phenolic resins [25]. Bio-based resins in particular are not utilized in industry because of problems with scalability [20]. Another issue is that studies which deal with the synthesis of sustainable resins don't actually delve into composite manufacturing leading to an incomplete understanding of the viability of sustainable materials. Ferdosian et al. [26] echoed similar sentiments by observing that studies on sustainable resins rarely focus on curing kinetics of the resins and mechanical properties of composites.

Vidal et al. [27] studied different panels for aircraft interior which were compared in a life cycle assessment study. The conventional panel consisted of a novel manufacturing method using cores made from polyetherimide and the conventional glass fibre reinforced thermosets with halogenated flame retardants and a honeycomb core made out of aramid fibres. The sustainable panels were made out of recyclable polymers and natural fibres as reinforcements. All sustainable panels were developed to ensure they fulfilled fire resistance requirements, including having surface density of the panels needing to be below 2 kg/m^2. All sustainable panels showed better environmental performance in the manufacturing stage, however, were offset by the conventional panel during use-phase owing to its lighter weight. This showcased an important property that the use-phase of an aircraft produces more emissions compared to materials and manufacturing, hence focus should also be put on having materials with similar properties.

Natural fibers as a green reinforcement are being researched upon to create bio-based composites. Among natural fibers, jute is the longest natural fiber to be an alternative for synthetic fibers. It offers advantages like biodegradability, thermal and acoustic insulation properties and lower specific weight compared to glass fibers. These fibers however suffer from having good interface properties due to matrix-like compatibility issues. Jute fibers also have been reported to have low flexural strength and modulus lying in the range of 30-107 MPa and 1-4 GPa [15] considered to be below the standard required for aerospace applications. Lunetto et al. [7] found in their review that the benefits of using bio-based fibres as a sustainable alternative is very limited. The benefits of recycling composites as a sustainable alternative are little. Literature on the use of natural fibres is still very limited, particularly in the aviation industry [7, 25].

New research has offered significant improvements in bio-based composites. In particular, Kumar at al. [15] created a bio-based resin which was reinforced with natural jute-fibers to create an environment-friendly composite with high-performance structural applications. They used vacuum assisted RTM to manufacture composites with a bio-based epoxy monomer and DDM (4,4'-diaminodiphenylmethane) and IPDA (isophorone diamine) as hardeners with jute fibers. They found that the bio-based composite did perform better than a composite made of synthetic fibers and commercial resin in tests of interfacial shear strength and had a higher modulus. The bio-based resin also exhibited water-resistant behaviour, although it didn't have good thermal properties.

2.5. Bio-Based Resins

An area of research for sustainable manufacturing technologies is in bio-based resins. Currently only petroleum-based epoxy resins are used in the aviation industry. The chemical industry has been looking for

alternatives to BPA, with aromatic molecules like vanillin and phloroglucinol being explored the most [17]. Fache et al. [28] described that “green” chemistry not only involves the use of bio-based starting products, it has to inculcate energy efficiency, waste reduction, safety towards human health and environment among others. New materials however require certification before they are used in commercial applications and within the aviation sector, certification of new materials takes around 11 years on average [10]. Another point to consider is that bio-based materials may not perform better environmentally simply due to a non-fossil source. The report by Rødsrud et al. [29] suggests that despite better environmental performance by some bio-based chemicals, the market favors their fossil-derived equivalents because of their low financial costs.

Renewable sources for thermosets include carbohydrates, lignin, vegetable oil (plant oil chemicals) and plant extracts.

- Carbohydrates: These are one of the most widespread organic substances in nature. Isosorbide has been shown to have a rigid structure due to its unique bridge-ring structure [11]. PLA (polylactic acid) can also be produced from this.
- Lignin-based aromatic phenols: Lignin holds a lot of potential in polymer science due to its complex structure containing many sites for further reaction. Lignin is present in all plants and creates about 20-30% weight in the biomass of trees [10]. The monomers extracted from lignin containing phenolic structures are suitable to produce benzoxazines and epoxies with desirable properties. Some of these are shown in Figure 2.4. Lignin also does not compete with food sources [30]. Lignin is available in potentially large amounts in biomass but extraction is difficult due to their highly polymeric nature, variability in amount depending on plant and method of extraction prevents them from being raw materials in industries.
- Plant oils: Soybean oil and castor oil are the main molecules in terms of plant oils. Soybean oil is used in adhesives and coatings while castor oil has its applications in rubber, lipsticks and medicine. Cardanol obtained from cashew nut shell liquid (CNSL) is also of great interest to researchers in bio-based thermosets. Cardanol however, directly cannot be used because it has a long aliphatic chain which doesn’t tend to be rigid [11].
- Plant extract: They include flavonoids, tannins and terpenoids, which have been studied for their application in bio-based thermosets.

In terms of these sources, lignin is the most promising due to its polymeric form. Bio-based Benzoxazine resins have also been developed in recent times from lignin as reported by Liu et al. [11]. Their characteristics include hydrophobicity, near zero cure shrinkage, high temperature stability and no by-products created during curing. Currently guaiacol, eugenol and vanillin are the most widely used lignin derived compounds for polybenzoxazine synthesis. Vanillin is particularly useful because it contains an aldehyde group which could remain unchanged during the synthesis of benzoxazine monomers and gets involved in the curing reaction. These resins tend to have higher T_g and are fire safe. Their main applications include fire-resistant resin, surfactant and corrosion resistant coating among others. T_g for high performance bio-based benzoxazine have been reported to be as high as 296° C [11].

For epoxy resins, currently two ways exist to create them from bio-based feedstocks:

- Direct reaction between epichlorohydrin and bio-compound. The compound however should contain active hydrogens, which are present in phenols and carboxylic acids.
- Epoxidation of C-C double bonds into oxirane.

Lignin derived monomers have had a lot of interest to increase the number of hydroxyl groups in them to produce high-performance epoxy products. The aldehyde group present in vanillin can react with amine to form Schiff base, which can be used to recycle epoxy resin. Eugenol is another molecule derived from lignin which has generated interest. It contains two functional groups of phenolic hydroxyl group and allyl group that can be modified further for different functionalities. A study focusing on synthesizing 80% bio-based resin system of eugenol showed a 39% higher Young’s modulus and 55% higher hardness compared to its BADGE-based counterpart [31]. Aliphatic bio-based epoxy resins are normally used in coatings [11]. Bio-based daidzen and luteolin epoxy resins, which come from natural flavonoids, demonstrate high mechanical properties as alternative to BADGE [15].

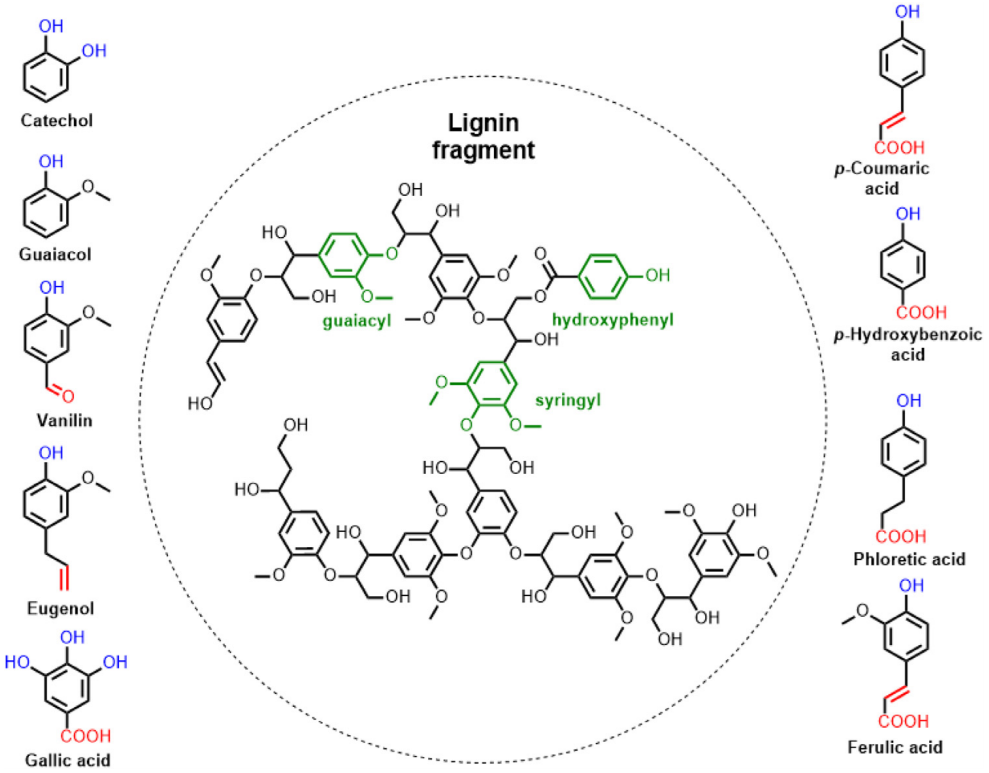

Figure 2.4: Derivatives of Lignin [11]

Apostolidis et al. [20] performed a study which dealt with replacing BADGE with PHTE (phloroglucinol triglycidyl ether) and using it with Epikure 04908 hardener in laminating systems. They used glass fibers as reinforcement for the composite and compared against the traditional BADGE system with the same hardener. Vacuum infusion was not possible even at 60° C because the viscosity of the resin system was still too high. Cure time was measured to be around 40 min. Through rheology analysis, a gel point time was obtained around 200 minutes. The cured resin system showed high thermal stability till 320° C. Glass transition temperature (T_g) was observed at 123° C. PHTE based resin system showed better thermo-mechanical properties compared to the BADGE based system. Problems do remain with this resin system because of high viscosity at room temperature requiring more reactive diluents which decreased the activation energy but also limit the amount of mass that can be mixed together. A recommendation given by the study was that PHTE could also potentially be utilized for frontal polymerization studies due to its high reactivity.

Qi et al. [21] focused on DGEM (Diglycidyl ether of magnolol) DDS resin system. DGEM was derived from magnolol which is naturally available. The T_g was reported to be 279° C and the storage and flexural modulus was around 1.5 times higher than its BADGE-DDS counterpart. It also showed extremely low viscosity of just $0.155\,Pa \cdot s$ at room temperature making it suitable for composite manufacturing techniques like vacuum infusion. The bio-based resin also showed very good flame retardancy characteristics. Magnolol is a bioactive compound, obtained from the bark of magnolia officinalis. Magnolol is multifunctional as it contains symmetrical bisphenol and diallyl groups. It is also highly aromatic enhancing its rigidity. Magnolol however is not without its own problems as it is currently very expensive in the market and the availability of it is low.

However, bio-based materials are not without issues. Biomass and its derivatives have extremely diverse structures differing in small amounts: example being isosorbide, isodide and isomannide differing because of the chirality of hydroxylated carbon, but their reactive performance varies greatly [11] leading to extraction issues. Problem arises because most lignin derivatives are monofunctional so they fail to be used directly to synthesize resins [11]. Not only this but environmental problems caused by the accumulation of bio-based thermosets would be the same as petroleum-based thermosets as there are no reports concerning the recycling of bio-based thermosets.

2.6. Vanillin

Vanillin holds a special status amongst molecular phenolic compounds as it is one of the only few derived from biomass today [30]. Bio-based molecules are industrially available but they are limited to aliphatic or cycloaliphatic compounds. The aromatic compounds used in the industry today are derived from petroleum. Vanillin is an organic compound which can be derived from lignin, a molecule which is makes up around 35% of woody biomass [32]. Fache et al. [32] explained that technological advances recently have made possible to derive vanillin from lignin.

Vanillin has some advantages like being a safe compound, aromatic in structure, two reactive functional groups and even can be used to make thermoplastic polymers. Vanillin is the main constituent in natural vanilla flavoring, in fragrances and perfumes. Other uses include base compound in the preparation of sunscreen. Vanillin derived from lignin has an aromatic intensity 20% stronger than the ones derived from petroleum [30]. Recently vanillin has been reported to be an excellent source to be used in composites. However, very little research has been published on composite characterization made of vanillin.

Vanillin can also be used to prepare hardeners for epoxy curing. Vanillin as a starting product can be used to make wide variety of polymers including: epoxies, phenolic resins, (meth) acrylic polymers, polyesters, polyacetals, polyaldimines and polybenzoxazines [28].

Studies conducted on vanillin reveal promising results. Kumar et al. [15] tested vanillin derived epoxy (VE) with DDM (4,4' diaminodiphenyl methane) curing agent for tensile and bending properties and water contact angle. These properties were compared with commercial epoxy- BADGE. The phosphorous moiety of VE gave flame retardancy properties in combustion. VE-IPDA showed a water contact angle of 94.4° compared to VE-DDM with 95.6°. This can be attributed to the hydrophobic moeieties of $-CH_3$ groups in the resin. Another study by Genua et al. [17] due to the bi-functional and tri-functional nature of DGEVA and PHTE they can be combined together to make a resin mixture.

Some of the derivatives of vanillin are shown in Figure 2.5. A derivative of vanillin known as DGEVA (Diglycidyl ether of vanillyl alcohol) has been reported to be an excellent epoxy monomer [17]. This is reported in the discussion below.

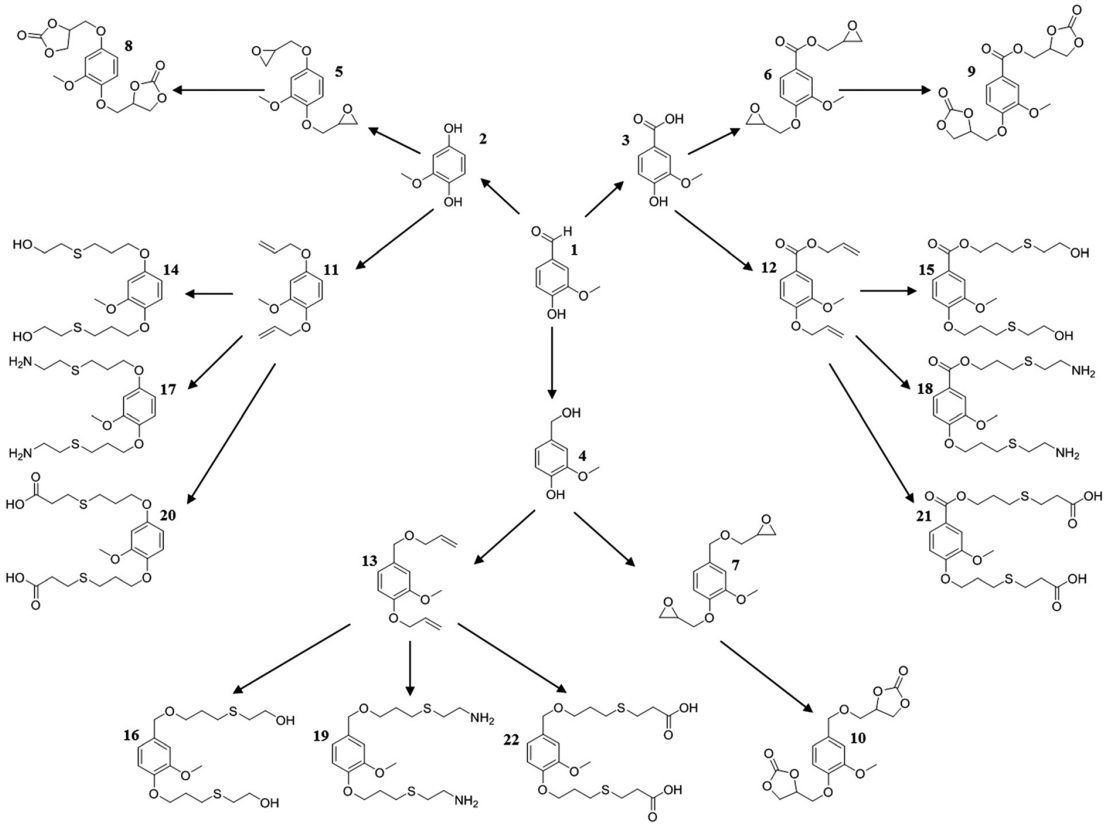

Figure 2.5: Vanillin Derivative Production Routes [32]

2.6.1. DGEVA

A study by Fache et al. [32] mentioned a procedure to produce DGEVA or VDE (Vanillin Diglycidyl Ether). Vanillin derivatives have different oxidation states. Reduction of it leads to vanillyl alcohol. As shown in Figure 2.5, the molecule labelled as ”1”, when reduced leads to molecule ”4” and consequently leads to ”7”, which is DGEVA. Vanillyl alcohol is a common commercial compound. Synthesis of DGEVA started from vanillyl alcohol. Vanillyl alcohol possesses benzyl alcohol and a phenol on which glycidylation occurred. This is due to protons in phenols being more acidic. It was synthesized using a biphasic phase transfer catalysis system as shown in Figure 2.6.

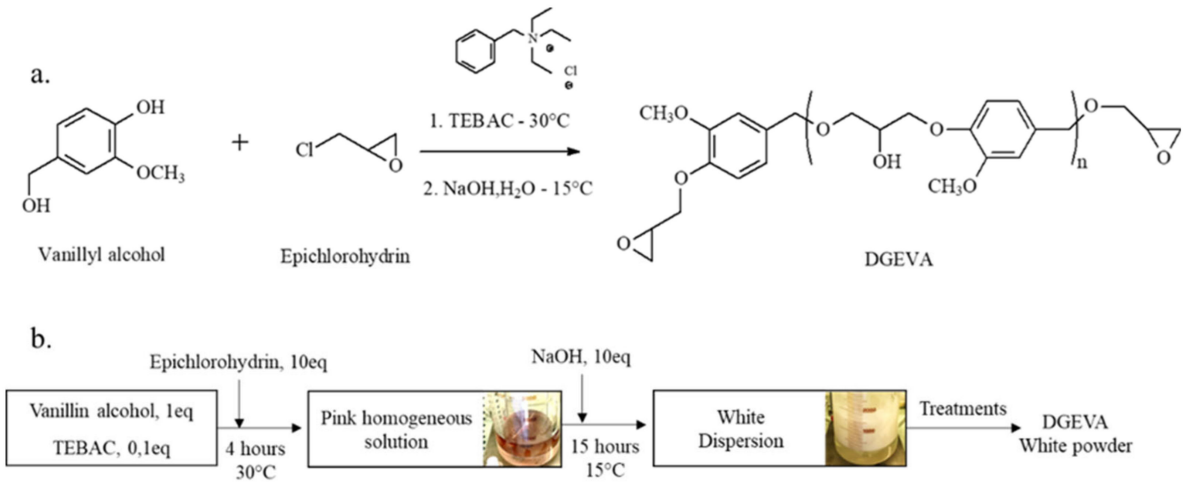

Figure 2.6: DGEVA Production [17]

2.6.2. Hardener

Aromaticity of the curing agents affects the final cure properties of the resin system. Currently, the aromatic diamine curing agents are utilized in the industry such as DDM (4,4’-diaminodiphenylmethane), DDS (4,4’ diaminodiphenylsulfone). Another commonly used one is known as DICY (dicyandiamide).

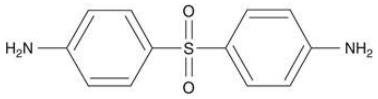

Figure 2.7: DDS Molecular Structure [23]

According to research performed by Gupta [23], DDS provided better curing characteristics when mixed with BADGE and PHTE. This was attributed to its had beter processibility as it came in a fine powder-like form which meant it dissolved uniformly in the epoxy monomers. Therefore, to keep the results consistent and comparable, the hardener chosen for this project was also DDS, commercially known as Aradur 9664-1 provided by Huntsman.

2.7. Gaps in Literature

Through the literature analyzed in the previous section, a few key points can be summarized:

- Bio-based resin systems rarely get characterized beyond their chemical properties. This means that their mechanical properties are not tested.
- VDE monomer cured with DDS has not been characterized yet, to the best of the author’s knowledge
- Composite characterization studies made with bio-based resins are scarce. A composite made of VDE-DDS resin system has not been found in literature.

These points act as the backbone of the experiments performed during the thesis project.

From the literature review it can be determined that a bio-based epoxy resin should have atleast the following characteristics:

- Glass Transition Temperature: For use in primary structures, the T_g of the resin system should be high enough. As discussed in the The Composite Materials Handbook-MIL 17 [33], the material operating limit was introduced so that a slight increase in temperature would not cause a significant loss in mechanical properties of the material and to avoid irreversible property changes. The operating temperature limit of epoxies in particular can be determined by obtaining T_g and subtracting 28° C from it, although the value can change depending on the specific application and when supported by data. T_g is also not supposed to be the sole basis for creating a temperature limit since it depends on the measurement technique used. Some report that the T_g requirement for aerospace service temperatures is around 130° C [14].
- Commercial epoxy resins have modulus values lying between 2-3.8 GPa [34]. Tensile strengths have been reported to be around 80 MPa [35]
- Fracture toughness properties: Commercially available thermosets have fillers and additives mixed in them to increase their fracture toughness as epoxies are brittle in nature. Some values of neat epoxies are found to be $0.75MPa\sqrt{m}$ [35].
- Viscosity for composite manufacturing: Ideal viscosity for vacuum infusion should be below $0.25\ Pa \cdot s$, though higher viscosities can be considered for other processes like RTM [14]. The temperature at which this viscosity is found is also important because at higher temperatures the resin itself would start to cure thereby not allowing enough time for the resin to infuse.

Therefore it was decided that for this thesis project the resin system comprising of VDE-DDS would be characterized thermally and physically along with its mechanical characterization. After obtaining data from this, an appropriate composite manufacturing method would be identified to ensure lesser void content within the composite. Finally, composite mechanical tests would be performed with matrix dominant behaviour to identify whether the bio-based resin system offered comparable properties.

2.8. Research Questions

Based on the literature review and the research gaps identified the following research question can be identified.

Research Question

What is the potential of VDE-DDS resin system to be used in primary aircraft structures?

To provide a complete solution to the proposed question concerning the recycling aspects of the new material and its mechanical properties, the following sub-questions are devised.

Sub-Research Question 1

What are the thermal and mechanical characteristics of the resin system?

Sub-Research Question 2

What is an appropriate method to manufacture composites with the resin system?

Sub-Research Question 3

How comparable are the composite properties made of VDE-DDS to a commercially available alternative?

Part II

Methodology

3

Thermal and Physical Characterization of Resin

For this project, the VDE monomer, supplied by Specific Polymers under the designation SP-9S-5-005, arrived in a wax-like solid form. To facilitate handling, the material had to be broken into smaller pieces using a hammer before it could be removed from its packaging. The monomer was then further processed into a fine, powder-like form through impact milling, utilizing the smallest available grain size for the milling process. BADGE monomer was provided by Huntsman as Araldite LY 3585.

3.1. Bio-Based Content

To understand how much bio-based content is within the final resin system, its stoichiometric ratio was calculated. The epoxy equivalent weight (EEW) of VDE was taken from the datasheet as 145 g/mol [36]. As can be seen in Figure 2.7, DDS contains 4 amine hydrogens which can react with the epoxy rings. Therefore the parts by weight for DDS could be calculated as follows:

$$W = \frac{(M_h/N)}{EEW_E} \times 100 \tag{3.1}$$

where M_h is the molar weight of the hardener, N is the number of amine hydrogens in the hardener, EEW_E is the epoxy equivalent weight of VDE.

With this the mass ratio of VDE:DDS came out to be 2.34:1. The molar ratio was further calculated to be 2.18:1. This mixing ratio was used to prepare the resin systems for all the tests performed for this thesis.

Since VDE monomer is fully bio-based and the DDS hardener is petroleum-based, the bio content of the resin system can be calculated according to the mixing ratio and their molecular weights. The bio-based content of the resin system came out to be 70% by weight.

3.2. Cure Cycle Estimation and Optimisation

Epoxy resins obtain their best characteristics when there is a high degree of cross-linking within the polymer structure. The final mechanical properties of the composite also get affected by this. Therefore, it is important to ensure that cross-linking occurs, which is usually done through a curing cycle. Since VDE-DDS is not a commercial resin system, its curing cycle had to be found. Experiments were carried out to determine the temperature and time required to reach a high degree of cure and then further tests were done to identify the post curing temperature. For the curing cycle, a cure kinetics model was also developed to get better insight on the curing cycle.

Epoxy curing tends to be an exothermic reaction and its enthalpy can be recorded [37]. This curing process is an irreversible change that occurs due to the ring opening of epoxy groups via a curing agent to produce a thermoset network. During this process the resin system goes through a lot physical changes, a few being the dramatic change in viscosity and the modulus of elasticity going from near zero to near 10^3 MPa. As the cure progresses, more branches are created which crosslink together to form a covalently crosslinked network. One of the best tools to observe this curing behaviour is differential scanning calorimetry.

Dynamic Scanning Calorimetry (DSC) is a measurement technique which records the enthalpy change in a material by measuring its heat transfer relative to a reference pan. DSC experiments can be performed in two ways: dynamic and isothermal. Dynamic DSC is conducted over a range of temperature while isothermal, as the name suggests, is done at a constant temperature over a period of time. For epoxies, dynamic DSC is particularly useful in observing the glass transition (T_g) temperature of the material while the isothermal test helps in understanding the cure behaviour.

3.2.1. Dynamic DSC

DSC runs were performed on mDSC250 by TA instruments. An initial run with heating rate of 10 K/min was incomplete because the peak wasn't completed as seen in Figure A.1. This lead to lowering the the heating rate to 3 K/min, 2 K/min and 1 K/min. The experimental runs were set up such that the resin would be cooled till -50° C and held isothermally at that temperature for 10 minutes to ensure it was at the same temperature. Then the temperature would be raised at a high heating rate (usually around 10° C/min) to 0° C, followed by heating till 300° C at the required heating rate. However, in a DSC machine it is important not to have the material degrade due to the machine's high sensitivity and so after the first slow heating run and observing another peak occurring after 250° C it was decided to always limit the heating rates till that temperature which would later be analysed with the help of TGA. Sealed aluminium hermetic pans were used for all DSC runs to ensure that no volatile gases escaped through the pans of the calorimeter.

Using these curves the enthalpy of the reaction can be calculated as shown in Equation 3.2. This is done by integrating the area under the curve whilst changing the baseline to account for the specific heat of the resin Cp. The integration is visualized. The enthalpy values were increasing with each decrease in the heating rate, therefore it was decided to decrease the heating rate further. Three other tests were done at heating rates of 0.75° C/min, 0.5° C/min and 0.25° C/min. These can be seen in Figure 3.1.

$$H_t = \int_0^t \frac{dH}{dt}\, dt \tag{3.2}$$

Where H_t is the enthalpy of the reaction, dH/dt is the instantaneous heat flow which is integrated over time when t=0 till t=t.

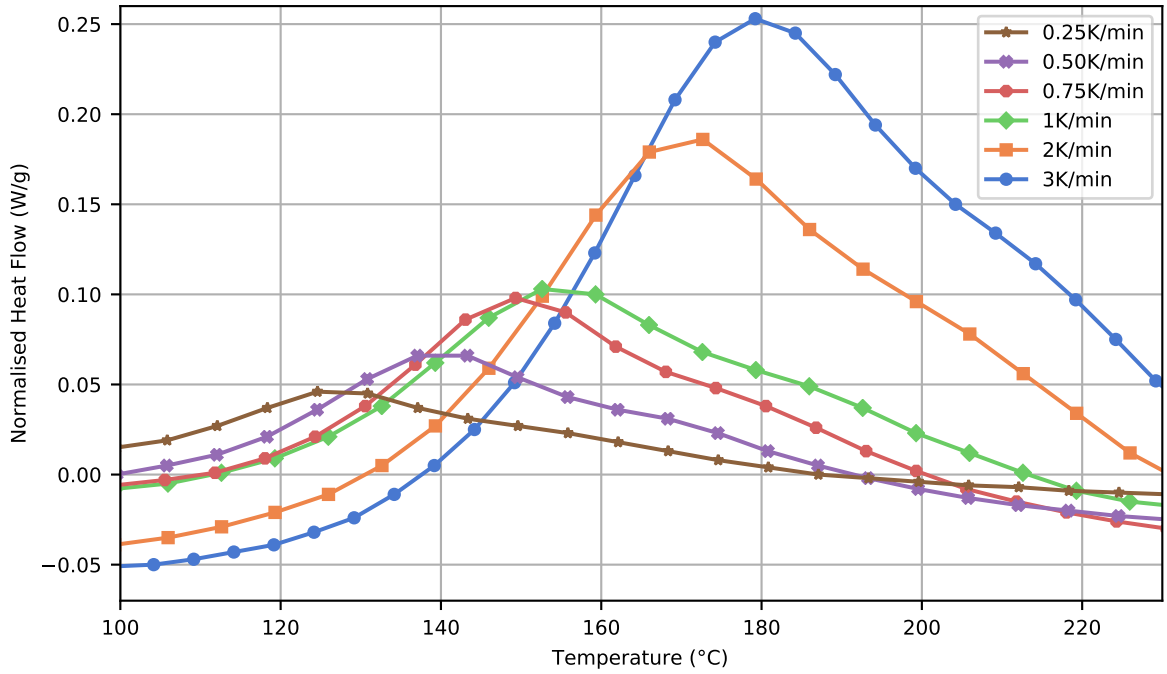

Figure 3.1: DSC Different Heat Rates

The heat rate of 0.5° C/min was chosen to calculate the total enthalpy of the curing reaction since it was

Table 3.1: Enthalpy Measurements of Different Heating Rates

Heating Rate (° C/min)	Enthalpy (J/g)
1	401.4
0.75	427.1
0.50	479.6
0.25	454.1

considered slow enough that the resin had time to cure properly but not slow enough that the heat flow couldn't be measured by the device as was shown by the heating rate of 0.25° C/min.

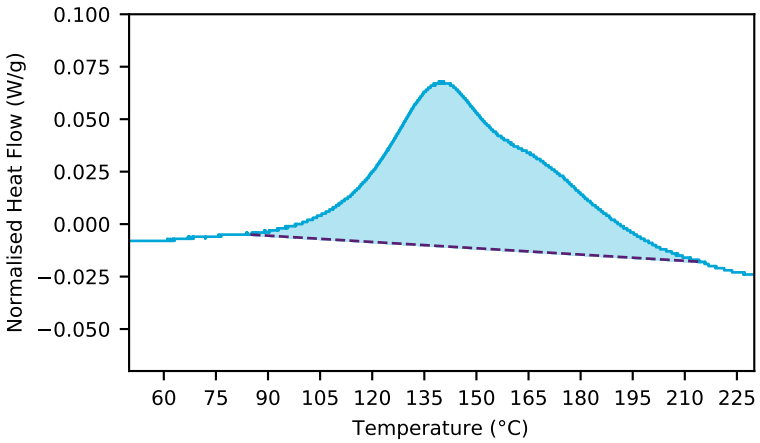

Figure 3.2: Baseline Shifting for 0.50 K/min Heat Rate

$$\alpha = \frac{1}{H_t} \int_0^t \frac{dH}{dt}\, dt \tag{3.3}$$

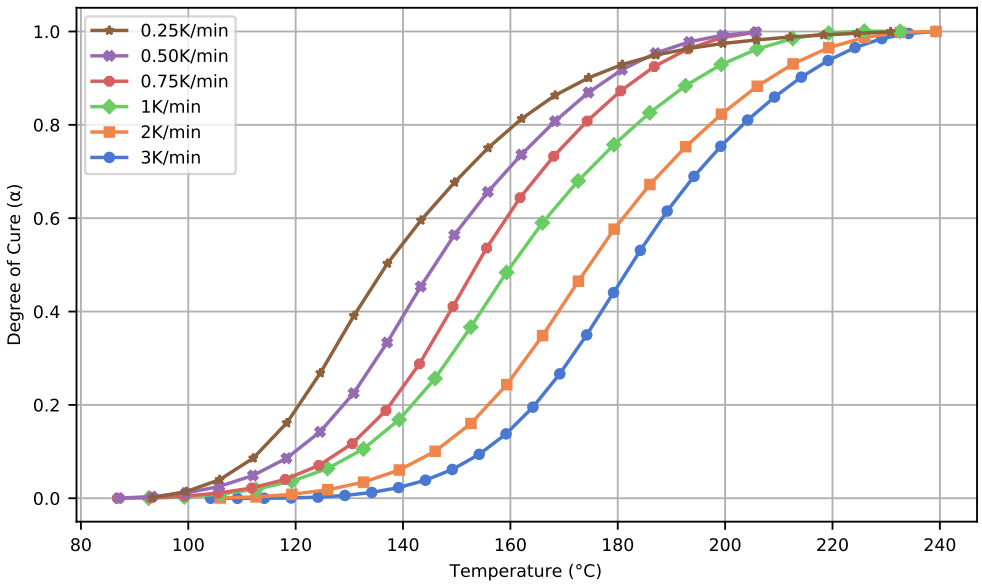

Figure 3.3: Different Dynamic DSC Runs

The degree of cure (α) can be calculated using Equation 3.3 at any point during the reaction. This is shown in Figure 3.2. The highlighted area in the figure is what the integration was done for which gave an enthalpy value of 479 J/g.

3.2.2. Isothermal DSC

Different isothermal temperatures were selected to see the heat of the reaction evolving at that particular temperature over time [38]. This is shown in Figure 3.4. For higher temperatures higher initial peaks are observed, however these peaks quickly start to converge with the axis. Again, integrating the area with baseline fitting and dividing by the total enthalpy calculated in the previous subsection gives the degree of cure. This was then plotted for all temperatures shown in Figure 3.5. Figure 3.5 also gives the curing time for the resin system at different temperatures. Ultimately, it was decided that curing cycle would be done for 2 hours at 160° C.

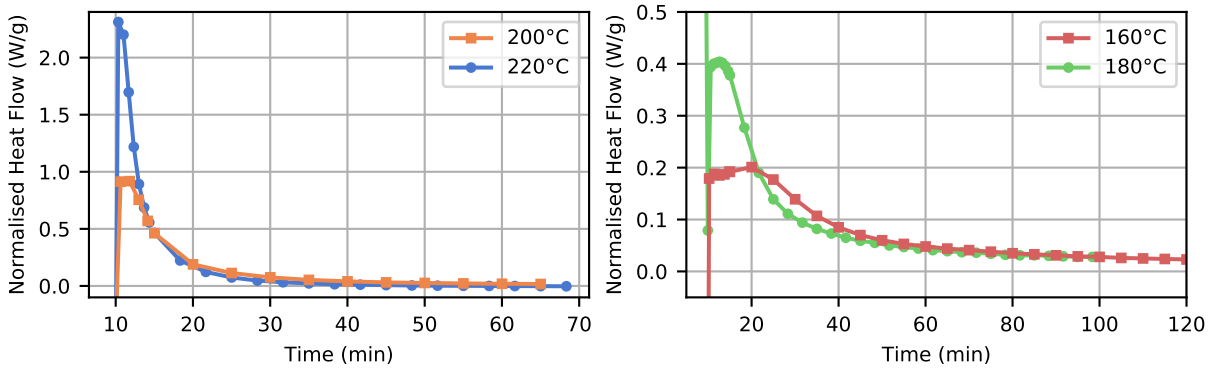

Figure 3.4: Isothermal DSC at Different Temperatures With Varying Time Scales

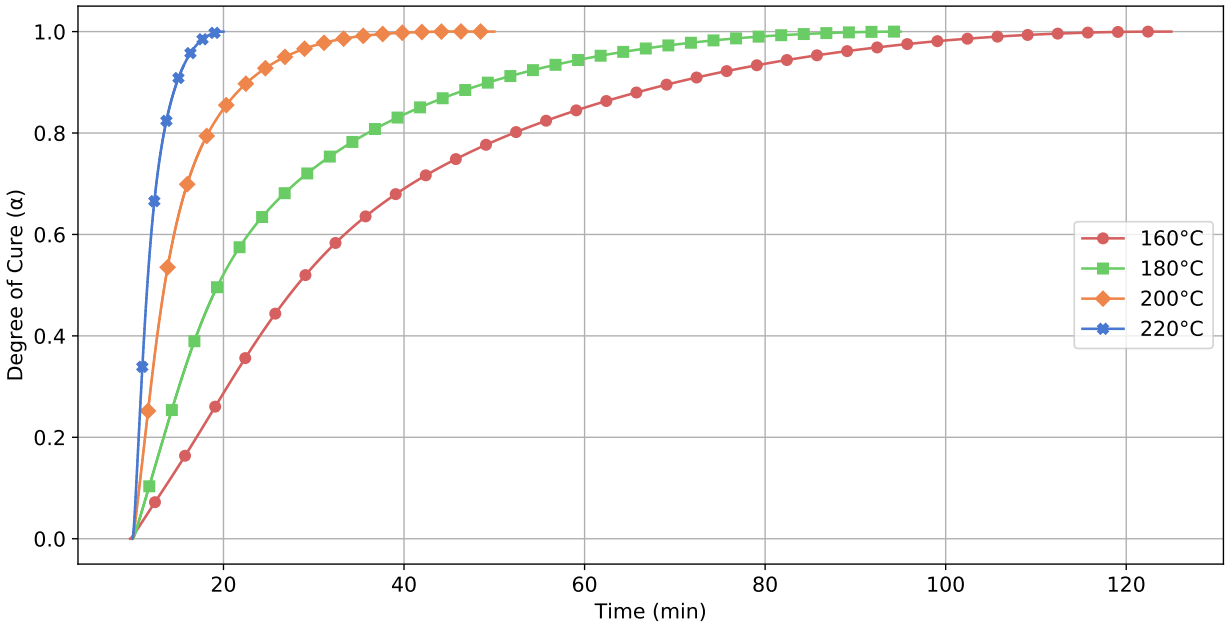

Figure 3.5: Degree of Cure at Various Isothermal Temperatures

3.2.3. Cure Model

The DSC data was analysed with the nth-order autocatalytic reaction equation given in Equation 3.4. Since the curing temperature was higher than the glass transition temperature a diffusion model was not used. Isothermal data taken from runs at 160° C, 180° C, 200° C and 220° C were taken to parameterize according to the equation.

$$\frac{d\xi}{dt} = k_1\xi^m(1-\xi)^{n_1} + k_2(1-\xi)^{n_2} \tag{3.4}$$

where

$$k_i = A_i e^{-E_i/RT} \tag{3.5}$$

where k(i) represents the Arrhenius equation, t is the reaction time, n_1 and n_2 are constants and ξ is the degree of conversion. A_i is the pre-exponential factor, E_a is the activation energy and R is the universal gas constant. Activation energy is defined as the minimum amount of energy required for a reaction to occur. Therefore, the activation energy can be calculated by the slope of $ln(d\alpha/dt)$ vs 1/T graph at low degrees of cure.

The activation energy (E_a) came out to be 65.3 kJ/mol. Multivariate linear regression analysis was done at the different isothermal dynamic heating rate measurements. The constants m, n_1 and n_2 along with other values are given in Table 3.2.

Table 3.2: Cure Model Values

A_1 [log(s^{-1})]	A_2 [log(s^{-1})]	m	n_1	n_2	E_1 $[kJ/mol]$	E_2 $[kJ/mol]$
3347.027	19473774	1.055	1.390	4.735	53.172	85.991

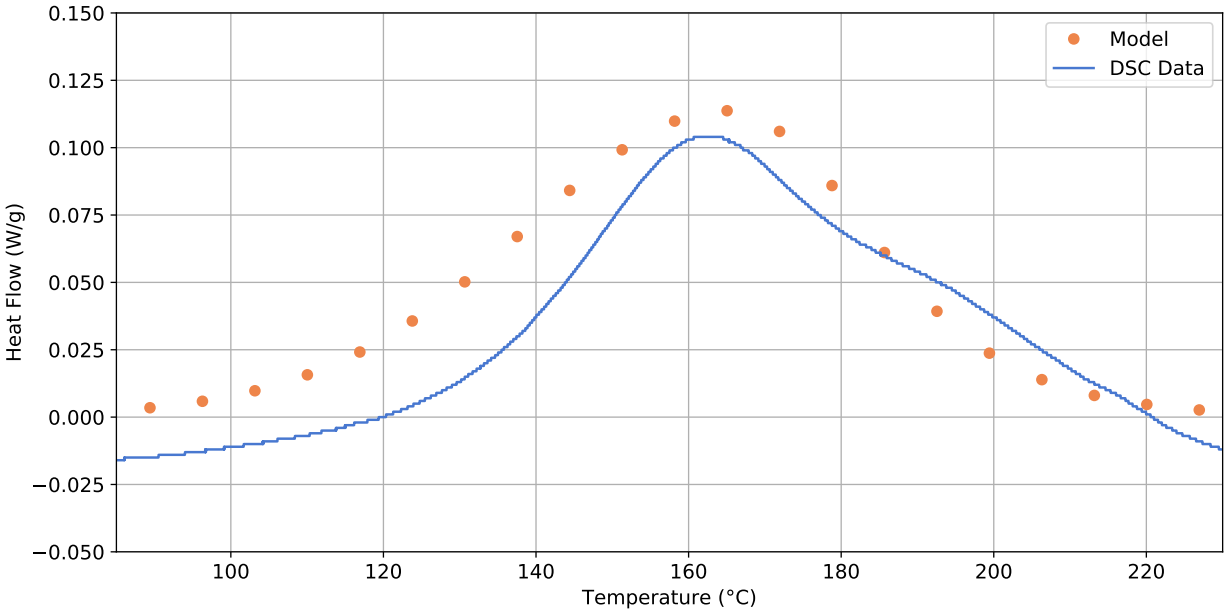

Figure 3.6: Heat Flow Evolved in a Dynamic DSC Compared to Model

With this model, the degree of cure over the extent of the reaction could be plotted for some temperatures as shown in Figure 3.7. Dynamic DSC data was also plotted alongside the model to see its accuracy as shown in Figure 3.6. This was done with the heating rate of 1 K/min since the time in the x-axis can be replaced with temperature.

The average error with this model was 0.061% which was considered satisfactory. As can be observed in the figure itself the heat flow predicted by the model and the experimental values are similar. The model does show that there is indeed some amount of residual cure left which was cross-checked with second heating runs done with dynamic DSCs. To test whether just four of the isothermal measurements were

necessary to predict other curing temperatures, experimental data at temperatures of 140° C, 190° C and 210° C was also collected. This was then compared with the degree of cure developing over time according to the model. This is shown in Figure 3.8.

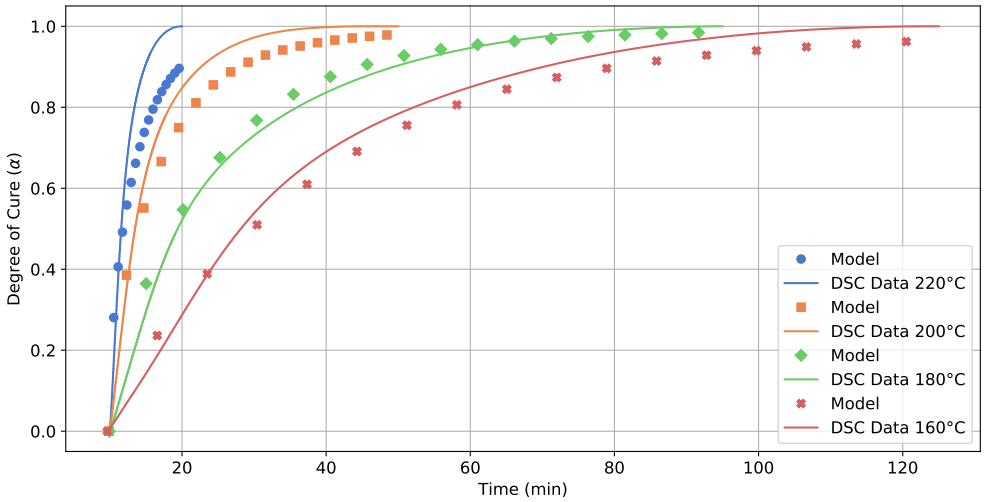

Figure 3.7: Degree of Cure Experimental Data vs Model

Observing this data gives a clear understanding of the cure kinetics and how it evolves over time through the different temperatures. Curing at 160° C and 180° C represent practical options as ways to cure the resin mixture for 2 hours and 1.5 hours respectively. However upon, looking at the test data from 140° C isothermal cure, it is seen that the resin reaches almost a fully cured state after 5 hours. It is generally accepted that a lower peak temperature during curing reduces thermal gradients, curing stresses and thus reduces residual stresses within the resin and might lead to less curvature in a composite [39]. It is also considered that a two-dwell cure cycle is better because it produces lower residual stresses by having an initial high exothermic peak and the second dwell for curing the resin. Another point to consider could be energy costs during the curing itself and how a higher temperature for a shorter time could be better or worse when compared to a lower temperature for a time that is more than twice as long. Ultimately, considering time limits, a curing cycle of 160° C for 2 hours was used within this project to cure the resin. A further post-cure cycle was also introduced which is discussed in Section 3.3.

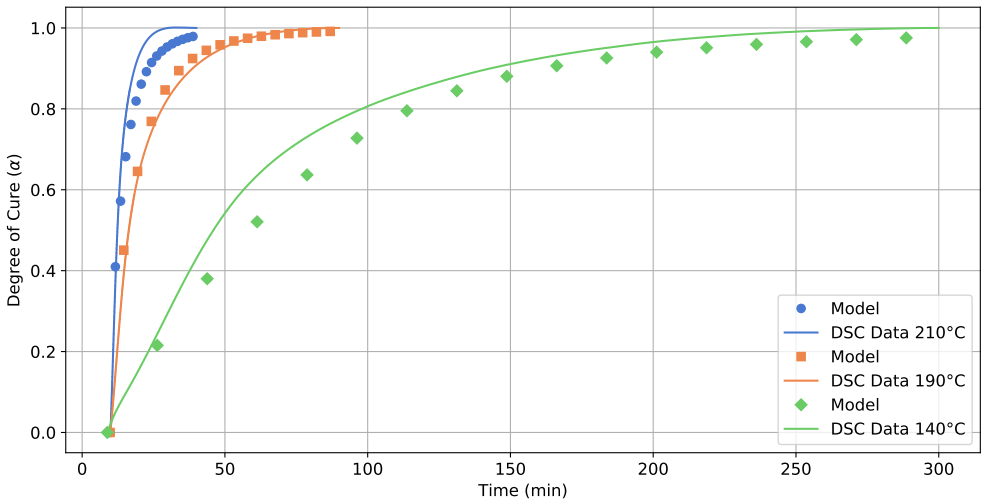

Figure 3.8: Degree of Cure Experimental Data vs Model different temperatures

3.3. Post Cure Cycle

As described in the previous section there was still some residual cure left even after curing at 160° C for 2 hours. To cure the samples completely, it was decided to post cure the samples to ensure maximum amount of cross-linking. DSC measurements are not preferred for checking this since the amount of heat released is rather small and therefore not detectable by the DSC equipment. A more sensitive technique is found in Dynamic Mechanical Analysis (DMA). A more cross-linked polymer would show a higher glass transition temperature (T_g) which is what was checked.

DMA was performed on the machine RSA G2 DMA by TA Instruments. Samples were cured at a lower temperature of 140° C for 2 hours so that there would be a higher amount of post-curing required. Samples were then post-cured at different temperatures for 30 minutes starting from 140° C at steps of 20° C going all the way till 220° C. It was decided not to perform post-curing at a higher temperature than this since from DSC data (Section 3.2) it could be seen that the material starts to degrade at temperatures of 240° C. As will be discussed further in the Section 3.4, the T_g can be taken as the peak of $tan(\delta)$. The results from post-curing at 140° C and 160° C were not valid since the samples didn't show a clear peak and there was a lot of noise in the data as well, as shown in Figure A.3. For the remaining temperatures, the trend is clear to see in Figure 3.9. Therefore, it was decided that the post-curing temperature would be set at 220° C. To determine the time for post-curing, a gel content test was performed.

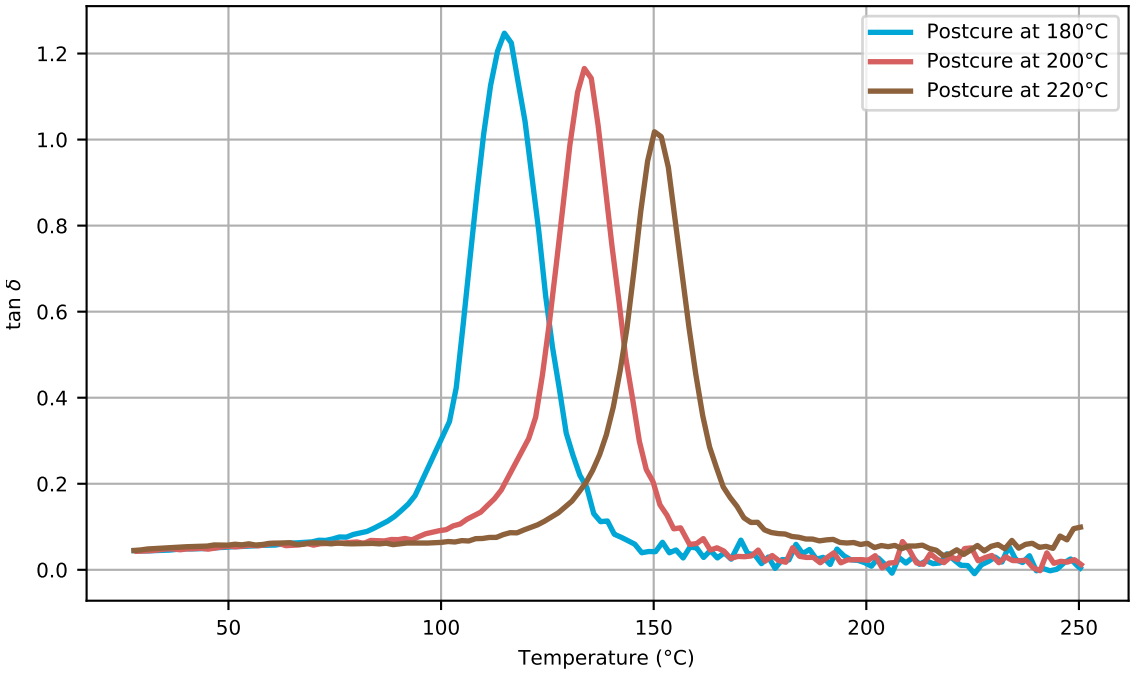

Figure 3.9: Changing T_g for Different Postcure Temperatures

3.3.1. Gel Content

To understand the time for post-curing, it was decided to test gel content by checking the resin's solvent stability. The solvent selected was toluene. Samples that had gone through just the curing cycle, ones that were post-cured for varying lengths of time were immersed in the solvent for a duration of 72 hours. The samples were weighed before immersion and kept in vials and after the immersion period was over, dried using filter paper and compressed air and weighed again. The results for this can be seen in Table 3.3.

The gel content can be calculated using the equation below.

$$GC\% = \frac{W}{W_0} \times 100 \tag{3.6}$$

For the cured resin mixture and the sample post-cured for half an hour, the gel content was 99.52% and 99.55%. For the sample that was post-cured for an hour, it was 100%. It was decided that post cure cycle

Table 3.3: Gel Content Specimen Weight

Sample Type	Mass Before Immersion (mg)	Mass After Immersion (mg)	Gel Content (%)
Cured	21.1	21.0	99.52
Post-Cured (0.5 h)	22.5	22.4	99.55
Post-Cured (1 h)	31.1	31.1	100

would be done at 220° C for one hour. The time for this cycle was not increased further because post-cure cycles are supposed to be shorter in duration and because it was noticed that slight discolouration would start to occur on the specimens when kept for longer. This could be attributed to oxidation occurring or that the material was starting to degrade. For some of the mechanical tests, these slightly discoloured samples were tested alongside to see whether it affected the mechanical performance. As will be discussed in Chapter 4, the oxidation did not significantly deteriorate the mechanical properties of the resin.

3.4. Glass Transition Temperature

An important characteristic of thermosetting polymers is its glass transition temperature. Glass transition is a phase transition in which a network polymer goes from a brittle glassy state with low molecular mobility to a rubbery state with high molecular mobility. This state is known as the glassy phase and the temperature at which the physical state changes into the rubbery phase is known as the glass transition temperature (T_g). This characteristic of the polymer offers insight into the temperature range till which the polymer would retain its mechanical properties.

Various methods exist to identify the T_g of a polymer including DSC and DMA which were used in this project. In a dynamic DSC, the T_g would be observed as a jump in the baseline while cooling. If the sample is being heated then the jump would be downwards. Both of these temperatures will probably not be the same but a lot of experiments are done while heating [40]. The abrupt change in the heat capacity is usually observable in two places in semi-crystalline polymers: glass transition and melting temperature. A typical DSC curve with the T_g is shown in Figure 3.10.

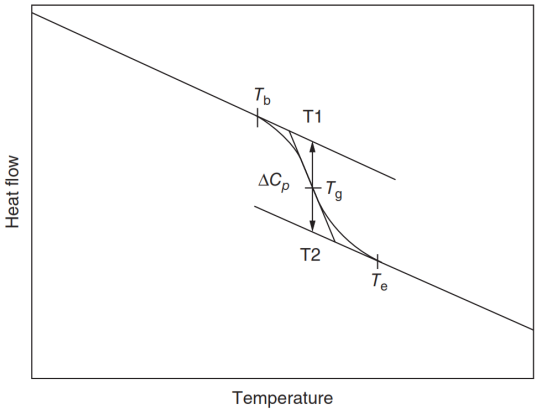

Figure 3.10: T_g Observed in a DSC Measurement [40]

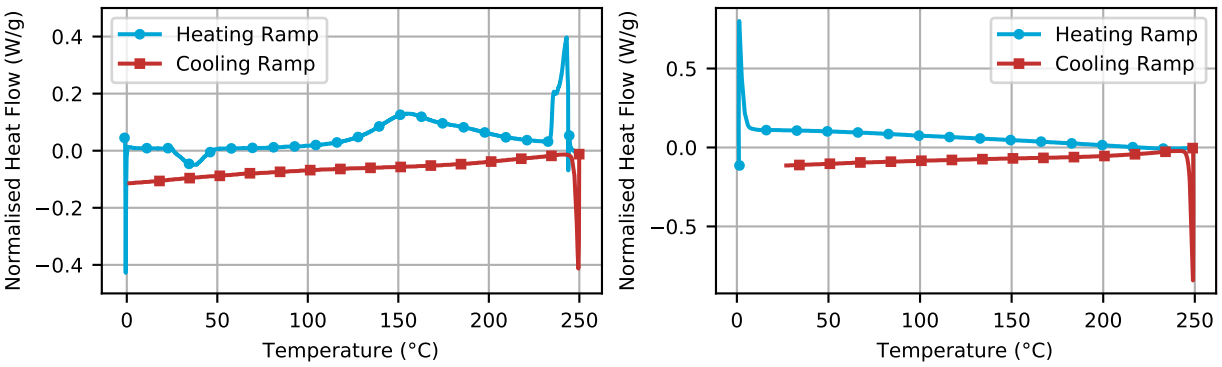

Figure 3.11: (Left) Initial and (Right) Subsequent Temperature Ramps in DSC

Some tests were done with VDE-DDS in the appropriate stoichiometric ratio to observe the transition regions but none were found. Figure 3.11 shows the first and second heating cooling ramp of an uncured sample. In this first heating run it can be seen that there is a transition region at around 35° C, which is most likely a phase transition as the VDE monomer melts into a liquid at this point with DDS dissolved in it, indicated by the endothermic nature of the process. At around 140° C an exothermic peak starts which ends at around 240° C. This is representing the curing reaction occurring. However, after this another peak starts to form after 240° C which is most likely when the material starts to degrade. This was further confirmed using TGA (Thermogravimetric analysis) and is discussed in Section 3.7. The first cooling run shows no transition regions and is simply a straight line. In a similar way, the second heating and cooling runs, both don't show any transition regions representing the glass transition region. This can happen due to a variety of reasons including large molecular mass of the polymer itself or little reaction enthalpy.

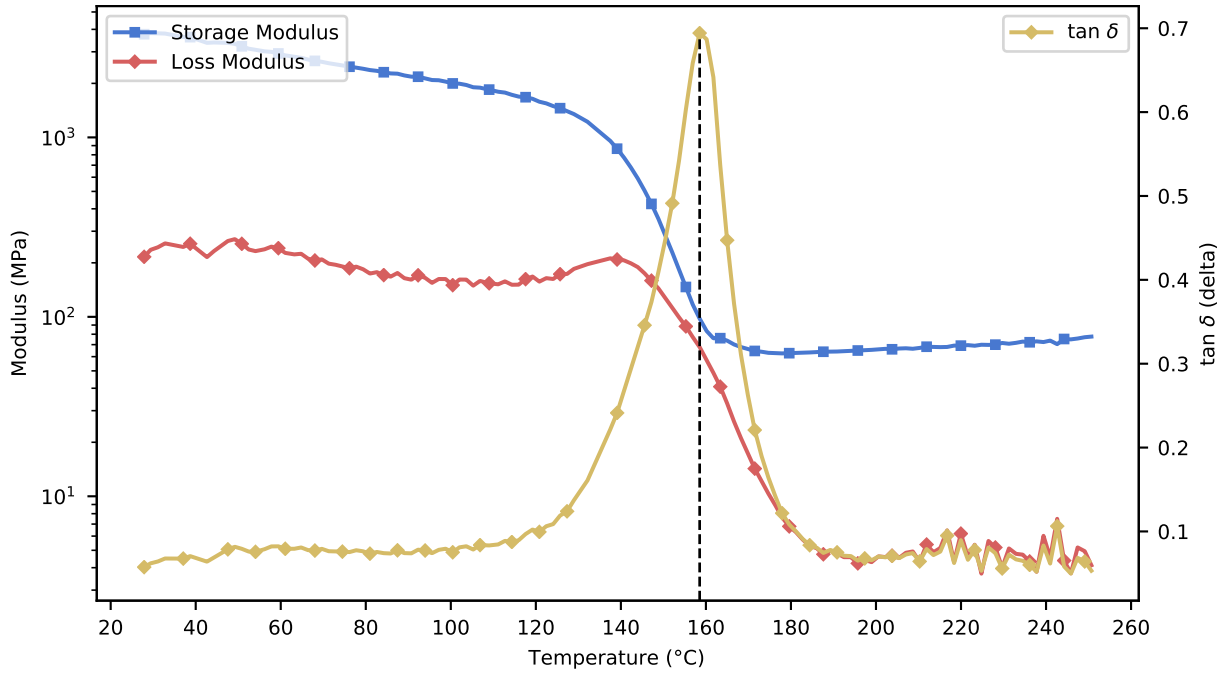

Figure 3.12: DMA Showing Peak of $tan(\delta)$

After this it was decided to use DMA to identify the T_g. DMA is a more sensitive technique when compared DSC for T_g measurement. The sample dimensions for conducting DMA was $35 \times 9 \times 2$ mm. The samples were cured and then post-cured in a steel mould with the specified dimensions according to TA Instruments' recommendations. The support span of the three-point bending setup was 25 mm. The test was conducted with a frequency of 1 Hz. A higher frequency would show a higher glass transition temperature.

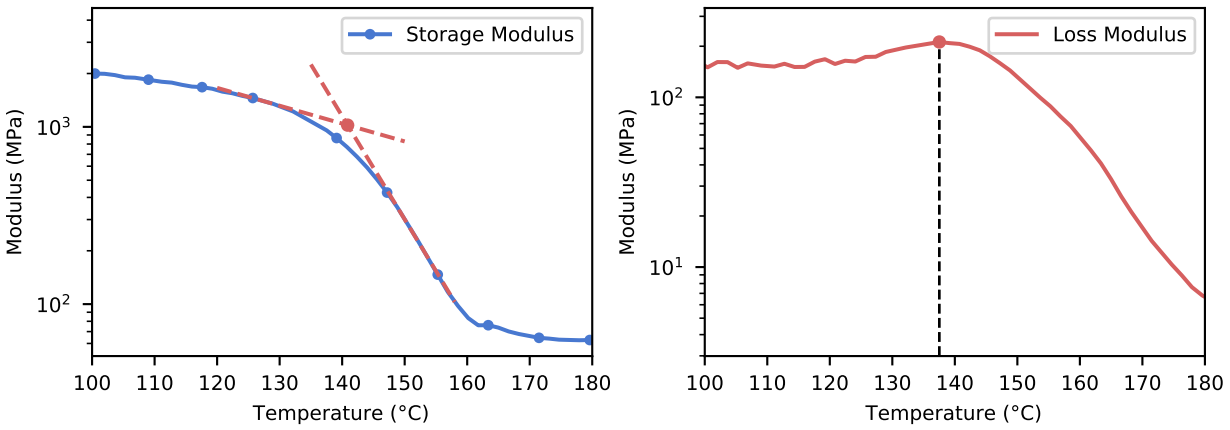

Figure 3.13: (Left) T_g from Storage Modulus and (Right) T_g from Loss Modulus Peak

Different analysis options exist to determine the T_g of the material from DMA. Since T_g is more of a temperature range rather than single temperature value, three different options are compared and analysed. The first method is to take the peak value of $tan(\delta)$, which is the ratio between the storage modulus (E') and the loss modulus (E"). The peak of $tan(\delta)$ is at 158° C as is shown in Figure 3.12. This is the point where the material has the highest viscous response to deformation. An option which provides a more practical T_g is the onset drop of E'. In this way, the T_g was 140° C as shown in Figure 3.13. When E' starts to decrease it means that the material is starting to lose its properties and this is usually the temperature limit for the material in practical applications as well. This can also give an understanding of the heat deflection temperature which happens under a constant load and is discussed in Section 3.5. The final method is to have it as the peak of E". This value is usually in-between the T_g values measured using $tan(\delta)$ and E'. However in this case, no clear peak of E" was present and the value was 137.52° C which is the least of all three methods. This is shown in Figure 3.13 as well.

Therefore, since the glass transition temperature is a range, it can be concluded that it is between 140-158° C, with the highest operational temperature probably being the lower value of this range. To further identify its operational temperature capabilities under load, Section 3.5 deals with the same.

3.5. Heat Deflection Temperature

To understand better at what temperatures the material is actually able to sustain a load, the heat deflection temperature (HDT) is commonly used. It determines at what temperature the material would undergo significant enough changes such that it loses its mechanical properties and undergoes a certain amount of strain whilst under a load. A standard called ASTM D648-18 "Standard Test Method for Deflection Temperature of Plastics Under Flexural Load in the Edgewise Position" was used to identify the HDT for the cured resin [41].

Due to time constraints, the experiment could not be conducted in an environmental chamber. Instead it was done in the same DMA three-point bendng setup since it provides the same values, just the specimen dimensions are of a different scale. As shown by Wadud and Ulbrich [42], DMA can be used for this purpose if the given stress and strain values are converted according to the specimen dimensions. The recommended stress to be applied according to the standard is 0.455 MPa. With this constant stress applied on the specimen, when it reaches a strain of 0.25 mm, the temperature is the heat deflection temperature of the material. Using these conditions and applying them to the DMA Isoforce mode across a temperature sweep, the HDT could be found out.

The first step was to calculate the required force to achieve for the specimen dimensions of $35 \times 9 \times 2$ mm which are recommended by the manufacturer to be used in the machine. The force can be calculated using the following equation:

$$F = \frac{2}{3}\sigma\left(\frac{T^2 W}{L}\right) \tag{3.7}$$

where F is the force, σ is the stress (equal to 0.455), T is the thickness of sample, W is the width of the sample and L is the span of the supports (taken here as 25 mm). This gives a required force of 0.4368 N.

Next, the required deflection, since that is what is measured by the machine, was calculated using the following equation:

$$d = \frac{\epsilon L^2}{6T} \tag{3.8}$$

where d is the deflection and ϵ is the strain.

Strain can be calculated according to the following equation:

$$\epsilon = \frac{6dT}{L^2} \tag{3.9}$$

With this equation the strain percentage comes out to be 0.121%. Putting this value into the previous equation gives the deflection value which comes out to be $63\,\mu m$.

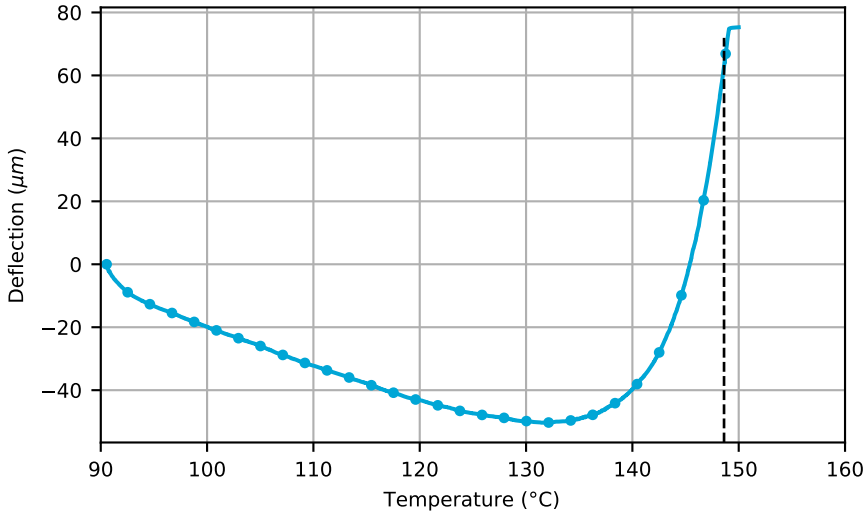

Figure 3.14: Masurement of HDT

Isoforce mode was used to conduct the DMA test with a temperature sweep. The force was set as 0.4368 N and the temperature range was set between 90° C and 150° C. The temperature at which it would reach a deflection of $63\,\mu m$ would be the HDT. However, with the increase in temperature, the material would start to expand and the deflection measured by the machine would be negative (upwards deflection of the probe) and then start to increase towards the positive side. This can be seen in Figure 3.14. The temperature at which the material gave a deflection of $63\,\mu m$ was 149 °C.

3.6. Thermal Expansion

As thermoset materials heat-up, they tend to expand. This comes in the form of dimensional changes which therefore increase the volume of the material itself. Higher range of operating temperatures would imply that the material would have to undergo these dimensional changes often which might lead to the creation of thermal stresses. The volumetric changes also have to be accounted for in the design of the structures in the form of tolerances.

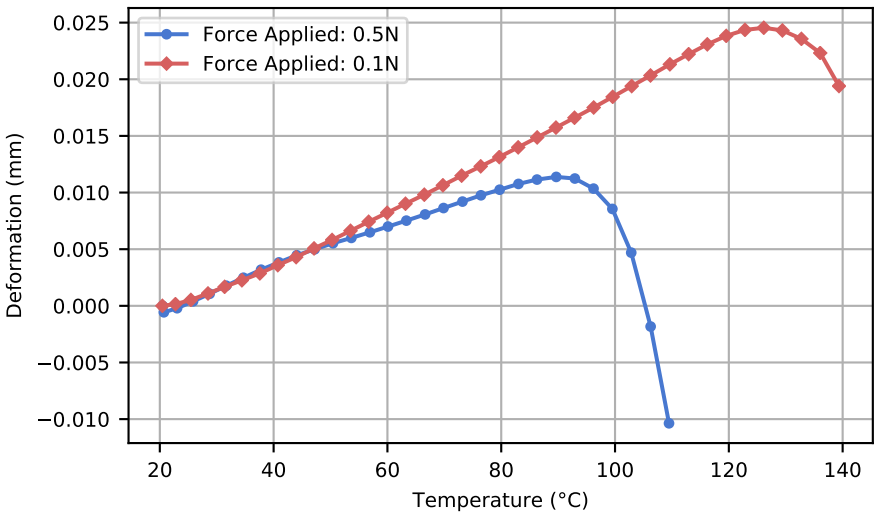

Figure 3.15: CTE Measurement

The coefficient of thermal expansion (CTE) was measured using the Perkin Elmer TMA 4000. The setup for thermo-mechanical analysis (TMA) consists of a probe which touches upon the surface of the sample and exerts a force. Upon introducing a variable temperature, the deflection of the probe changes, which is recorded by the machine. Tests were conducted with different applied forces of 0.5 N and 0.1 N. The data recorded is shown in Figure 3.15. The behaviour shown by the material was unexpected because instead of expanding, it seemed like the material started to shrink at different points. The tests were repeated again which gave similar results. However, one of the tests left a visible mark on the sample as can be seen in Figure 3.16. This could explain what the data was showing in that the probe had simply penetrated the surface due to the high force. This was only for the test where the force was 0.5 N but it is possible that micro-indentations could have been made by the probe with the lower force and that is what was registered as the deformation as well.

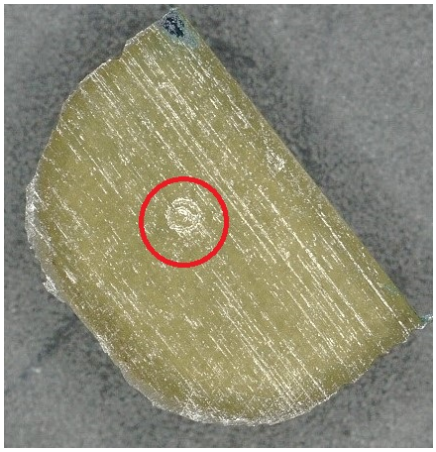

Figure 3.16: Indentation on the Specimen Circled in Red

Nevertheless, the two parameters with which the specimens were tested gave a similar slope in the initial stages which is what was used to calculate the CTE. CTE is calculated using the following equation:

$$\alpha = \frac{\Delta L}{L \Delta T} \tag{3.10}$$

where α is the thermal expansion coefficient, ΔL is the deflection measured by the probe over temperature range ΔT and L is the thickness of the sample. The thickness of the sample was 4.01 mm. With this, CTE

value came out to be $58.12\,\mu m/m°C$. Comparing this with other cured resin values, it is noticed that the CTE for VDE-DDS is lower than its competitors like BADGE-DDS for which it was $84.45\,\mu m/m°C$ [23].

3.7. Degradation Temperature

Thermal degradation occurs in thermoset networks through chemical bond scission that happens due to the increased kinetic energy in the molecules. Through bond scission smaller volatile molecules are formed and released from the material which is measured by TGA. Since the sample size in a TGA measurement is rather small, the rate of bond scission compared to the mass lost due to volatiles is slower and hence can be considered to be the bottleneck [43]. Another point to consider is that some degradation products are non-volatile and hence the specimen would continue to have the same weight. The TGA curve shows the initial degradation temperature but using it for further conclusions about the material's properties would not be considered appropriate since the material would be far out of its operating temperature.

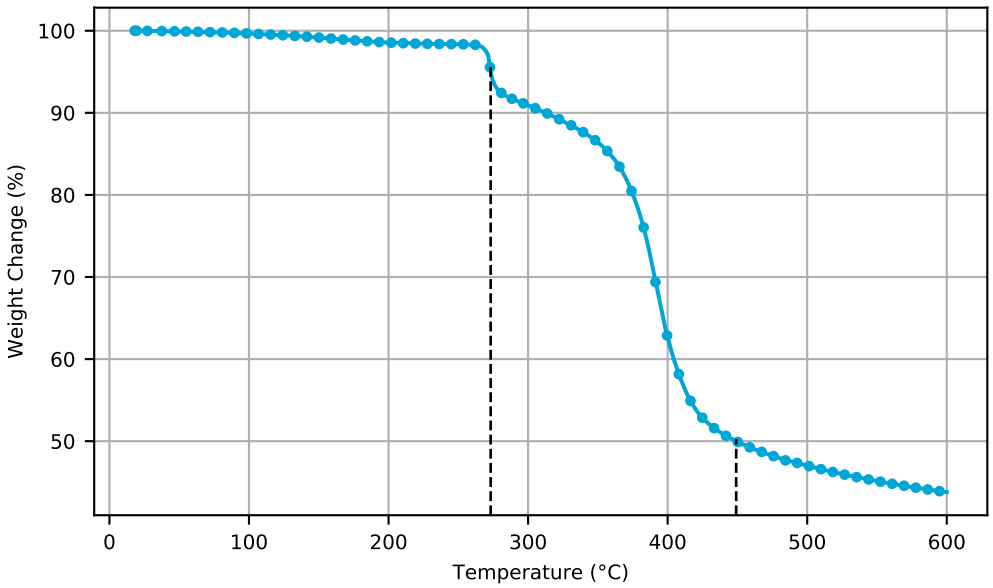

Figure 3.17: TGA for VDE DDS

Thermogravimetric analysis (TGA) helps in understanding the behaviour of the material at elevated temperatures. The principle of TGA is that it contains a micro weighing scale where the sample is kept, which is enclosed inside a furnace within which there is a constant supply of air flow and the weight of the sample is then measured according to the changing temperature. For this experiment, a ramp rate of 10° C/min was used. SDT Q600 instrument was used to do TGA. An air flow rate of 20 ml/min was used. The starting weight of the sample was around 12 mg. The measurement is shown in Figure 3.17.

Table 3.4: TGA Weight Loss

Weight Change (%)	Temperature (°C)
5	273
50	450

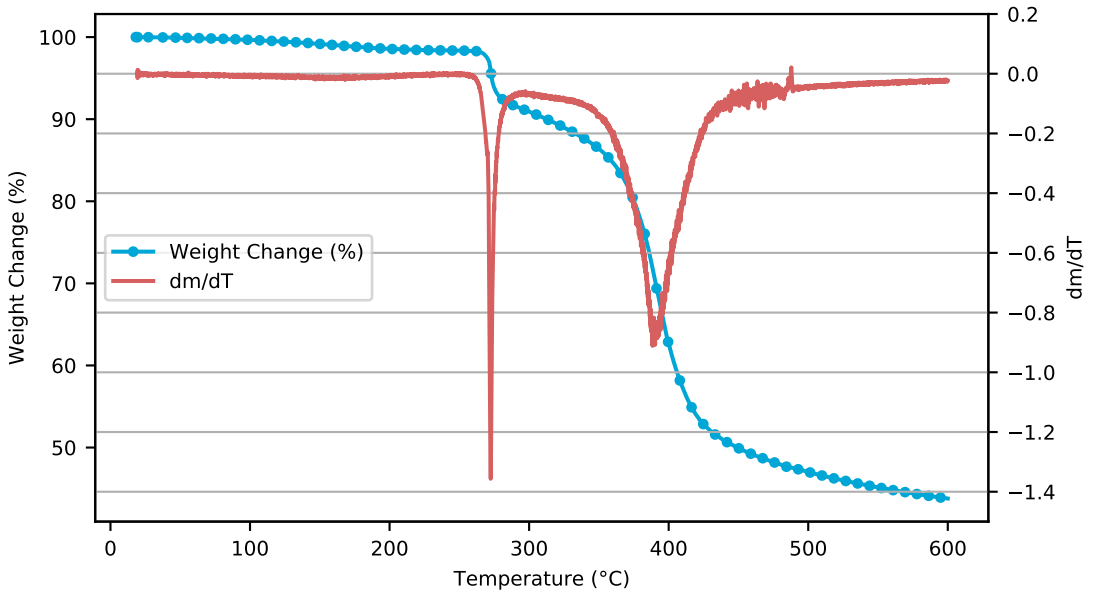

Figure 3.18: Weight Change with Rate of Weight Change

The rate of change of mass can also be plotted by taking the derivative of the weight change. This is plotted in Figure 3.18. It was observed that there is a major rate of mass change occurring near 270° C and then another occurring just before 400° C. The graph shows that dm/dt stabilizes for a short time before it starts to increase again and the weight loss occurs dramatically after this period. It can be speculated that the side chains substituents of the epoxy resin are what break-off first during the initial high rate of weight change [44]. This would also explain how the change in mass stabilizes after this and the next major rate of weight change is when the primary epoxy chain itself starts to break. The remaining mass left is the polymer char yield. A study focusing on BADGE mixed with DETDA hardener investigated the chemical process of the bonds breaking [45]. They found that the initial stage of degradation was started by breaking of cross-linked and ether bonds, which was then followed by polycondensation and carbonization subsequently. It was found that these reactions ultimately produced carbon chains and char-like clusters.

3.8. Rheology

Rheological experiments were performed on the HAAKE MARS III rheometer by Thermo Scientific to find how the viscosity of the uncured resin developed with increasing temperature. Due to unavailability of disposable plates, it was not possible to study the pot life and gelation time of the resin. Instead, the study focused on the processing parameters for composite manufacturing. One of the popular choices for flat composite plate manufacturing is vacuum infusion since it makes good quality panels and the fiber volume content can be controlled. Commercial epoxy resins available today for vacuum infusion generally have viscosities ranging between 100- 250 m Pa-s.

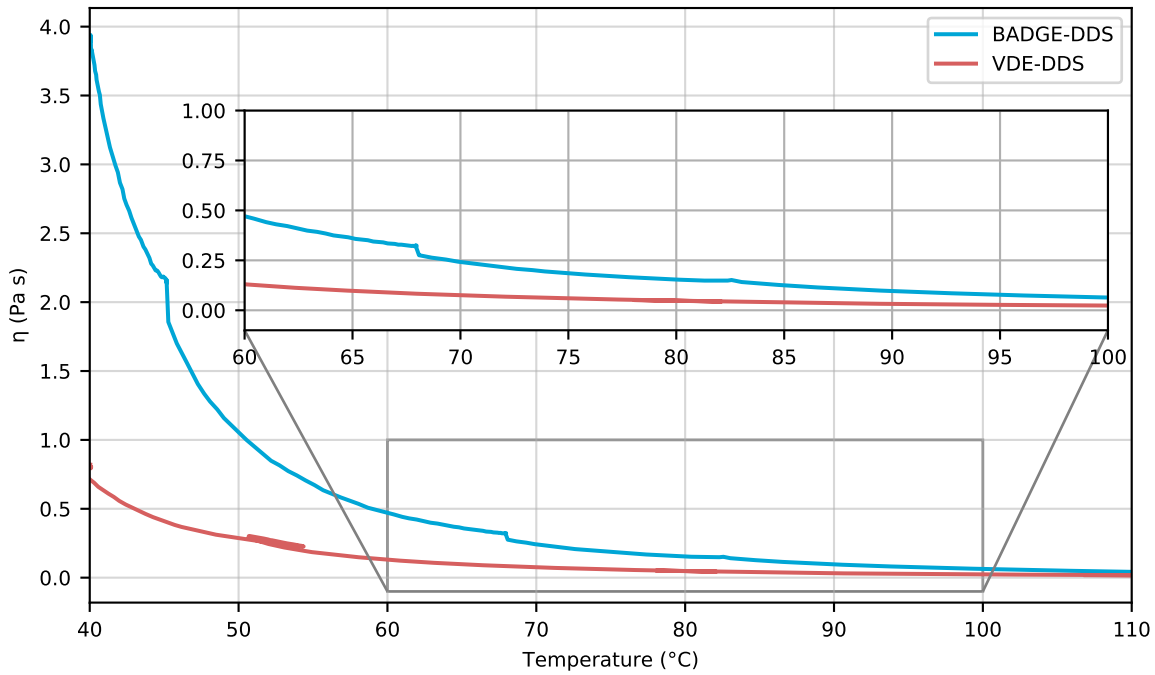

Figure 3.19: Viscosity Developing Against Temperature

The viscosity was measured by VDE-DDS mixture from 40° C to 110° C so as to not let the resin cure whilst it was in the rheometer. 20 mm diameter aluminium plates were used with the resin being kept at the elevated temperature of 40° C for 15 minutes before the experiment started so that it was uniformly at that temperature. A comparison was provided by BADGE-DDS as can be seen in Figure 3.19. As was seen in Section 3.3, VDE undergoes a phase change at around 40° C while BADGE remains a liquid throughout. However, VDE-DDS mixture always showed a lower viscosity compared to BADGE-DDS. The difference in their viscosities does tend to decrease as the temperature goes higher but after 110° C it is assumed that the resin would start to partially cure. It is important to note that the resin viscosities shown in the figure do reach the values recommended for vacuum infusion however it does so at elevated temperatures of 60-70° C. This is not ideal as the fibers and the mould would have to be kept at these elevated temperatures for the duration of the infusion, since a hot resin coming into contact with colder fibers would immediately increase in viscosity and stop flowing. VDE-DDS lies right at the cusp of a smaller scale process like vacuum infusion and an industrial process like resin transfer moulding (RTM). RTM would be ideal but given its higher demand for equipment would be hard to fulfill in this case. Another factor to keep in mind is the gelation of the resin at higher temperatures. While through DSC it was found that the resin reaches lower degrees of cure at 120° C even after 5 hours of curing, it is still not known how that would affect the viscosity. In conclusion, the resin holds potential to be used in across a wide range of manufacturing methods.

3.9. Surface Hydrophilicity

Different epoxies have different surface energies, and interact with water in different ways. Hydrophilic materials have water contact less than 90°, whereas hydrophobic surfaces have water contact greater than 90°. This value affects an epoxies properties as more hydrophilic materials would have a tendency to absorb more water, which would lead to degradation in thermal and mechanical properties of the resin.

For this experiment two different cured epoxy samples were prepared which were then put in front of a water contact angle measuring setup. The software used for water contact angle measurement was KSV Attension Theta. The software calculates the contact angle by first measuring the angle made by a calibration ball 4mm in diameter which is spherical and all its edges are visible. After this the sample is put in the setup (see Figure 3.20) and the contact angle is measured (see Figure 3.21).

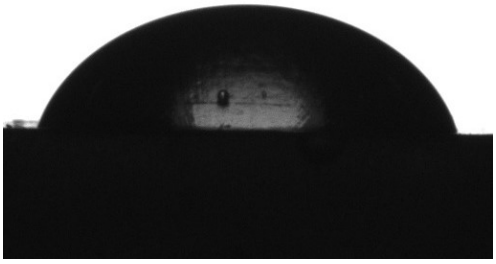

Figure 3.20: A Water Droplet on Resin Sample

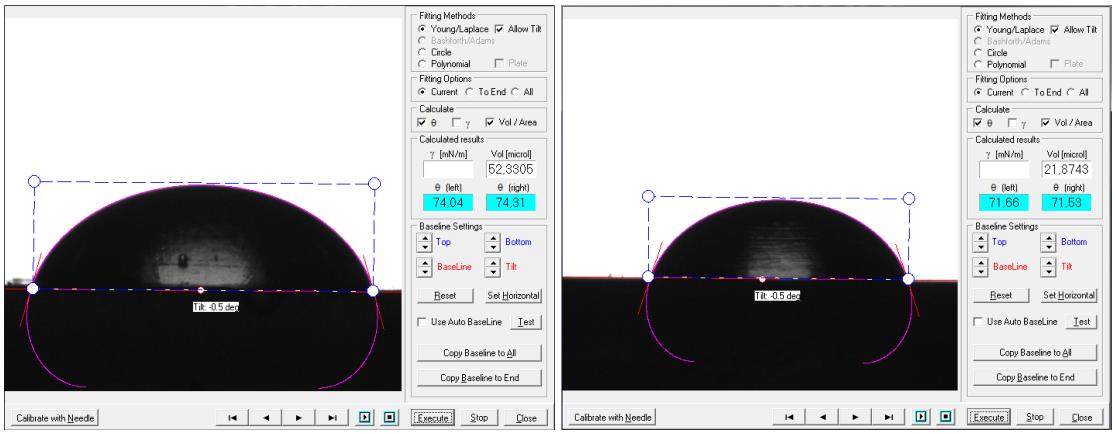

Figure 3.21: Measurement of the Water Contact Angle

Table 3.5: Water Contact Angle Measurements

Sample Number	θ (Left)	θ (Right)	Average Angle (°)
1	71.19	67.19	69.19
2	74.04	74.31	74.17
3	71.66	71.53	71.59

The different measured water contact values are given in Table 3.5. The average water contact angle value comes out to be 71°, which means that the surface is hydrophilic in nature.

New research work being done on bio-based additives like haxanoic acid and resveratrol are used to enhance the hydrophobicity of coatings [46] could help in preventing exposure of water to the resin..

3.9.1. Water Absorption

Samples were put in a vial of water for different amounts of time to understand how much water gets absorbed by the fully cured resin. Too much water intake can cause issues in the structure. most surfaces are indeed coated with other polymeric substance for water repellency but it shouldn't be left to chance.

The water absorption values are too high compared to other commercial epoxies, the study by Gupta [23] found that for BADGE-DDS water absorption after 2 weeks was only 0.96% higher compared to its initial mass. In applications where contact with water occurs regularly, hydrophobic coatings should be employed to not affect the properties of the resin. How the water absorption does indeed affect the thermal and and mechanical properties of the resin is beyond the scope of this project.

Table 3.6: Water Absorption

Sample Number	Time	Initial Weight (mg)	Final Weight (mg)	% Change
1	24 hours	36.1	36.3	+0.55%
2	48 hours	43.8	44.3	+1.14%
3	1 week	99.1	102.7	+3.63%
4	2 weeks	57.3	60.45	+5.49%

3.10. Density and Cure Shrinkage

The density of the fully cured resin was found through Archimedes' principle as described in ASTM D792 "Standard Test Methods for Density and Specific Gravity (Relative Density) of Plastics by Displacement" [47]. Different samples were weighed in distilled water and air and their density was calculated according to the density of water at that specific temperature.

Figure 3.22: Weight Measurement of Sample Immersed in Water and in Air

Table 3.7: Specimen Specifications for Density Measurement

Sample Number	Water Temperature (° C)	Specimen Weight in Air (g) **A**	Immersed Specimen Weight (g) **B**
1	21.0	1.0836	0.1907
2	21.1	1.6423	0.4013
3	21.2	3.8007	0.9166
4	21.3	0.2647	0.0651
5	21.4	3.7254	0.9008

The density is calculated using the following formula:

$$\rho = \frac{A}{A - B}(\rho_o - \rho_l) + \rho_l \tag{3.11}$$

Where ρ_o is the density of water and ρ_l is the density of air. As can be seen in the table, the water temperature increased between each specimen because the ambient room temperature was around 22° C so the temperature of the water increased slowly. This was recorded during each trial to account for any discrepancies.

The density of the resin came out to be $1.296 \pm 0.043\, g/cm^3$.

When the resin starts to cure, the polymer network undergoes cross-linking. This increases the density of the cured resin and causes the material to shrink. It is this shrinkage which causes internal stresses in the final composite material, as the fibers themselves have little to no shrinkage within the curing temperature ranges [48]. Carbon fiber, for example, has a negative coefficient of thermal expansion. Therefore, a lower amount of shrinkage is preferred in industrial applications.

Cure shrinkage is important because it can help with good surface finish of the composite. Cure shrinkage however is not to be confused with what manufacturers call mould shrinkage which is a measurement of linear shrinkage of the material. Linear shrinkage cannot be calculated directly and some assumptions have to be made like isotropic contraction and plane strain condition.

BADGE-DDS and VDE-DDS based epoxy resins were tested for cure shrinkage.

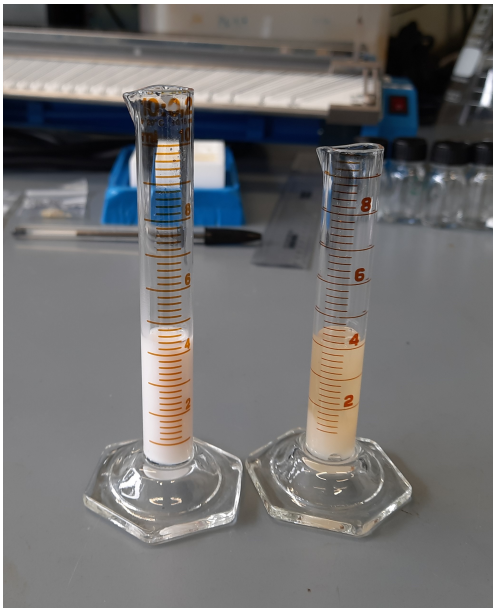

Figure 3.23: Cure Shrinkage Measurement (Left Cylinder for BADGE-DDS and Right for VDE-DDS)

Table 3.8: Samples of Uncured Resin for Density

Sample	Mass of Resin (g)	Volume (ml)
BADGE	4.8127	4.15
VDE	4.8206	4.02

With this information, the uncured resin density can be calculated. For BADGE-DDS the density comes out to be $1.15\, g/cm^3$ and for VDE-DDS it comes out to be $1.17\, g/cm^3$. As calculated earlier the density of cured VDE-DDS is $1.296\, g/cm^3$ and for BADGE-DDS it is $1.217\, g/cm^3$ [23]. Thus, the cure shrinkage can be calculated as:

$$Shrinkage = \frac{V_{cured} - V_{uncured}}{V_{uncured}} \tag{3.12}$$

Volume can be represented by mass and density and since the mass of the sample remains the same it would be cancelled out leaving just the density, so the following formula is applied:

$$Shrinkage = \frac{\rho_{uncured}}{\rho_{cured}} - 1 \tag{3.13}$$

Shrinkage for BADGE-DDS came out to be 5.5% and for VDE-DDS it was 7.04%.

4

Resin Mechanical Characterization

It is important to know the resin behaviour on a macro scale. The bulk properties of the resin system helps in understanding its usage in composites. To accurately evaluate the mechanical properties of the resin, its tensile strength, flexural strength, and fracture toughness were measured following ASTM D638, ASTM D790 and ASTM D5045 respectively. These would be used as a benchmark to compare against other epoxy resins currently used in aerospace applications. Given the thermal and physical characteristics of the resin system, it was expected that the resin would give comparable properties, if not better.

4.1. Tensile Strength

To find important parameters such as tensile strength and tensile modulus, tensile tests were carried out. Samples were created according to the type 5 specimen given in ASTM D638- ”Standard Test Method for Tensile Properties of Plastics” [49] on the Zwick Roell UTM 10kN machine. Due to previous experience with a similar resin [23], the specimens were first tested with a 1kN load cell to identify whether its failure load would be below that value to get more accurate readings for the failure load. The pre-test revealed that the loads were higher, but by a small amount, therefore a 10kN load cell was used.

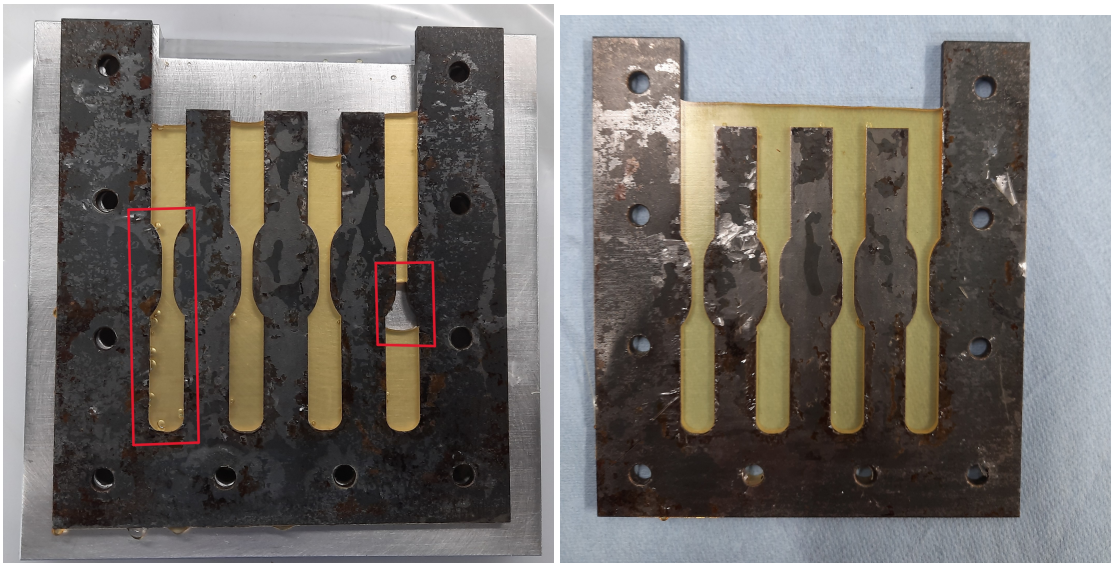

Figure 4.1: Tensile Specimens Produced with Defects (marked in red) and Good Samples

Initial moulding of the specimens introduced problems like air bubbles and complete gaps in the specimens produced as shown in Figure 4.1. The problem was identified to be lack of degassing and something known in injection moulding as the Venturi effect [50], which occurs due to different flow rates occurring inside the mould. To solve the air bubbles, it was simply decided to degas the resin for longer in the speed mixer. However the venturi effect could not be completely mitigated due to the shape of the mould and the

specimens themselves. Some techniques which help to force the air out of the mould is to have a better design with more air vents. Another is to pour the resin in parts and shaking the mould to let the air out. This process gave good results as can be seen in Figure 4.1.

Table 4.1: Specimen Dimensions

Specimen Number	Section Width (mm)	Section thickness (mm)
1	3.22	3.90
2	3.32	3.89
3	3.18	3.90
4	3.19	3.91
5	3.15	3.89

The dimensions of the specimen are given in Table 4.1. A crosshead rate of 1 mm/,min was used as defined in the standard. A total of six specimens were produced however one of them broke from the clamps while testing and was hence not included in the calculations. Accurate strain data was not measured due to a gauge region smaller than what could be measured by the extensometers. Since, the slope of the graph would remain the same, the tensile modulus of the material was calculated using the grip-to-grip separation of the machine. The specimens were held in the grips using hydraulic clamps to prevent slippage. Figure 4.2 shows the manufactured tensile specimens and the specimens being tested.

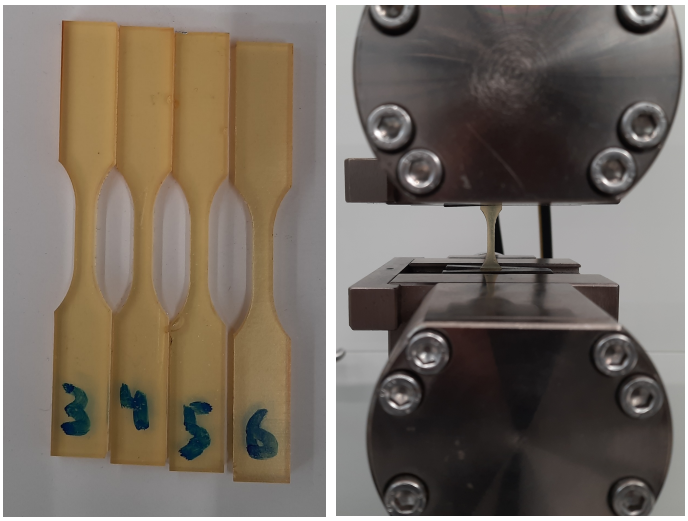

Figure 4.2: Tensile Specimens and Specimen Being Tested

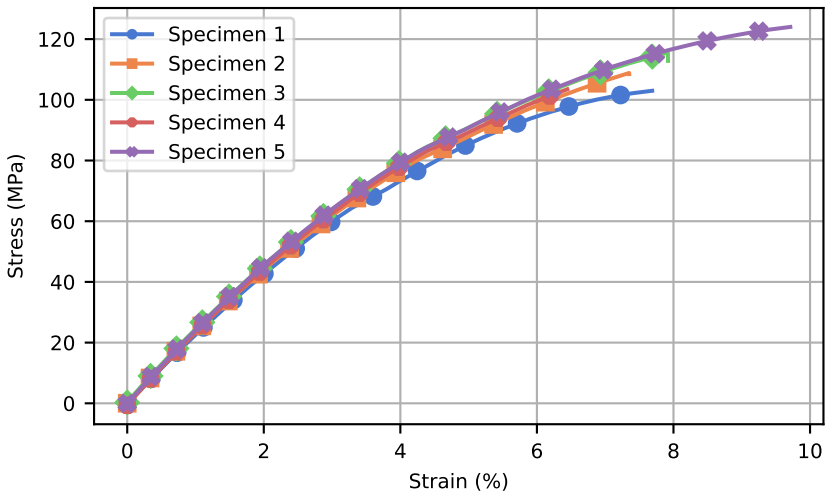

Figure 4.3: Tensile Stress-Strain Curve Obtained

The stress-strain curves shown in Figure 4.3 show typical behaviour observed in thermoset plastics. The initial region is linear in nature, which was used to calculate the tensile modulus. The specimens show uniform behaviour indicating that their manufacturing and testing conditions remained similar. After the initial linear-elastic region it can be observed that the material undergoes more deformation. This indicates that the material is not brittle.

The tensile stress was calculated by dividing the maximum load sustained by the specimen by its area in the gauge region. The tensile strength came out to be 110.978 ± 7.94 MPa. The tensile modulus was calculated to be 2.12 ± 0.058 GPa. A previous study measured the tensile modulus of BADGE-DDS to be 1.29 GPa [23] for comparison. Further discussion is given in Section 7.2.

4.2. Flexural Strength

Another important characteristic of a resin is its bending properties. The most common way to test this is the three-point bending test where the specimen is supported on two ends while a force is applied on from the top similar to DMA as discussed in Section 3.3. This maximum force sustained by the material gives its flexural strength and its elastic resistance to deformation gives its flexural modulus. ASTM D790-"Standard Test Method for Flexural Properties of Unreinforced and Reinforced Plastics and Electrical Insulating Materials" [51] was followed for the specimen dimensions and loading rate. The support span was chosen as eight times the width. Given that on average the width of the samples was around 4 mm the support span was chosen as 64 mm. The radii was the loading nose and supports was taken as 5 mm as mentioned in the standard.

Table 4.2: Specimen Dimensions for Three-Point Bending

Specimen Number	Specimen Width (mm)	Specimen Thickness (mm)
1	10.10	3.95
2	10.15	3.95
3	10.16	3.94
4	10.08	3.96
5	10.20	3.98

Using a mould piece, a sheet of resin was created which was then cut into the required specimen dimensions using a Secotom-60 cutting machine. The specimens are shown in Figure 4.4 and their dimensions are given in Table 4.2.

Figure 4.4: Specimens Created for Three-Point Bending Test

The rate of crosshead motion is given through Equation 4.1 where R is the rate of crosshead motion (mm/min), L is support span (mm), d is the depth of beam (mm) and Z is a constant which is equal to 0.01.

$$R = \frac{ZL^2}{6d} \tag{4.1}$$

Solving the equation for the specimen dimensions gives a crossshead speed of 1.7 mm/min. An interesting observation during testing was that the specimens were not breaking within the strain limit of 5% given in the standard. The maximum deflection allowed is given by Equation 4.2 where D is the midspan deflection (mm), r is the strain (which is equal to 0.05 mm/mm in this case), L is the support span (mm) and d is the depth of the specimen (mm).

$$D = \frac{rL^2}{6d} \tag{4.2}$$

Solving for this, the maximum deflection came out to be 8.53 mm. However, the specimens were routinely having a midpsan deflection greater than this value without breakage. It was ultimately decided to test the samples until they broke since it wouldn't have any effect on the calculation of the flexural modulus or the strength.

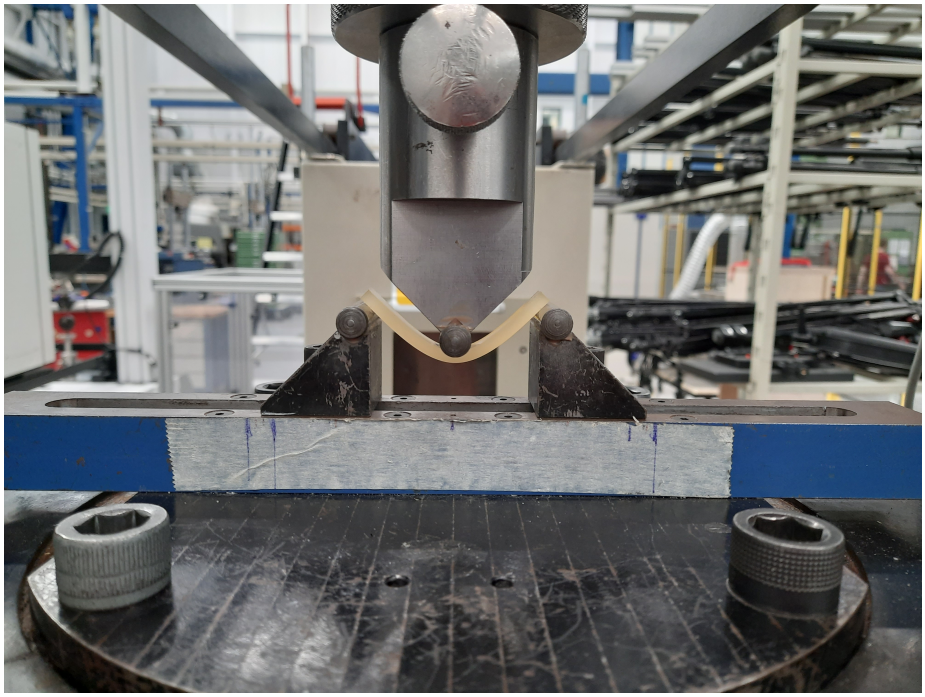

Figure 4.5: Three Point Bending Test in Action

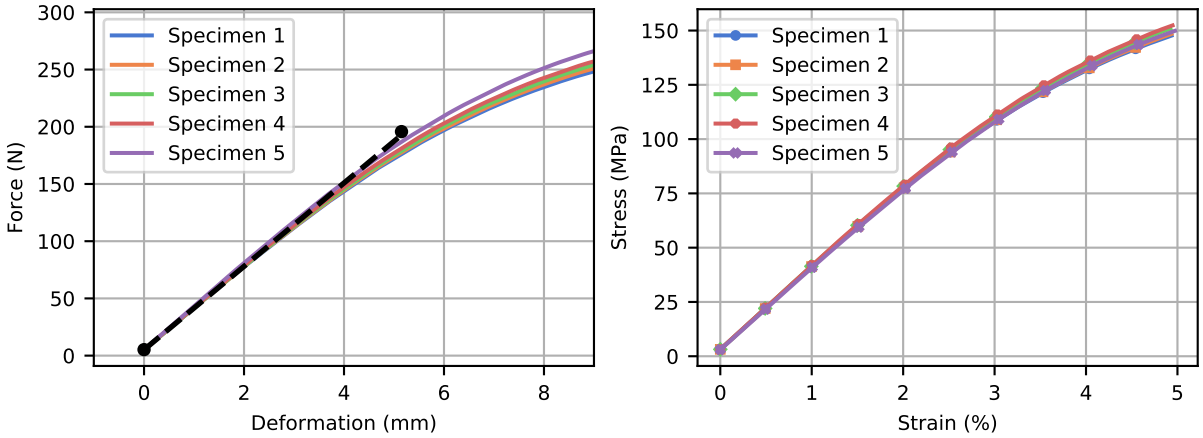

Figure 4.6: Load Deflection and Stress Strain for 3-Point Bending Test

The calculation of flexural stress is done through Equation 4.3 where σ is the stress in outer fibers at midpoint (MPa), P is the load at a given point on the load-deflection curve (N), L is the support span (mm), b is the width of the specimen (mm) and d is the depth of the specimen (mm). The flexural modulus is calculated through Equation 4.4 where E is the flexural modulus and m is the slope of the tangent to the initial portion in the load-deflection curve as shown in Figure 4.6.

$$\sigma_f = \frac{3PL}{2bd^2} \tag{4.3}$$

$$E = \frac{L^3 m}{4bd^3} \tag{4.4}$$

The flexural strength came out to be 165.289 ± 3.32 MPa and the flexural modulus is 3.84 ± 0.02 GPa. These values were quite high as will be discussed in Section 7.2. For example, a study focusing on an

epoxy and hardener combination of BADGE and DDM reported flexural strength of 120 MPa and modulus as 2.4 GPa [52].

The testing procedure was considered unusual because none of the samples broke before the midspan deflection limit defined by the standard. Generally, epoxy resins are brittle in nature. Therefore, it was decided to run a dynamic DSC test on the specimens to check that partial curing was not the cause of this increased flexibility. Another sample from the tensile specimens batch was taken to be compared with after the test was done. No difference was found between the two and there were no exothermic peaks indicating that the resin had cured. The scan was done from a temperature of -50° C till 250° C.

4.3. Fracture Toughness

An important characteristic of a resin is its fracture toughness which is its ability to resist crack growth. Epoxy thermosets are have little resistance to crack growth which makes them brittle. This is particularly important for resins being developed to be used in composites since a lot of failure modes in composites start out as cracks within the matrix. Recent developments have gone into using different fillers to act as toughening mechanisms for epoxy resins but generally resulting in decrease in mechanical and thermal properties [53]. Studies haven't found a direct correlations between other properties like the glass transition temperature or fragility with fracture toughness [54]. In commercial usage, neat epoxies are rarely used and are often mixed other energy dissipating materials like rubbers or thermoplastics [55]. Another way is to include inorganic fillers which can improve the mechanical strength as well as the fracture toughness. For the purposes of this project, neat epoxy resin was tested to understand its baseline behaviour as adding different fillers would skew the results and would make it difficult to make comparisons.

The critical stress-intensity factor (K_{IC}) of the plastic material is characterized through the test method ASTM D5045- "Standard Test Methods for Plane-Strain Fracture Toughness and Strain Energy Release Rate of Plastic Materials" [56]. The geometry used for this project was the single edge notch bending (SENB).

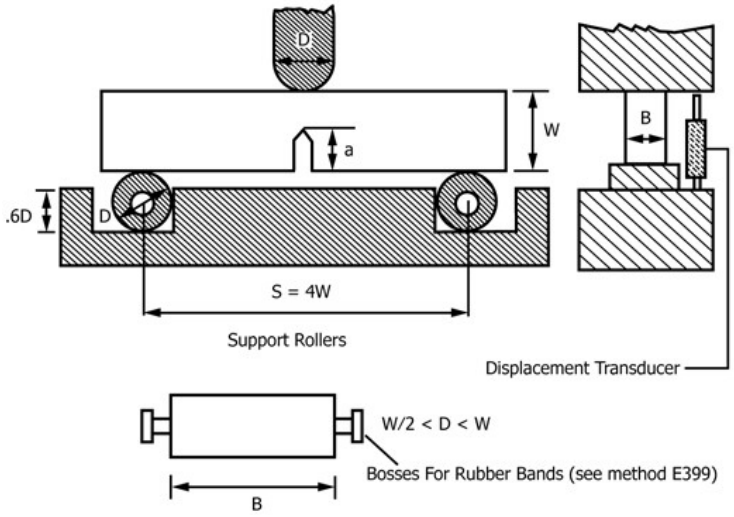

Figure 4.7: SENB Testing Schematic [56]

A plate was manufactured with the same mould used for three-point bending specimens which gave a thickness of about 4 mm. Then using a Secotom-60 cutting machine specimens were cut into dimensions of length near-about 34 mm and width 8 mm. ASTM D5045 mentions the support span to be equal to four times the width of the specimen and given that the specimen width was close to 8 mm it was decided to keep it constant for all samples at 32 mm so as to not change the testing setup too much which might interfere with the results. The diameter of the support roller and the indenter was 6 mm. The crosshead rate was given as 10 mm/min.

As shown in Figure 4.7, the testing apparatus is similar to the three-point bending setup. The main difference lies in the specimen preparation. The samples are supposed to have an initial notch created

in the center which is usually done through a razor blade. A pre-crack is then initiated within this notch by tapping on a fresh razor blade inside the notch. This pre-crack is supposed to be atleast two times longer than the width of the notch. The setup for creating the initial notch included a way to approximately observe how big the notch was, which was later accurately confirmed through optical microscopy using a Keyence VR 5000 digital microscope. Following this the cracks were initiated through the process of tapping razor blades. The cracks were then observed through the microscope as well and their dimensions were noted down as shown in Figure 4.8.

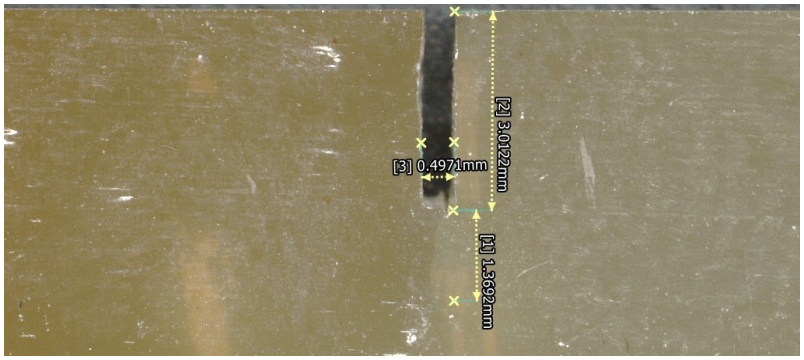

Figure 4.8: SENB Specimen with Crack Dimensions Observed Through Microscope

Sample Number	Thickness (mm)	Width (mm)	Length (mm)	Notch Dimensions (mm)			
	B	W	L	a	w	A	δa
1	3.94	8.34	33.90	4.38	0.49	3.01	1.36
2	3.96	8.37	33.60	3.83	0.54	2.34	1.49
3	3.94	9.30	33.99	4.40	0.51	2.88	1.42
4	3.94	8.90	34.05	3.81	0.47	2.40	1.41
5	3.95	9.15	36.60	4.58	0.51	2.69	1.88
6	3.94	9.17	36.70	5.19	0.51	2.96	2.23

Table 4.3: Dimensions for SENB Samples

Sample preparation was difficult, however six samples with valid notch and pre-crack lengths were obtained. One criteria for correct specimen dimensions is the value of x which is defined as the ratio between a and W. It is stipulated that $0.45 \leq x \leq 0.55$. The values of x are given in Table 4.4. So, out of the total six valid specimens only four were of the correct crack size. However, all specimens were tested to observe the difference between the proper and improper specimens.

Table 4.4: Dimension Accuracy

Specimen Number	x (a/W)
1	0.52
2	0.45
3	0.47
4	0.42
5	0.50
6	0.56

The load-deflection curve of the specimens is shown in Figure 4.9. The variation in the maximum load of the different samples and their deformation can be observed quite easily. The differences in the sample size and the crack lengths are to play a part in this variation however some trends can be observed with this. A smaller crack to width ratio (x) gives a better probability of higher load before breaking, which is to be expected. Specimen 5 which has crack to width ratio closest to 0.5 has a fracture load at 42.9 N.

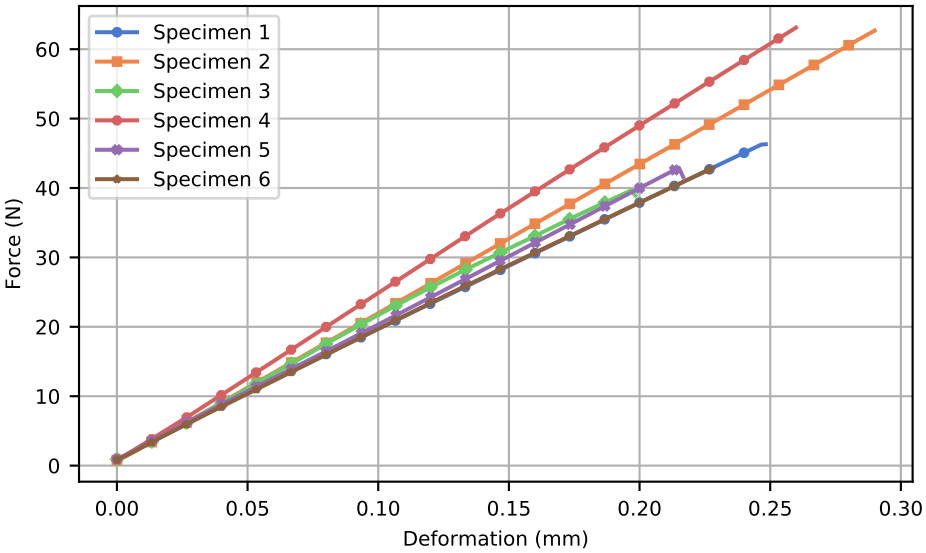

Figure 4.9: Load Displacement Curve for SENB Samples

Following this K_q can be calculated as given in Equation 4.5 where P_Q is given through a compliance curve, B and W are the dimensions of the specimen and f(x) is given in Equation 4.6.

$$K_Q = \left(\frac{P_Q}{BW^{1/2}} \right) f(x) \tag{4.5}$$

and

$$f(x) = 6x^{1/2} \left[\frac{1.99 - x(1-x)(2.15 - 3.93x + 2.7x^2)}{(1+2x)(1-x)^{3/2}} \right] \tag{4.6}$$

P_Q is calculated by creating a compliance line as shown in Figure 4.10. The trendline is similar to the actual force recorded which is pretty neat. After this another line was created which had a 5% greater compliance and both were plotted together. The standard mentions that if the it lies in between the two lines then P_Q can be taken as P_{max}. Since this is the case, P_Q for this particular specimen was taken as 42 N.

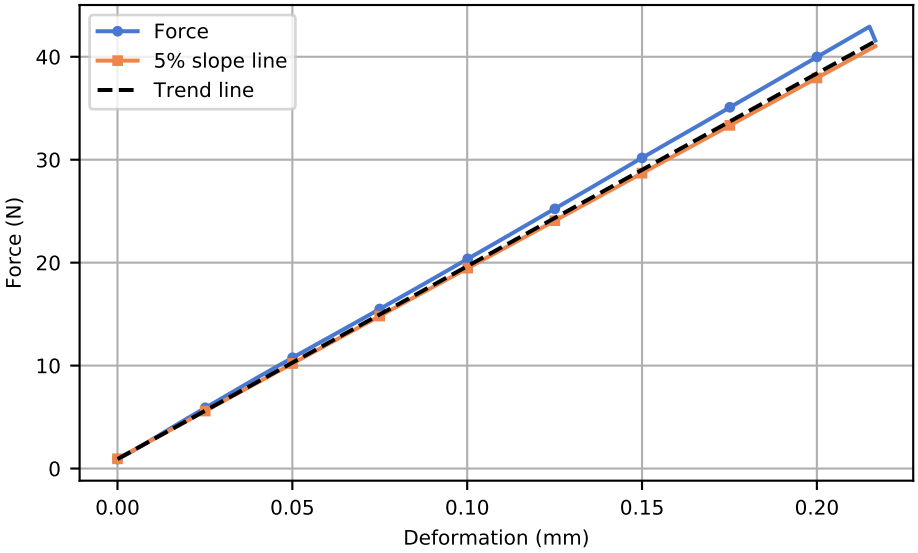

Figure 4.10: Compliance Line for K_{IC}

K_Q was then calculated for all specimens and is reported in Table 4.5.

The validity criteria is given by Equation 4.7 where B is the specimen thickness, a is the total crack length and the term (W-a) represents the ligament of the specimen. The right-hand side of the equation contains the calculated K_Q value and σ_y which is the yield stress, as was calculated in Section 4.1 which was 110.67 MPa. If these values are greater than the term on the right side then the test is considered to be valid and the corresponding K_q can be considered equal to K_{IC}. The table below shows the values.

$$B,\ a,\ (W-a) \geq 2.5 \left(\frac{K_Q}{\sigma_y}\right)^2 \tag{4.7}$$

Table 4.5: K_Q and Validity Criterion for SENB Test

Specimen Number	B ($\times 10^{-3}\, m$)	a ($\times 10^{-3}\, m$)	W-a ($\times 10^{-3}\, m$)	K_Q ($MPa \cdot m^{1/2}$)	$2.5\,(K_Q/\sigma_y)^2$ ($\times 10^{-3}\, m$)
1	3.94	4.38	3.95	1.48	0.44
2	3.96	3.83	4.53	1.62	0.53
3	3.94	4.40	4.89	1.02	0.21
4	3.94	3.81	5.08	1.45	0.43
5	3.95	4.58	4.56	1.21	0.29
6	3.94	5.19	3.97	1.51	0.46

Excluding the samples which didn't follow the correct crack dimensions, K_Q can be considered equal to K_{IC} which is the critical stress intensity factor. The mean K_{IC} value comes out to be $1.33 \pm 0.23\, MPa \cdot m^{1/2}$.

5

Composite Manufacturing

As mentioned in Chapter 2, bio-based epoxy systems are rarely characterized in their composite usage leaving significant gaps in terms of their applicability. Issues arise with composite manufacturing due to the resin's high viscosity at room temperatures or high reactivity causing very small working times.

For VDE-DDS, different methods were tested to understand the quality of the composite plate produced for further specimen testing using different manufacturing methods. As discussed in Section 3.8, since the resin has high viscosity at room temperature, it would be suitable for a manufacturing process like RTM which allows the resin to spread amongst the fibers more evenly. An alternative could be to add reactive diluents to it so that viscosity decreases, at the cost of decreased mechanical properties, however this was beyond the scope of the project and a fair comparison would not be made. Since the facilities available during the project duration weren't adequate for RTM, it was decided to perform hand layup and cure under a vacuum to optimize the dwell cycle for curing the composite, allowing the resin to infuse with the fibers then apply that cycle in an autoclave to reduce void content.

5.1. Vacuum Bagging and Oven Curing

Hand layup with vacuum bagging is considered to be the easiest in terms of manufacturing since it can be done by hand and simple tools, however it produces defects in the composite including bad surface finish, high void content and ultimately not allowing any control over the fibre volume content in the composite.

An optimum method for the layup procedure is to have each layers' calculated resin amount already in separate containers. After each layer is laid-up the amount of resin for that particular layer can be put on the fibres and spread with a brush. A general rule of thumb in composite manufacturing is to use 50:50 mass ratio for fibre and resin. So, for example, having a carbon fiber sheet of 200 gsm would mean that a square meter area of carbon fibre would weigh 200 g. Using the 50:50 ratio, it would require 200 g of resin. So for a plate with a size of $250 \times 250\,mm$ would weigh around 12.5 g for one layer. If the total number of layers is ten then the amount of resin needed would equal around 125 g. Adding equal amount of resin should be enough for the process. Using this mass ratio, the theoretical fiber volume fraction can also be predicted given the density of the resin. This would come out to be around 42% but since some of the resin would be left over and squeezed out during the layup and curing process it can be assumed that the actual volume fraction would be higher given that there are less number of voids produced. Ideal value of fiber volume fraction in a composite is considered to be 60%.

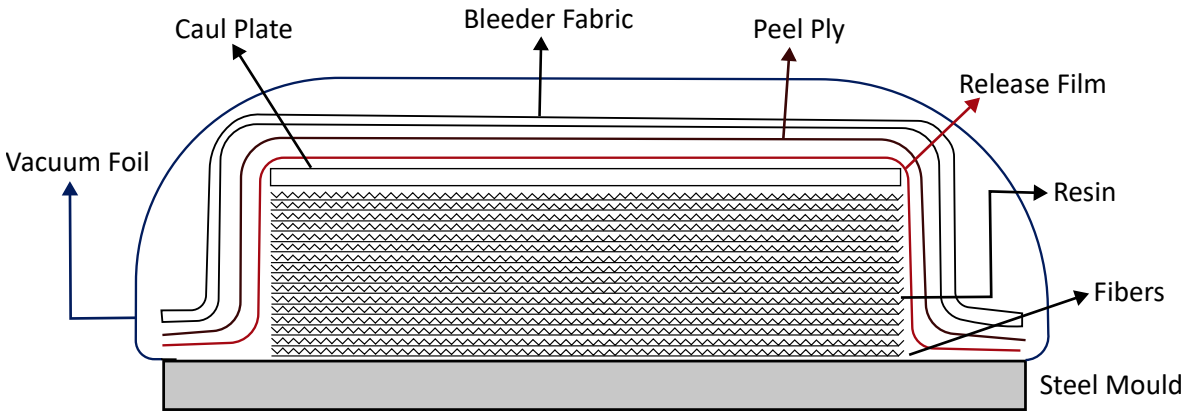

Figure 5.1: Annotated Schematic of Composite Mould

The layup schematic is shown in Figure 5.1. The MCTechnics Nylon WL8400 vacuum foil was used because of its temperature resistance upto 232° C. Airtech Nylon Stitch ply Econostitch suplied by MCTechnics was used which had a ceiling temperature of 232° C. The polyester Airweave N10 breather fabric was used as bleeder fabric to absorb all the excess resin. An unperforated release film A400 made of FEP (fluorinated ethylene propylene) supplied by MCTechnics was used given its application temperature going up to 260° C. Difference in the use of perforated and unperforated release film was also checked and found to be negligible.

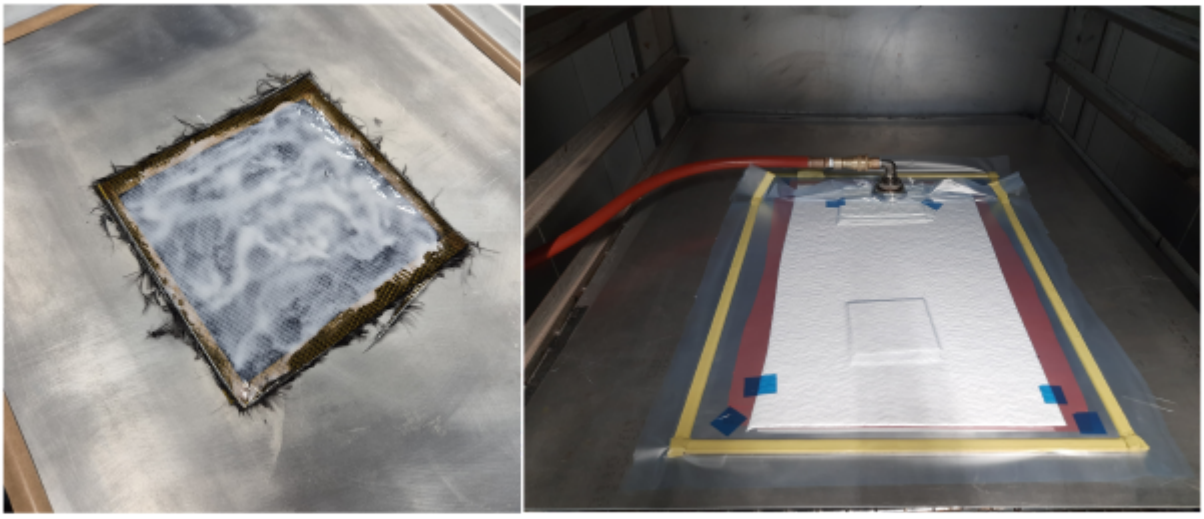

Figure 5.2: (Left) Lay-up Procedure and (Right) Mould with Vacuum Bag Inside Oven

Most of the trials with the manufacturing were conducted with BADGE-DDS instead of VDE-DDS for two reasons. Firstly, for comparison purposes, the mechanical properties of the composite made of VDE-DDS had to be compared with an existing product which was BADGE-DDS. Hence the composite of BADGE-DDS would have to be made anyways and since it has a higher viscosity, as was discussed in Section 3.8, its manufacturing parameters would translate well into the parameters for VDE-DDS. The second reason was the high cost of VDE monomer which meant that no room for trials existed and only the final test specimens could be manufactured with it. Only a small composite plate of VDE-DDS was manufactured initially using the basic cure cycle to understand its quality and to start experimenting with the dwell temperatures.

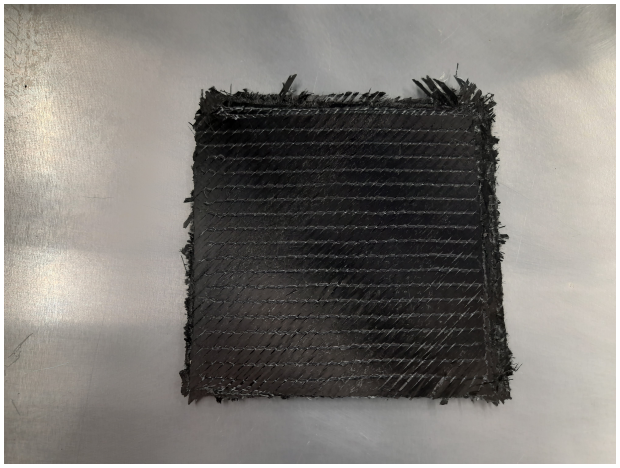

Figure 5.3: Initial VDE-DDS Plate

Figure 5.3 shows the first composite plate made out of VDE-DDS. The surface finish was reasonable and it had no visible dry spots on the surface. Upon examining the cross-section under a microscope (Figure 5.4) it could be seen that the composite had a lot of voids, some having a span of more than 1 mm. During testing these would be the stress concentration regions and the composite would fail because of the voids and not due to the material, making the comparisons ineffectual between the two materials.

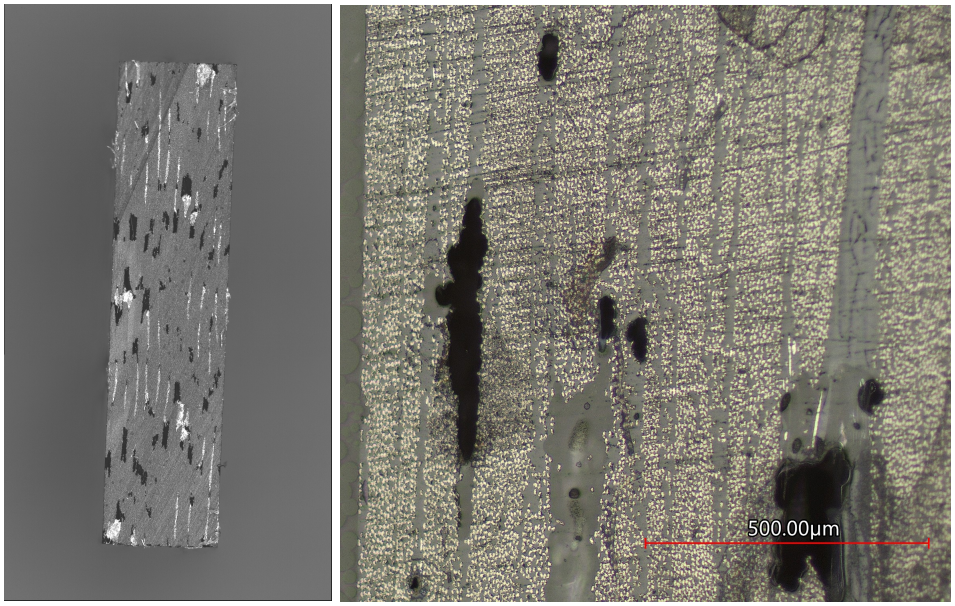

Figure 5.4: (Left) Stitched and (Right) Close-up of Cross-Section Under Microscope

Using ImageJ software's void content macro, a quantitative estimation was made on the void content of the panel. Using three different images captured at different magnifications the average void area was calculated and divided by the total surface area of the specimen. The average void content came out to be 16%, which is considered to be very high and the composite unusable. It was noticed that some regions had more voids compared to others which meant that the resin had not adequately infused with the fibers during the layup process. This would be the focal point during the optimization process since the autoclave would remove most of the voids due to its high-pressure environment. Further manufacturing optimization was done on composites with BADGE-DDS.

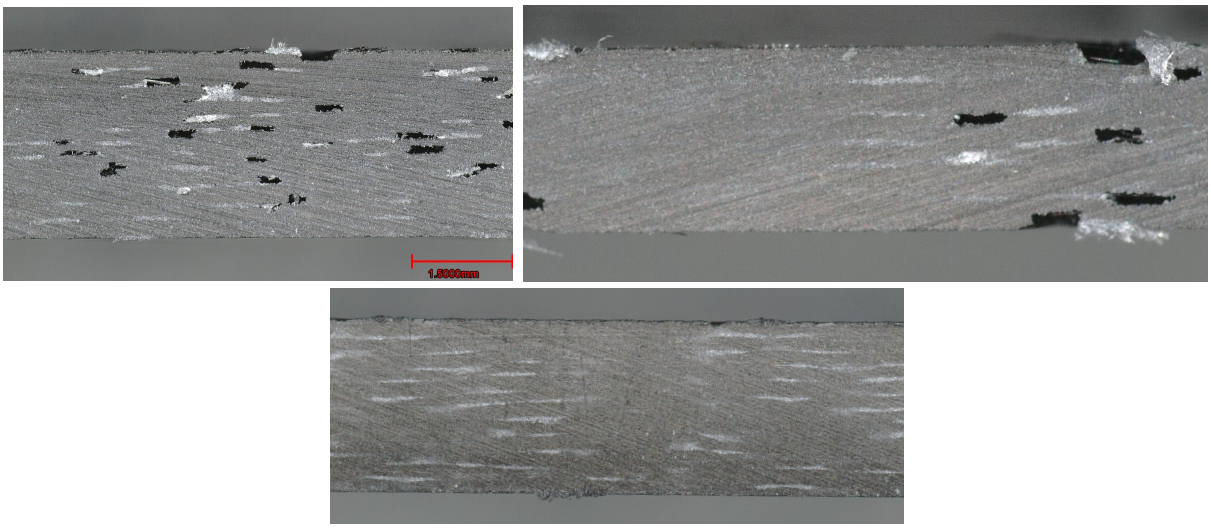

Figure 5.5: (Clockwise from Top Left) Initial Dwell Cycle, Optimized Dwell Cycle and Autoclave Composite Cross-Section Under Microscope

Different dwell cycles affected the number of voids in the final composite. The aim of introducing a lower temperature dwell cycle was mainly to reduce dry spots within the composite. The void content was qualitatively checked by optical microscopy and quantitatively with the resin burn-off test, which is discussed in Section 5.2.1. An initial dwell at 70° C was done at a vacuum before the curing cycle started, cross-section of which is seen Figure 5.5 (top-left). It was hypothesized that this would reduce dry spots because under pressure the excess resin would be squeezed out of the laminate. The temperature was selected based on rheology data collected earlier, 70° C being the point where both BADGE-DDS and VDE-DDS had low enough viscosities to flow easily. It was also before the point where the resin system would start to cure as was shown in Figure 3.3.

This did give better results compared to the initial composite made of VDE-DDS, however optically the voids could be seen to be in large numbers. The voids were also sporadically spread throughout the laminate, creating some sections with less and others with more voids. This cycle was further improved by creating an initial dwell at 70° C without any vacuum and then turning on the vacuum after half an hour and then starting with the cure cycle. This would ensure that the resin reached a temperature where it had a lower viscosity so it would infuse better with the fibers and wet them out completely. After this, like the previous method, the excess resin would be squeezed out under the vacuum. This did provide a better laminate in terms of quality and its cross-section is shown in Figure 5.5 (top-right). Considering the project's timeline, more focus was not given to optimization of this cycle further and it was decided to translate these dwell cycles into the autoclave curing cycle. The final autoclave part's discussion is given in Section 5.2, its microscope cross-section is given in Figure 5.5 (bottom), showing no macro-voids. This quality was considered to be suitable for testing.

5.1.1. Composite Plate Dimensions

The final plates manufactured were of size 450×450 mm. The plate was made such that three types of test specimens could be extracted from it namely, ILSS (Inter-laminar shear stress), IPSS (In-plane shear stress) and compression testing samples. The decision to make a single plate was based on the fact that it was being manufactured using hand layup, so to reduce variability on the quality of the laminates produced, it was decided to manufacture it in one go. Various tries as mentioned before helped in understanding the parameters for the cure cycle of the two different resins. Unfortunately, since both cured at different temperatures they couldn't be put in the autoclave at the same time, which would have reduced the variability even more.

12 plies of biaxial non-crimp carbon fibre was used. The fabric itself was stitched using polyester 83 dtex. The areal weight of the fabric was 200 g/m^2. The fibres themselves were the AKSACA A42 1600 tex (24k) carbon fibres with a density of 1.78 g/m^3. The tensile strength of the fibres was 4200 MPa and the

tensile modulus was 240 GPa [57]. The layup was done based on the ASTM standards for each of the tests. The final layup was $[\pm 45]_{6S}$. This was achieved through keeping the final six layers at an angle of 90°. However, for the impact strength, the same layup procedure could not be followed because that required a higher thickness and some [0/90] layers mixed in between. To achieve this configuration, the fibres themselves were cut at a 45° angle to get a [0/90] layer and placed in between the normal [+45/-45] layers. The final layup for the impact strength plates was $[(\pm 45)(0/90)]_{10S}$. A minimal thickness of 5 mm is required by the standard. However that couldn't be achieved due to limited availability and high cost of VDE monomer. Therefore, it was decided that a good balance to still perform the test would be to do it with 20 plies instead. Another criteria mentioned in the standard is to test five different specimens however due to the time constraints of the project, only three were tested for each resin system and compared.

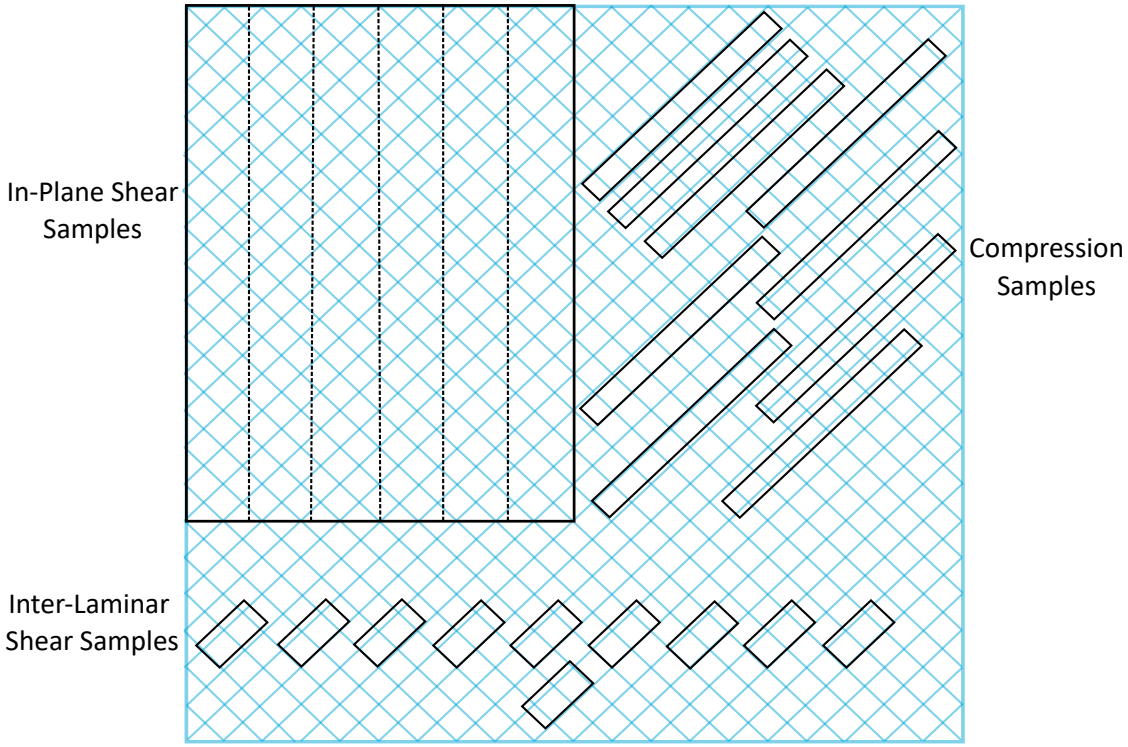

Figure 5.6: Schematic of Composite Plate

5.2. Autoclave Curing

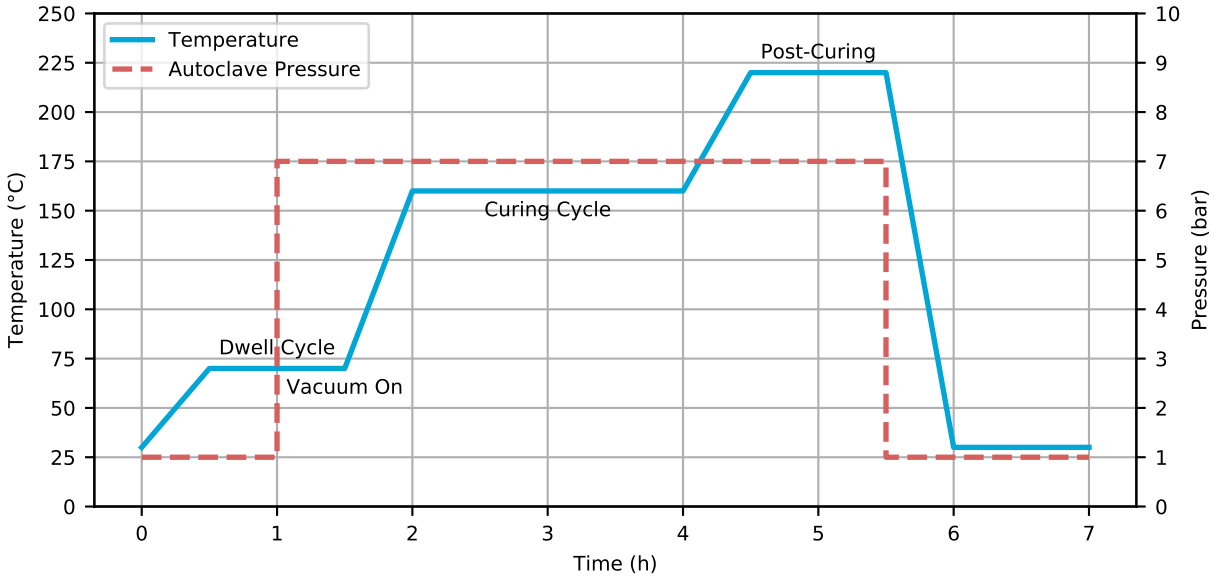

Figure 5.7: Final Cure Cycle in Autoclave

Using the autoclave is expensive and resource intensive which is why it wasn't the preferred method to start with. However, due to the high void content associated with vacuum bagging, it was decided to move forward with the autoclave. Hand layup process was followed to spread the resin on the fibers. A pressure of 7 bar was selected inside the autoclave. The dwell cycle discussed earlier was initiated followed by the curing cycle as shown in Figure 5.7.

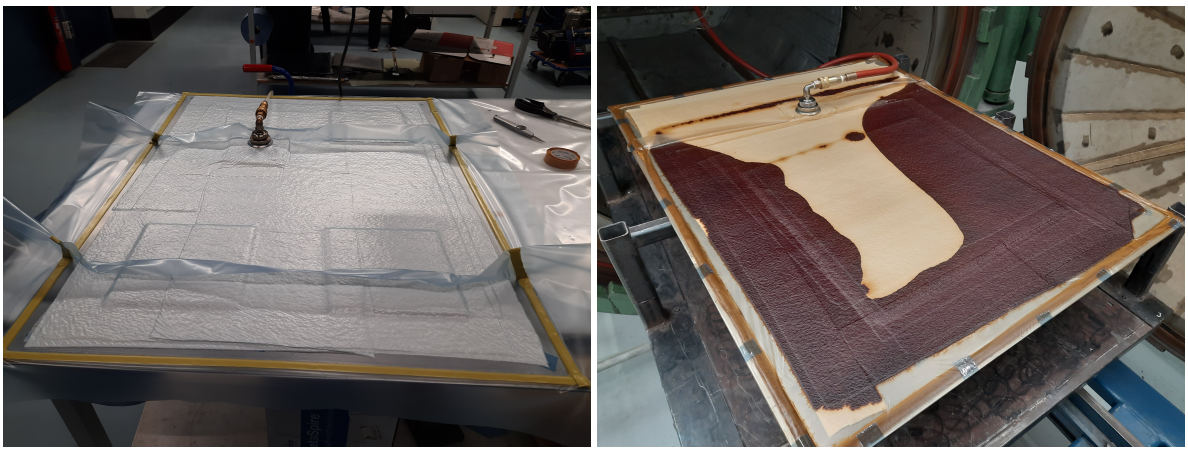

Figure 5.8: (Left) Layup on Mould Before and (Right) After Curing in Autoclave

Figure 5.8 shows the mould with the layup prepared to be put inside the autoclave for the impact plates and the single plate for the other tests after curing. The resin movement can be seen through the second image, which seems to be uniform in all directions implying a homogeneous lamination of the fibres. The vacuum hose was kept as far away from the plate as possible since there was a possibility that resin could deposit inside and cure under the high temperatures. The plates for the impact test represented a challenge because three were being cured on a single mould and keeping the vacuum hose at the same distance from each plate was difficult. The resin movement also had to be taken into account for this.

5.2.1. Laminate Quality

Laminate quality was tested following ASTM D3171-22 "Standard Test Methods for Constituent Content of Composite Materials" [58]. Quality testing was done for composites made from each iteration of the dwell cycle optimization. Square and rectangle samples were cut out from each composite plate from different areas (Figure 5.9) and had their weight and density measured as described in Section 3.10. Following this, they were put in crucibles and placed in a muffle furnace. The furnace was allowed to ramp up to a temperature of 595° C and stabilizing there for 20 minutes. Following this the furnace cooled down and only the fibers remained in the crucible. The weight of the fibers was measured which allowed to calculate the weight of the resin. Dividing the weight by the density of its respective components gave the volume and adding both volumes and dividing each component's volume by the total volume gave the volume fraction as shown in Table 5.1.

Figure 5.9: Composite Specimens Ready to be Put in Furnace

Fibre density was taken to be $1.78\ g/cm^3$ [57], the density of BADGE-DDS was known to be $1.21\ g/cm^3$ along with VDE-DDS being $1.29\ g/cm^3$ as discussed in Section 3.10. For each composite plate, four samples were cut and tested, the average values for each are given in Table 5.1.

Table 5.1: Constituent Volume Content for Different Cycles

Specimen	V_m (%)	V_f (%)	V_v (%)
Initial Dwell Cycle	56.28	43.22	0.49
Optimized Dwell Cycle	61.40	40.17	-1.58
Autoclave Cycle	59.83	47.48	-7.32

These results are different to the ones observed through the microscope in that the values are small and even go negative. This is usually the case when the fiber densities are incorrect. Unfortunately, there was only a singular datasheet for the fibers which meant that the constituent fractions couldn't be corrected. A clear pattern does emerge from the values and it is of decreasing void content in the composite. This validated the design of the dwell cycles and also demonstrated that the plate manufactured with the autoclave contained very little voids compared to the previous plates. Hence, samples were cut from the composite plate made in the autoclave for mechanical testing. The final manufactured plate for VDE-DDS is shown in Figure 5.10.

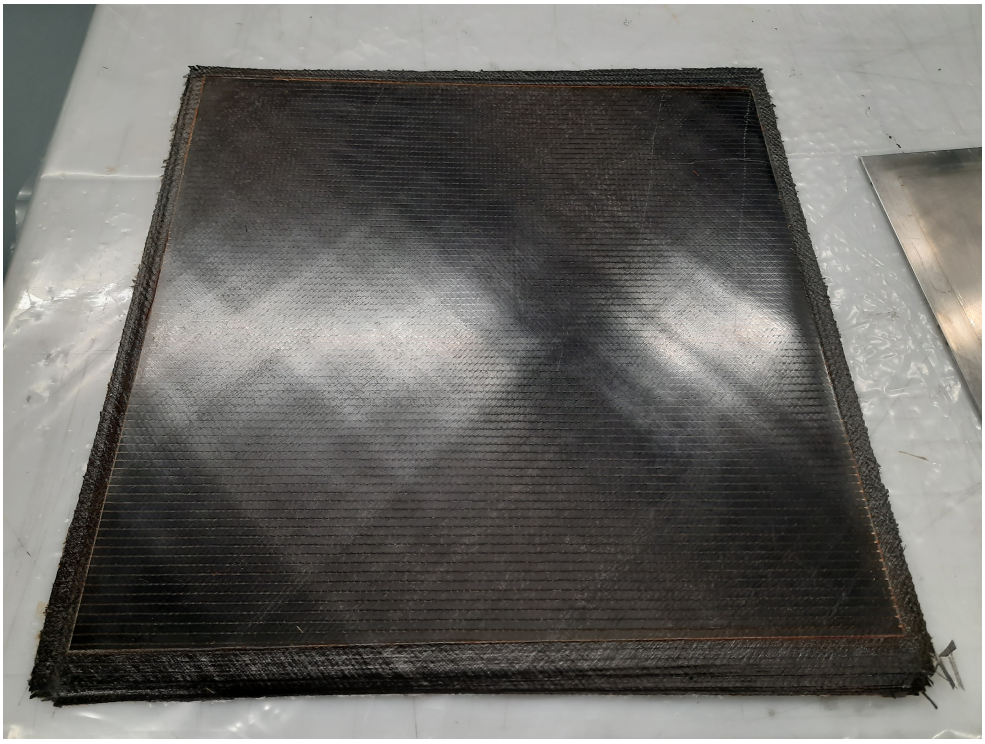

Figure 5.10: Final Plate Manufactured

6

Composite Mechanical Testing

Composite mechanical tests were selected to compare matrix-dominant behaviour for a direct comparison of VDE-DDS against BADGE-DDS. To keep the variation as limited as possible, the plates were manufactured in the same way and the samples were taken from the same plate. They, however, weren't cured together because the curing cycle for BADGE-DDS and VDE-DDS differ.

IPSS specimens were of standard tensile specimen geometry. Compression and ILSS samples were taken from the plate by cutting it at 45° angle as shown in Figure 5.6. The obtained specimens were then tested as discussed below.

6.1. IPSS Test

In-plane shear test was chosen since the in-plane shear behaviour is independent of fiber properties and depends on the matrix yield strength and interface properties [59]. Due to the large difference in the strength and stiffness properties of the fibers and the matrix, loads applied along the fiber direction tend to be linear because the loads are taken up by the fibers, while those transverse to the fiber direction are controlled by the matrix and the interface regions.

ASTM D3518- "Standard Test Method for In-Plane Shear Response of Polymer Matrix Composite Materials by Tensile Test of a $\pm 45°$ Laminate" was followed to perform the IPSS test [60]. The standard mentions the use of a symmetric laminate with dimensions of $250 \times 25\,mm$. Samples of this size were cut and tested in Zwick Roell 20 kN UTM machine. The strain on the samples was measured using an extensometer with a gauge length of 50 mm. The extensometer however could only measure the strain up until 8 kN to protect the extensometer in case the sample broke earlier. The strain values after this point were measured by the machine's grip movement. The loading rate of the specimens was around 5 mm/min. The specimen dimensions are given in Table A.1.

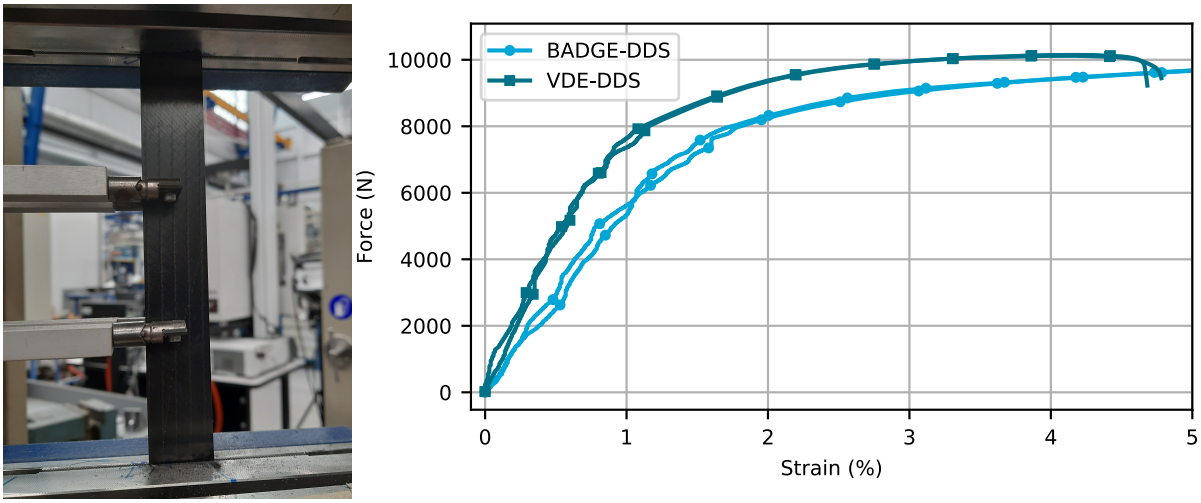

Figure 6.1: IPSS Test in Action & Load Displacement Curve for IPSS

The load-deflection curve for some of the samples is shown in Figure 6.1. It can be observed that there is an initial region of elastic deformation where the graph is linear. This is followed by a non-linear region which is when the matrix undergoes plastic deformation. This region becomes parallel to the x-axis after undergoing more strain which shows the fibers taking up the load and deforming elastically. The samples made of VDE-DDS shows a higher modulus based on the slope. An issue faced during this test was the slippage of the samples from between the grips, which was fixed by clamping the samples more tightly.

The response of the material shows that the stiffness of the composite made with VDE-DDS is higher due to its lower strain at the same force compared to BADGE. The maximum shear stress on the specimens can be given by the following equation:

$$\tau_{12}^{m} = \frac{P^{m}}{2A} \tag{6.1}$$

where, τ_{12}^{m} is the maximum in-plane shear stress, P^{m} is the maximum force applied on the specimen below 5% engineering strain and A is the cross-sectional area of the specimen.

The shear modulus is calculated using the following formula

$$G_{12}^{\text{chord}} = \frac{\Delta\tau_{12}}{\Delta\gamma_{12}} \tag{6.2}$$

where, G^{chord} is the shear modulus of elasticity, $\Delta\tau_{12}$ is the difference in shear stress between two selected points and $\Delta\gamma_{12}$ is the difference in engineering shear strain between the two points. The points selected were over a range of $2000\mu\epsilon$.

For VDE-DDS, the shear strength came out to be 85.75 ± 0.52 MPa and the shear modulus was 6.58 ± 0.68 GPa. Comparing that to BADGE-DDS, where the shear strength was 81.84 ± 4.85 MPa and the shear modulus was 5.49 ± 0.52 GPa. These results are discussed further in Section 7.3.

6.2. Compression Test

Compression testing was performed to understand the matrix' contribution in the composite in providing strength whilst under compressive loads. The most compression failure mode in studies is fiber kinking [12]. This is caused by fiber misalignment initially which leads to plastic deformation of the matrix and finally a kink band forms. In the same study it was also found that the elastic modulus of matrix has the greatest influence on the compressive strength of a composite. The primary cause of failure in compression is the plastic yield behaviour of the polymer matrix rather than fiber fracture.

The compression test was done according to ASTM D6641- "Standard Test Method for Compressive Properties of Polymer Matrix Composite Materials Using a Combined Loading Compression (CLC) Test Fixture" [61]. The samples were cut from the original plate at an angle of 45° to get samples with a layup of [0/90] as is mentioned in the standard. The specimen dimensions were $140 \times 13\,mm$ with a thickness close to 3 mm. KFG-5-120-C1-23 uni-axial strain gauges from Kyowa were used. They were attached on one side to measure the deformation along the sample in the axial direction. Nine samples were tested for each material and six of them gave accurate results. The remaining ones were not taken into consideration for the strength and modulus because their load values were too low or the strain gauges provided wrong values, possibly due to incorrect application of the same. The samples along with them in the CLC fixture are shown in Figure 6.2. The sample dimensions are provided in Table A.2.

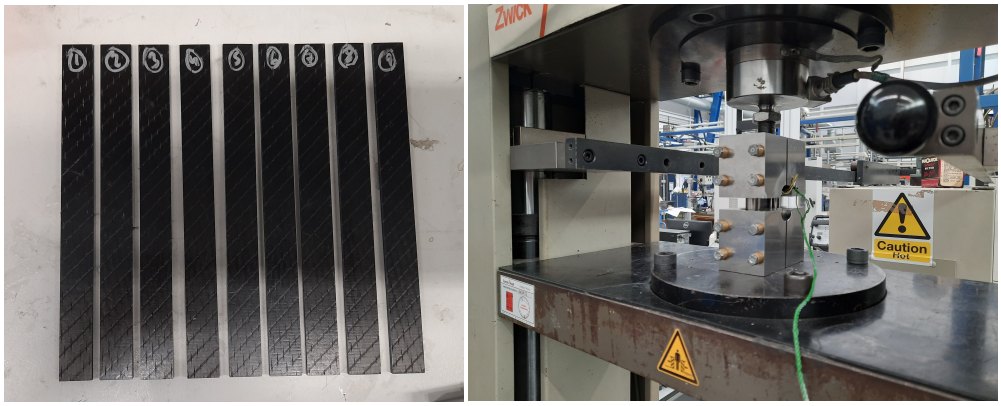

Figure 6.2: Compression Testing Samples and Fixture

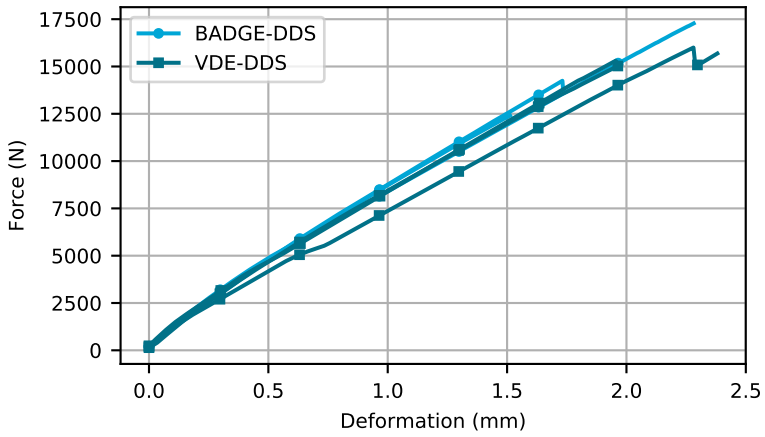

Figure 6.3: Load Deformation Graph from Compression Test for Some Samples

The load displacement curve obtained from the compression test is shown in Figure 6.3 for some of the samples. Both types of samples showed uniform behaviour and had the same amount of variation within their data. The failure occurred within the gauge section for all valid specimens.

The compressive strength of the laminate is calculated by the following equation:

$$F^{cu} = \frac{P_f}{wh} \tag{6.3}$$

where F^{cu} is the compressive strength of the sample, P_f is the maximum load on the specimen, w is the width of the specimen and h is the thickness.

The compressive modulus of the specimen can be calculated by:

$$E^c = \frac{P_2 - P_1}{(\varepsilon_{x2} - \varepsilon_{x1})wh} \tag{6.4}$$

where E^c is the compressive modulus, P_1 is the load at ε_{x1}, similarly P_2 is the load at ε_{x2}, ε_{x1} is the lower end of the strain and ε_{x2} is the upper end.

The compressive strength of BADGE-DDS came out to be 499.02 ± 40.26 MPa and the compressive modulus was 3.87 ± 0.18 GPa. For VDE-DDS the strength was 532.95 ± 36.90 MPa and the compressive modulus was 4.29 ± 0.29 GPa.

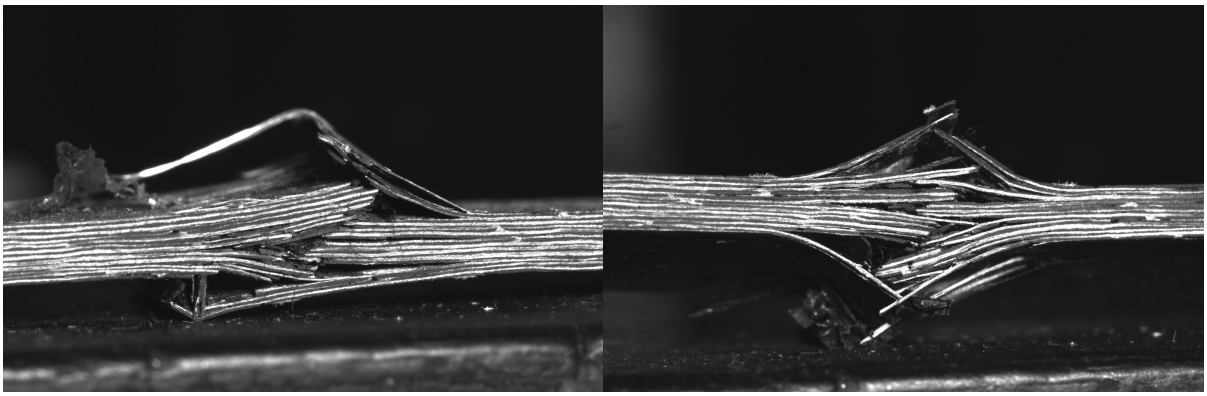

Figure 6.4: VDE-Composite Specimens Failing in Compression

Figure 6.4 shows the a close-up of the compression samples after testing. The type of failure observed here is called wedge splitting [62] and some inter-laminar failure. This is characterized by two shear fractures occurring and in-between a wedge is formed. This type of failure is given as a valid failure criteria in ASTM D6641. Figure 6.5 represents a failure type of through-the-thickness shear. This failure mode can be seen propagating through the thickness of the specimen. This is caused by fiber waviness or misalignment causing stress concentration regions. This type of failure mode is common in thinner composite structures.

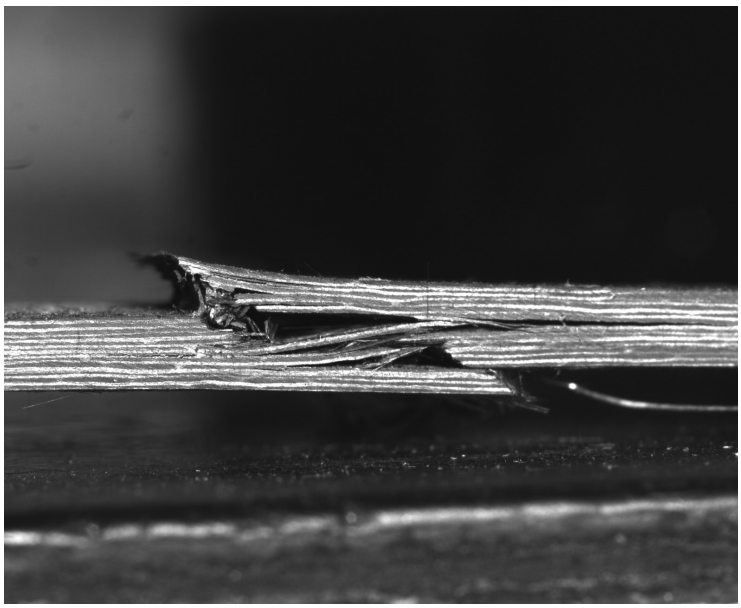

Figure 6.5: BADGE-Composite Specimens Failing in Compression

6.3. ILSS Test

The inter-laminar shear strength also known as the short-beam test was conducted on both BADGE and VDE composites to understand the behaviour of the resin with the fibers. Good adhesion of the resin with the fibers would imply a higher inter-laminar strength. As mentioned before, the role of the matrix in a composite is to hold the fibers together and transfer load to them which is characterized by a composite's inter-laminar shear strength. ASTM D2344- "Standard Test Method for Short-Beam Strength of Polymer Matrix Composite Materials and Their Laminates" was followed for this test [63]. This test is done under a three-point bending setup in which force is applied from top while the specimen is placed in between two support rollers. The specimen thickness determines the the length and width of final samples to be used for testing. Given the different thickness values of BADGE and VDE samples, a common value of 2.5 mm was taken. The length of the specimen is supposed to be six times the thickness, therefore

that was taken to be 15 mm and the width is supposed to be twice the thickness, therefore it came out to be 5 mm. The specimen dimensions are given in Table A.3. The span for the support rollers was set at 10 mm, the diameter of the rollers themselves being 3 mm. The indenter roller had a diameter of 6 mm in consultation with the standard.

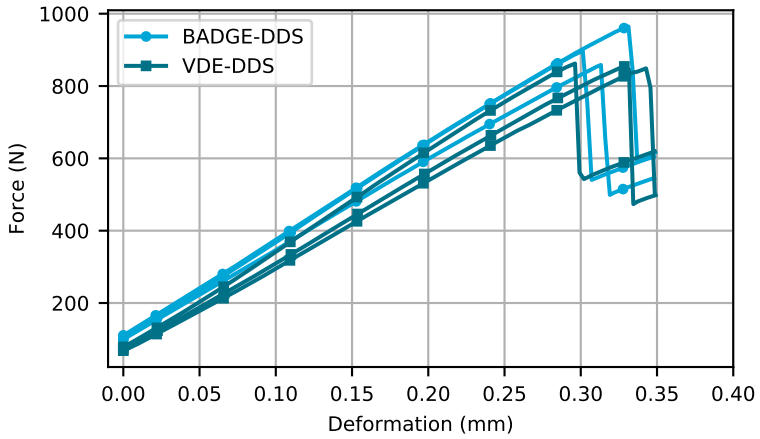

Figure 6.6: Load-Displacement Curves for ILSS Test

The above load-displacement curves were obtained and further processed for calculations. The short beam strength can be calculated using the following equation:

$$F_{sbs} = 0.75 \times \frac{P_m}{b \times h} \tag{6.5}$$

where F_{sbs} is the short-beam strength in MPa, P_m is the maximum load on the specimen in N, and b and h are the specimen width and thickness respectively.

After observing the results, a scatter amongst the data for VDE-based composite can be seen. This is unlike the previous tests where scatter amongst the BADGE-based composite was found. A possible reason for this could be the region of the plate from which the samples were cut might have had some irregularities in that particular area.

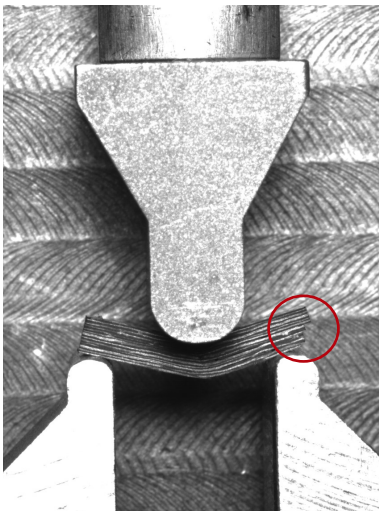

Figure 6.7: VDE-Composite Specimen with Inter-Laminar Shear

In Figure 6.7 it can be seen on the right side that the layers shift away from each other which is the expected failure mode in this test. Other failure modes can also be observed like the one in tension as shown in

Figure 6.8. The beam strength was not calculated for these samples as they wouldn't provide accurate information of the specimen strength.

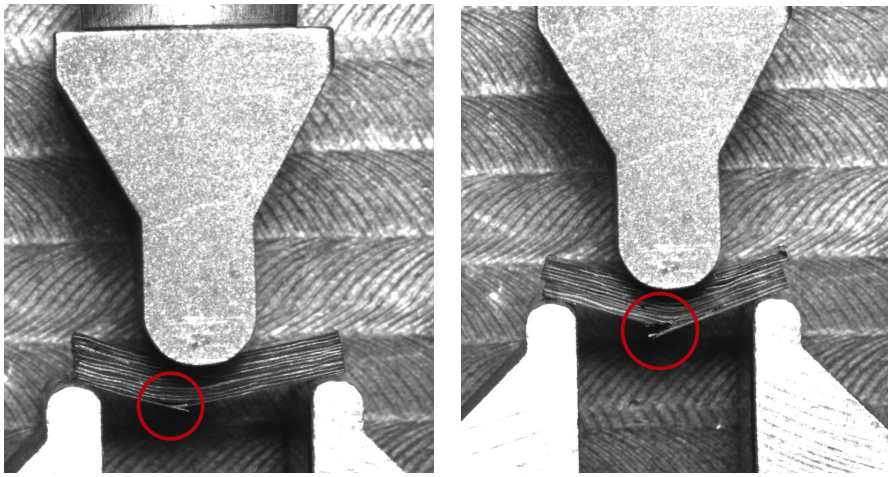

Figure 6.8: VDE-Composite Specimens Failing in Tension

The inter-laminar shear strength for VDE-DDS was calculated to be 58.17 ± 2.37 MPa and for BADGE-DDS it was 52.53 ± 3.72 MPa.

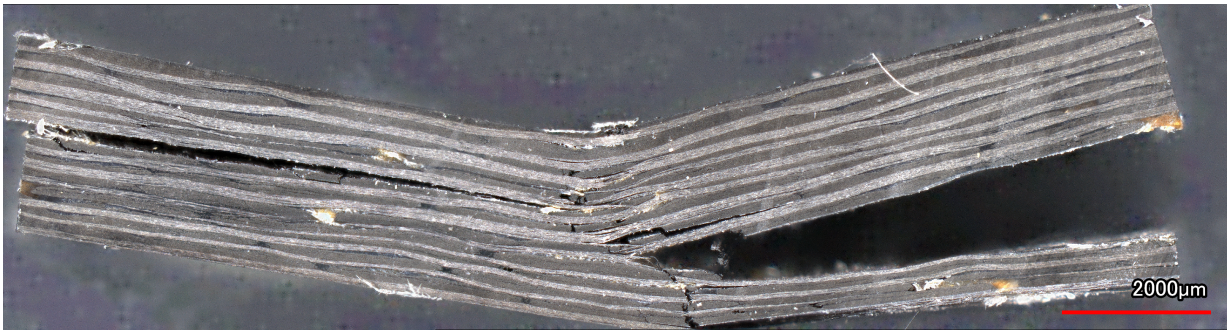

Figure 6.9: A Stitched Cross-Section of VDE-Composite Specimen After ILSS Test

Some inferences can be drawn from Figure 6.9. The first failures appeared as voids within the layers that can be seen in the center. From there the cracks propagated further along the 0° fiber layers. This was when the layers shifted with respect to each other causing the final failure of the laminate. Another crack can be seen propagated through the layers downwards from the middle across the layers, probably caused by extra loading on the specimen after failure occurred.

6.4. Impact Test

The impact test was done to understand the low-velocity impact behaviour of the composite and to compare the response of the different materials when used as a composite matrix. The standard ASTM D7136-"Standard Test Method for Measuring the Damage Resistance of a Fiber-Reinforced Polymer Matrix Composite to a Drop-Weight Impact Event" [64] was used to perform the test. A 200×200 mm plate was made, out of which the desired dimensions of $100 \times 150\,mm$ were cut and put under the impact tower to be tested. Only three samples of each material were manufactured and tested due to high cost of VDE monomer. The stacking sequence of the composite was $[(\pm 45)(0/90)]_{10S}$. The same bi-axial fibres used earlier were used in this laminate as well. For the [0/90] layers, the fibres were cut at a 45° angle. Using a high-speed camera the speed of the impactor was measured which was then used to calculate the initial velocity following which all other calculations were made. The camera's recording speed was 6400 FPS (frames per second). Out of all the tests performed in the project, the impact test is most prone

to deviations due to different testing setups and manufacturing errors. Therefore, it was tried to keep most of the conditions the same for this test for the two materials. The same testing height of 0.6 m was used for both composite panels. The nominal thickness of BADGE-DDS plate was 4.10 mm and for VDE-DDS it was 3.94 mm. Using an average thickness of 4 mm for both types of specimens and having a ratio of 6.7 J/mm for the impact energy to specimen thickness, the drop height was calculated to be 0.6 m.The impactor had a mass of 4.80 kg with a nose diameter of 16 mm.

The impact velocity was calculated frame-by-frame with the help of a scale kept in the foreground in the camera's view as shown in Figure 6.10.

Figure 6.10: Impact Test Setup with a High-Speed Camera

The theoretical impact energy from the dropped height was 26.8 J. Although all tests were conducted from the same height, the velocity of the impactor was different in most cases which meant the impact energy was also different for all but two of the specimens. This was most likely due to internal friction present in the impact tower itself which caused different amounts of loss in speed of the impactor. These values are reported in Table 6.1.

Table 6.1: Different Velocities and Impact Energies for the Specimens

Specimen Number	BADGE		VDE	
	Velocity (m/s)	Impact Energy(J)	Velocity (m/s)	Impact Energy(J)
1	3.04	22.17	2.90	20.18
2	2.66	19.98	2.66	16.98
3	2.78	18.54	2.56	15.72

Figure 6.11: (Left) Front and (Right) Back of a VDE-DDS Specimen After Impact

Figure 6.11 shows the aftermath of the impact test on one of the specimens. From the front, the damage is visibly limited to the impactor diameter. Upon observing the damage location from the back, it can seen that delamination occurred in a wider area. Not only that but the damage propagated throughout the thickness of the sample. This shows that the impact energy was quite high on the samples. A similar pattern was seen in all the tested samples.

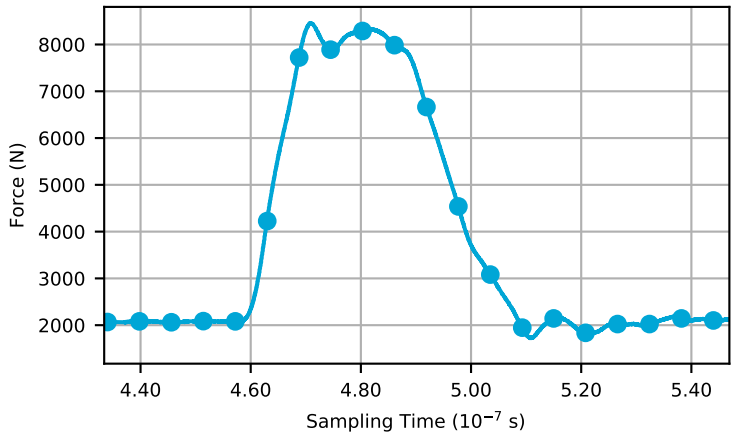

Figure 6.12: Force Plot Received from Testing

A force-time curve was obtained from the test which is shown in Figure 6.12. This was filtered and smoothed with a Savitzky-Golay filter algorithm and was arranged according to time given the sampling rate of 5 MHz. The velocity of the impactor was calculated using the equation give below:

$$v(t) = v_i + gt - \int_0^t \frac{F(t)}{m}\, dt \tag{6.6}$$

where v is the velocity at time t, V_i is the initial velocity, as reported in Table 6.1, g is acceleration due to gravity, taken here as $9.81\, m/s^2$, F is the measured contact force and m is the mass of the impactor.

The displacement of the impactor was calculated using Equation 6.7.

$$\delta(t) = \delta_i + v_i t + \frac{gt^2}{2} - \int_0^t \left(\int_0^t \frac{F(t)}{m}\, dt \right) dt \tag{6.7}$$

where δ is the impactor displacement at time t and δ_i is the displacement from reference location, taken here as zero.

The absorbed energy can be calculated by:

$$E_a(t) = \frac{m\left(v_i^2 - v(t)^2\right)}{2} + mg\,\delta(t) \tag{6.8}$$

where E_a is the absorbed energy at time t.

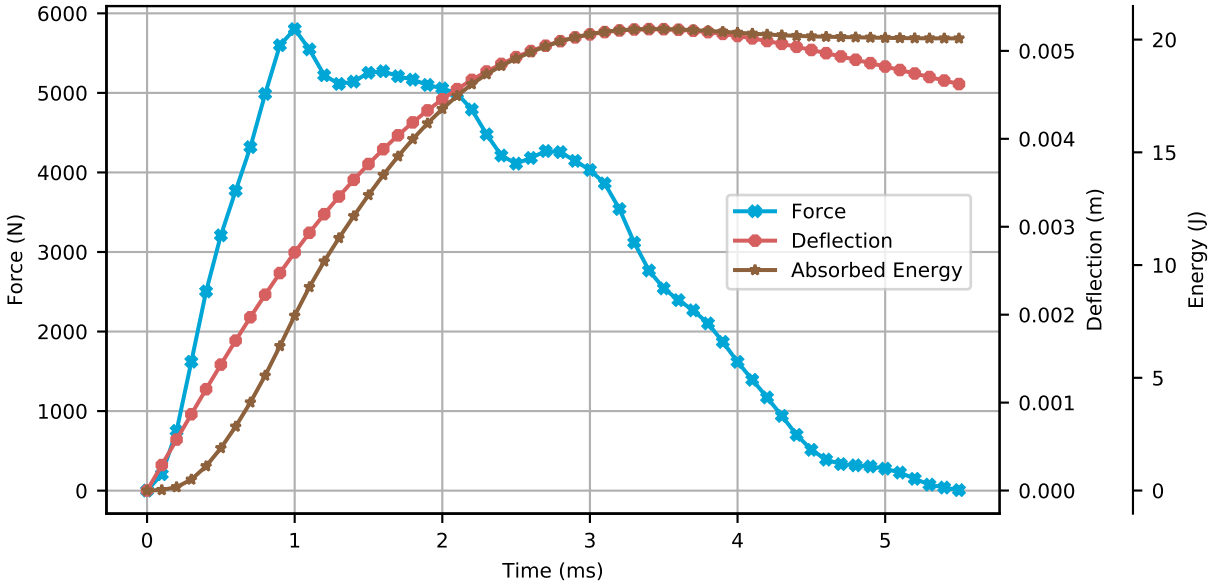

Figure 6.13: Force, Deflection and Absorbed Energy Against Time

The different values are plotted against time and is shown in Figure 6.13 for one of the specimens. The plot shows the deflection of the impactor reaching a peak shortly after the peak in the force is reached which follows the correct trend since it takes that much time to dissipate the force. The absorbed energy reaches a peak and then reduces as well indicating that not all energy was absorbed and was dissipated as elastic response by the material. This can be seen further in Figure 6.14. The graph shows the evolution of force against the displacement of the impactor. From this plot it is inferred that a lower deflection at the final point would lead to a higher elastic response from the material. On average, the BADGE specimens showed a more elastic response compared to the VDE samples. The area under the curve of a force-delfection curve also gives the total absorbed energy by the specimen as shown in Figure 6.15. These values are reported in Table 6.2.

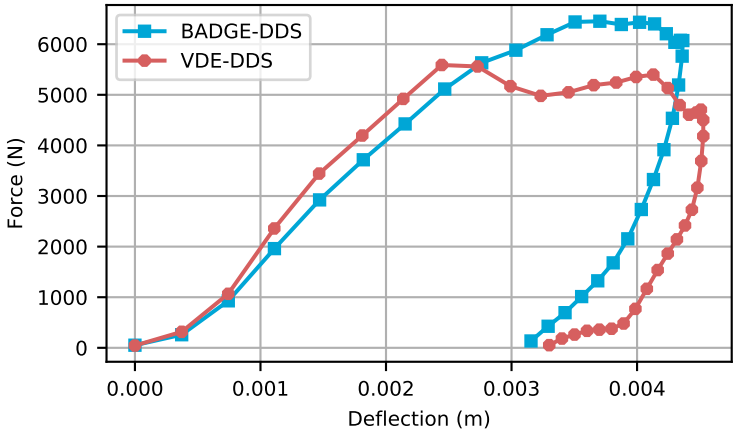

Figure 6.14: Force Deflection Comparison

Table 6.2: Impact and Absorbed Energy of the Specimens

Specimen Number	BADGE		VDE	
	Impact Energy (J)	Absorbed Energy (J)	Impact Energy (J)	Absorbed Energy (J)
1	22.17	21	20.18	19
2	19.98	19	16.98	15
3	18.54	16	15.72	14

Another parameter which can be inferred from this test is the bending stiffness of the material. This is shown in Figure 6.15 for a VDE-DDS specimen. Bending stiffness is calculated as the slope of the force-deflection curve. On average, VDE-DDS specimens had a bending stiffness of 2.4 kN/mm while for BADGE-DDS specimens it was 2.1 kN/mm.

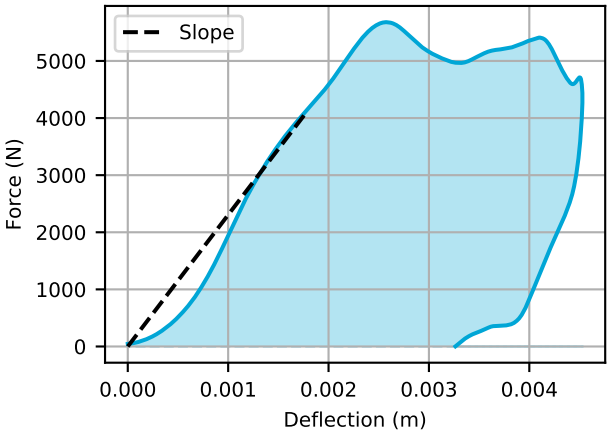

Figure 6.15: Slope Showing Bending Stiffness and Area for Energy Absorption Calculation

The energy deflection comparison graphs also provide an insight into how the material behaves. As shown in Figure 6.16, VDE-DDS specimen initially absorbs more energy with a smaller deflection showing an increased resistance to damage propagation, however it soon reaches a peak and starts to crack further. The ultimate absorbed energy is higher for the BADGE-DDS sample with a smaller deflection before the impactor returns upwards. This was investigated further by identifying the matrix-cracking energy which is shown in Figure 6.17.

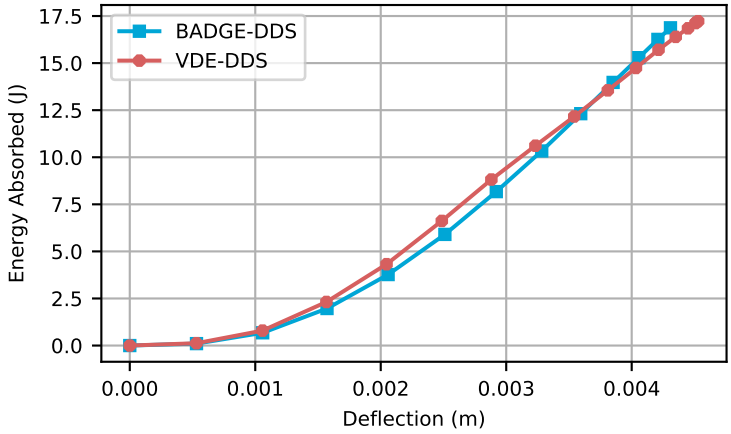

Figure 6.16: Absorbed Energy-Deflection Comparison

Upon plotting the force and energy against deflection, the energy needed till the first crack in the matrix occurs can be identified. It is generally accepted to be the first peak in the force-deflection curve. Finding the energy at that point gives the matrix-cracking energy. A higher matrix cracking energy would mean that the material is able to absorb more energy before it transfers the impact damage to the fibers. A study found that matrix cracking and delamination were the most common damage mechanisms on carbon-epoxy laminates due to low velocity impacts [65]. Hence, this is also an important parameter which is shown in Figure 6.17. On average, BADGE-DDS specimens had a higher matrix cracking energy compared to its VDE counterparts. This is discussed further in Section 7.3.

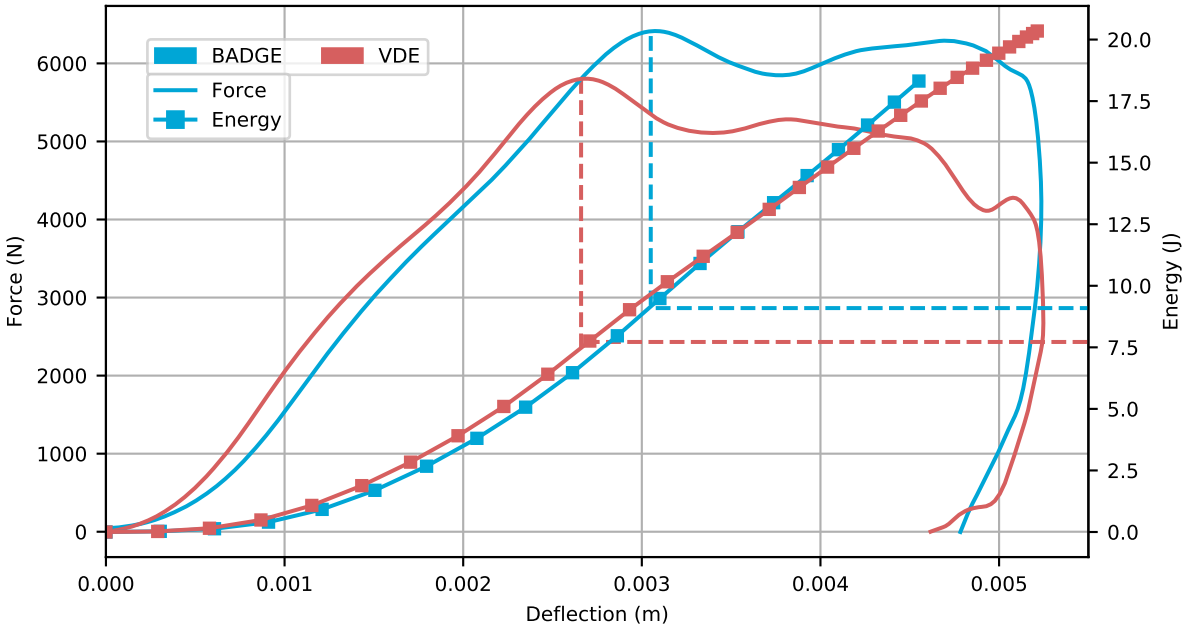

Figure 6.17: Matrix Cracking Energy Comparison

Part III

Outcomes

7

Results and Discussion

7.1. Thermal and Physical Characteristics of Resin

The various thermal properties investigated during the project are reported in Table 7.1.

Table 7.1: Thermal Characterization Results

Property	Value	Measurement Technique
Cure Cycle	160° C for 2h + 220° C for 1h	DSC & DMA
T_g	158° C	DMA
HDT	149° C	DMA
CTE	$58.12\ \mu m/m°C$	TMA
Degradation Temperature	273° C (5% weight loss)	TGA
	450° C (50% weight loss)	
Viscosity	$0.12Pa \cdot s$ (at 60° C)	Rheometry
Water Contact Angle	71°	High-Resolution Camera

The cure cycle was estimated by analysing the heat of the reaction using DSC, first over a range of temperature and then using the enthalpy value from that in isothermal measurements to determine the time. Analysis of that data revealed that some residual cure was left in the resin. A post-cure cycle was introduced to cure the resin completely. Samples were post-cured at different temperatures and analysed in DMA to determine the post-cure temperature. The sample with the highest recorded T_g in DMA was chosen. For the optimal time, a gel content test was done on samples post-cured for different periods of time. Ultimately, the cure cycle was found to be 160° C for 2 h and post curing at 220° C for 1 h.

T_g was found by using DMA since DSC showed no clear peaks in the dynamic heating and cooling ramps. The results showed the T_g to be between 140° C and 158° C depending on the analysis technique used. Figure 7.2 shows different resin systems compared for their T_g and fracture toughness values.

HDT was calculated for the resin system to be 149° C, also using DMA. This result lies in the middle of the T_g values obtained through two different methods of peak of $tan(\delta)$ and the onset drop in E'. As was discussed in Section 3.4, the drop in storage modulus represents the loss of mechanical properties in the material. VDE-DDS retains some of its mechanical properties even in its transition state.

Armed with this knowledge and considering that the requirements for epoxies used in the aerospace sector are to have operational capability till 150° C [66], VDE-DDS can be considered a new alternative in terms of its thermal characteristics. The heat deflection temperature of materials can be increased by using filler materials or by simply reinforcing the material with fibers, however this ultimately doesn't affect the T_g of the material.

CTE of the resin system was measured using TMA, in which a probe pushes down on the material and measures the deflection from that point over a temperature range. However, due to the pointed nature of the probe, it simply went into the material thereby giving wrong results after a certain temperature.

The CTE measured at lower temperatures was $58.12\ \mu m/m\ ^{\circ}C$. The CTE should be as low as possible, specially for a polymer's usage with carbon fibres, since CF has a negative CTE causing stresses within the composite if the temperature were to increase or decrease. This is very common in aircrafts as they gain and lose altitude over the period of an entire flight, requiring the need for a more thermally stable material combination in a composite. CTE of VDE-DDS was found to be lower than that of BADGE-DDS.

TGA provided valuable insight into how the resin behaves at elevated temperatures. A 5% mass loss was observed at around 273° C and 50% of the total mass was lost at around 450° C. The change in mass loss revealed that the mass loss occurred in two stages. The first stage of quick weight loss is around 280° C and the second one being around 390° C. It is speculated that these temperatures are where the side chains of the resin molecules break-off followed by the scission of the epoxy chain.

Viscosity of VDE-DDS was measured over a range of 40° C-120° C. A lower viscosity resin would aid in manufacturing processes by having easier processibility and therefore, less costs. Results showed that the resin had suitable viscosity for a process like RTM but not low enough for vacuum infusion. The surface's hydrophibicity of the fully cured resin was also checked. A water contact angle of 71° C was found. Water absorption test was also done to see the amount of water absorbed by the material over various periods of time. After a 24 hr immersion period, an increased weight of 0.55% was found. This was found to be more than that of its commercial epoxy counterparts. It is recommended to use hydrophobic coatings on the surface of VDE-DDS since it has been reported that excess water absorption can lead to a decrease in the mechanical properties of the resin [67].

Table 7.2: Physical Characterization Results

Property	Value
Density	$1.296\ g/cm^3$
Cure Shrinkage	7.04%

The physical characteristics of the resin include the density and cure shrinkage, which are reported in Table 7.2. The density of VDE-DDS is on the higher side compared to BADGE-DDS. A higher density would lead to higher weight of a composite and not necessarily higher mechanical properties since the load is taken up by the fibers in a composite. the density of the two resin systems differs by 6%.

Cure shrinkage of VDE-DDS lines up with common thermosetting epoxy systems having cure shrinkage normally between 5-7%. Ideally, the cure shrinkage should be as little as possible because while curing the carbon fibres would also be undergoing their own shrinkage due to their negative CTE, thereby causing residual stresses within the final composite.

Through these thermal and physical characteristics, it can be concluded that VDE-DDS can be used as a material for aircraft primary structures since it meets the high temperature requirements and has appropriate processing parameters. It follows a standard curing cycle while displaying good physical characteristics. One shortcoming that could arise is the rate of water absorption by the material's surface. However, this could easily be mitigated by use of hydrophobic coatings, as is the case for most aircraft manufacturing processes today to ensure that it reaches certification standards.

7.2. Mechanical Characteristics of Resin

After thermal and physical characterization of the resin, its mechanical properties were studied. Three tests were done on the resin system to characterise it. Tensile and flexural tests were done to identify its strength and modulus. Fracture toughness test was also performed to observe the resin system's resistance to crack growth, an important parameter for a material to potentially be used in composites.

These properties are compared against values found in literature of some commercial epoxy systems used in the aerospace industry. This is shown in Figure 7.1. The resin systems compared include Araldite® LY 8605 / Aradur® 8605 which is a low viscosity epoxy system used in RTM processes and reaches a T_g of around 150° C [68]. Other resin systems like Araldite® LY 1556 / Aradur® 34055 and Araldite® LY 1568 / Aradur® 3492 were also included. These are all BADGE-based epoxy systems with cycloaliphatic amine based curing agents [69] [70]. A Bisphenol F based resin with an aromatic amine curing agent was

also selected called EPIKOTE™ Resin 862 / EPIKURE™ Curing Agent W [71]. Pure resin systems of BADGE-DDS and TGDDM-DDS were also included [72, 73].

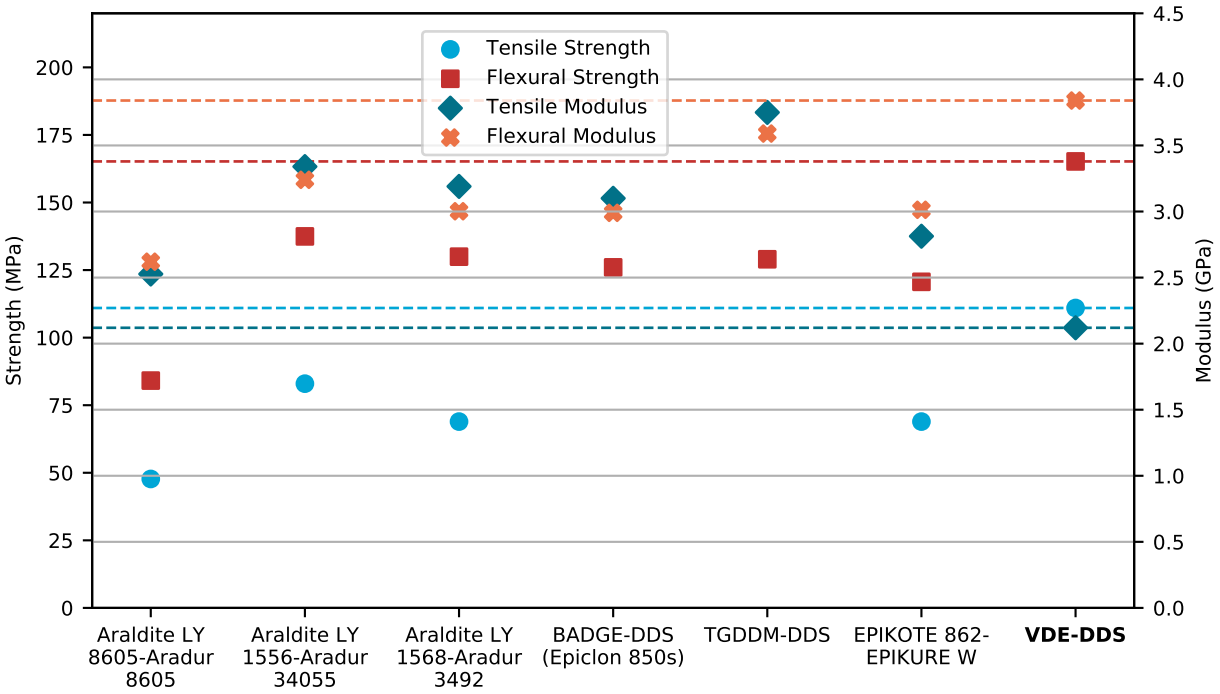

Figure 7.1: Comparison of Different Mechanical Properties of Resin (Data obtained from [68, 69, 70, 71, 72, 73])

The tensile strength of the VDE-DDS was 110.9 MPa which is on the higher side when compared to other aerospace-grade epoxies as shown in Figure 7.1. As can be seen in the graph, in terms of strength, VDE-DDS is very high but comparing its modulus, the value seems to be on the lower end. In the context of usage in a composite, a resin should have high modulus and strength if possible. The strength of CFRP composites is constrained by the difference in the mechanical properties of the resin and the fibers, which is why a higher strength and modulus is required. A lower tensile modulus, however, translates into better fracture toughness. Brittle materials tend to have easier crack development compared to more elastic materials. This is shown in Figure 7.2.

For the flexural strength of the resin, it can be observed through Figure 7.1 that both the strength and the modulus of VDE-DDS lies on the higher end. This is an important characteristic as not only is the resin stiffer, it has the ability to withstand more stress compared to others. For composite properties like impact toughness, the flexural strength is important since that is when the matrix would start to crack and eventually lead to breakage in the structure. A resin system with higher modulus would also be able to resist these kind of impact events for a longer period of time. However, an important point to consider is that epoxies tend to show isotropic behaviour and a large difference in tensile and elastic modulus values of VDE-DDS was not expected. Other resin systems shown in Figure 7.1 have similar values for their modulus values. It would be worth repeating these tests for VDE-DDS in the future to get conclusive results.

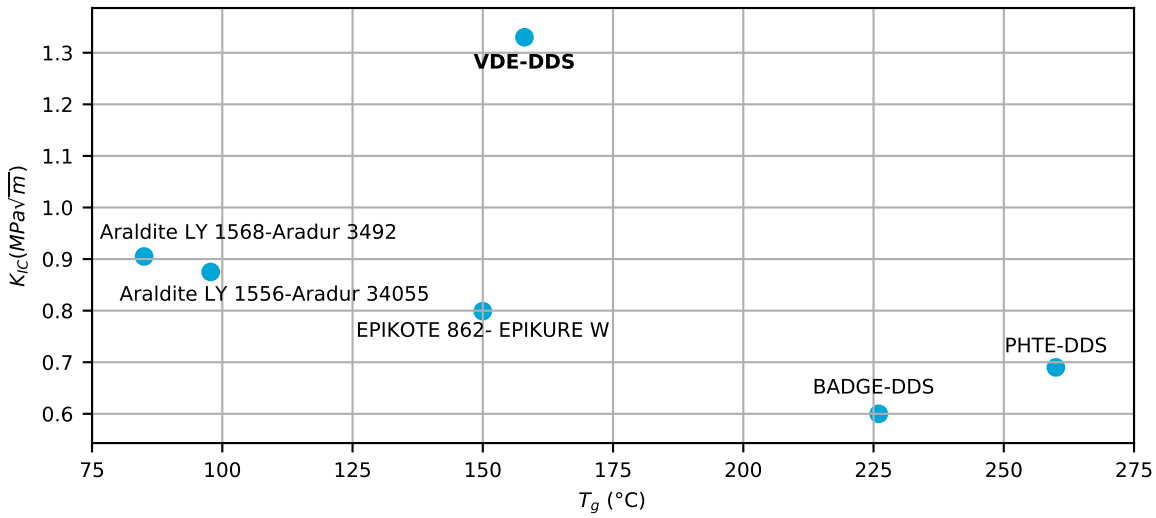

Figure 7.2: Fracture Toughness vs T_g for Various Resin Systems (Data obtained from [23, 69, 70, 71])

Figure 7.2 shows a comparison between different resin systems and their T_g. An ideal-case for an epoxy resin system would be in the top-right of the graph. Unfortunately, VDE-DDS doesn't provide the highest T_g in when compared to others. This property depends on the temperature range of the application but, in general, it is beneficial for the material to have a higher T_g. However, this is compensated by a very high K_{IC} value. This holds high potential because resistance to crack growth is one of the most important characteristics for any composite matrix material. Brittle materials tend to have a lower K_{IC} value. This can be attributed to the fact that brittle materials have easier crack formation which is why rubbery filler materials are added to commercial epoxy systems. These, however, tend to decrease the T_g as well. Overall, VDE-DDS offers good operational capability in terms of temperature and toughness. Further work can be done on this to identify the crack propagation through the resin and to mix it with fillers to improve its toughness. Mechanisms like crack tip yielding or crack deflection should also be studied to understand VDE's place in the aerospace epoxy industry.

After a thorough characterization of the resin system was performed, focus was shifted to composite manufacturing and testing. As was discussed in Chapter 2, not a lot of studies focus on this part which is why it was essential to this project. Since composites can vary greatly, from matrix to fibers, it was decided to do a comparison directly against the most widely used epoxy monomer-BADGE. The hardener and the fibers were kept the same to make accurate comparisons. The tests were chosen such that they were matrix-dependent. The manufacturing conditions were kept uniform by manufacturing a single plate and cutting test specimens out of it. Since the curing cycle was different, the plates couldn't be manufactured in the same cycle, the parameter being the only difference during manufacturing.

7.3. Composite Mechanical Tests

The results of the IPSS, compression and ILSS test are shown in Figure 7.3.

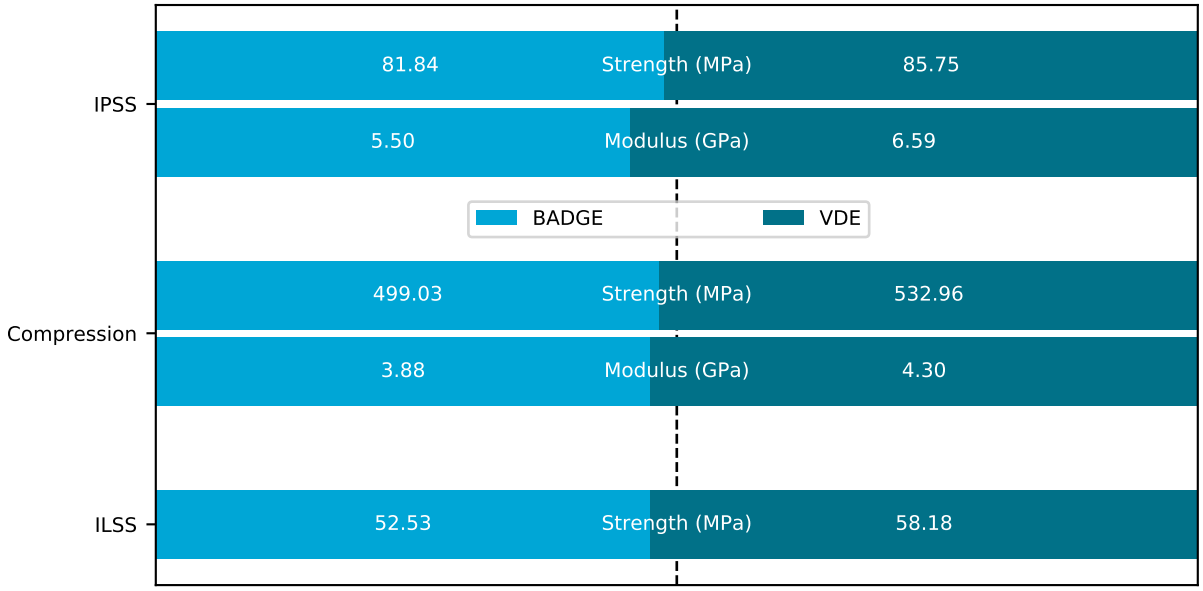

Figure 7.3: Composite Mechanical Tests Comparison

A clear picture emerges from these tests that composites made out of VDE-DDS performed better both in terms of strength and stiffness. A more thorough analysis is presented below.

7.3.1. IPSS

The IPSS strength is comparable to the matrix yield strength which was calculated in Section 4.1. This shows how matrix dependent the test is and how the final failure occurs due to the matrix failing. Figure 7.4 shows the disparity between the measured values of VDE-DDS strength in the resin and composite whilst showing how close it is for the BADGE-DDS system (BADGE-DDS tensile strength value taken from [23]). The difference in performance can be attributed to different specimen sizes, the one used in tensile test being smaller and manufacturing quality of the composite itself. The difference was 1% in case of BADGE-DDS and 29% for VDE-DDS.

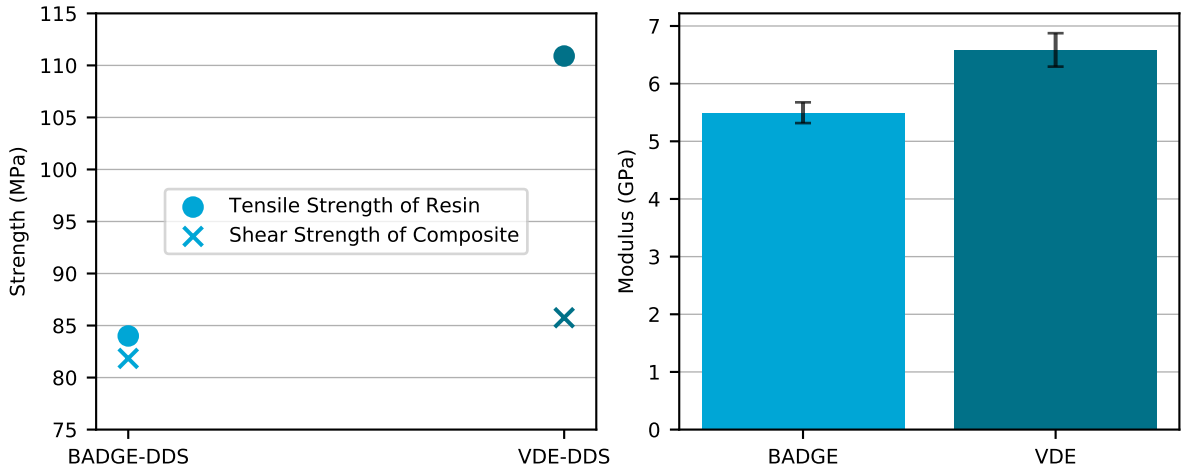

Figure 7.4: Comparison Between VDE and BADGE Samples in IPSS Test

The average modulus was also calculated for the specimens which shows a difference between the two kinds of samples. Even taking into account the standard deviation, VDE-DDS samples tend to be stiffer as shown in Figure 7.4. This was unexpected as VDE-DDS had a lower modulus value in coupon tensile testing as discussed in Section 7.2. Overall, VDE-DDS composite had a higher modulus by around

20% and higher strength by 4%. This could possibly be due to a stronger interface region in VDE-DDS composite. In the future, a test performed with acoustic emission sensors could also shed light into how the fibers break during testing and could reveal the discrepancy between the tensile strength of the resin system compared to its composite's in-plane shear strength.

7.3.2. Compression

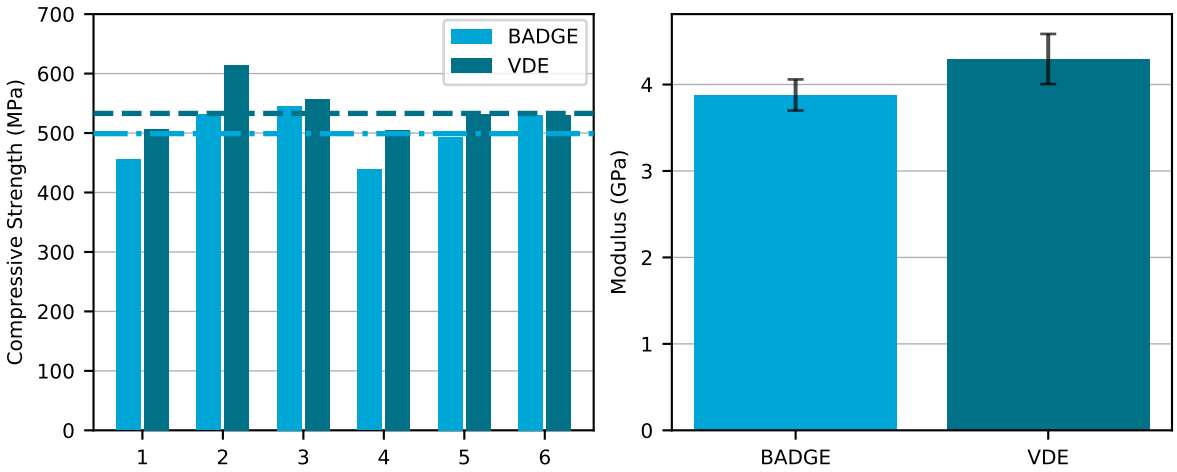

Figure 7.5: Compressive Strength and Modulus Comparison

Compression tests revealed that VDE-DDS samples had more strength and were stiffer as well. Upon analysing each specimen's compressive strength, it can be seen that there is not a lot of variation between the samples including the BADGE-DDS specimens. This could be attributed to low void content within the composite and uniform manufacturing for the samples. The average compressive strength for VDE-DDS specimens was 6% higher compared to the BADGE-DDS samples and the modulus was 10% higher. The final failure in compression test occurs due to matrix cracking and a higher compressive strength indicates that VDE-DDS had better shear strength properties.

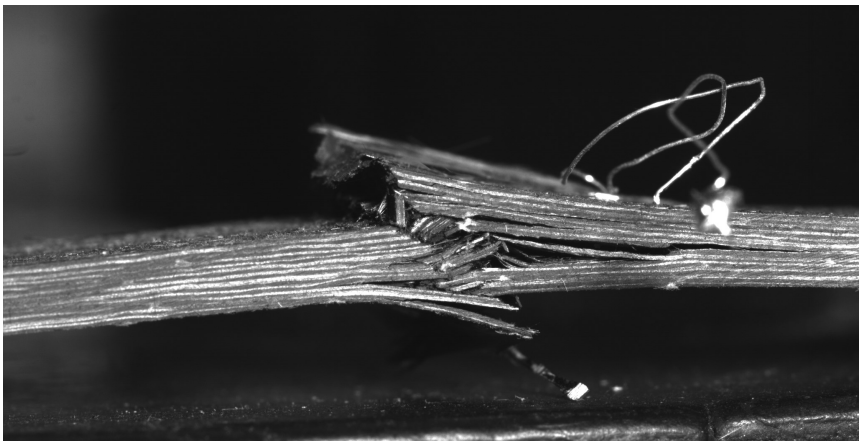

Figure 7.6: Compression Failure for a BADGE-DDS Sample

7.3.3. ILSS

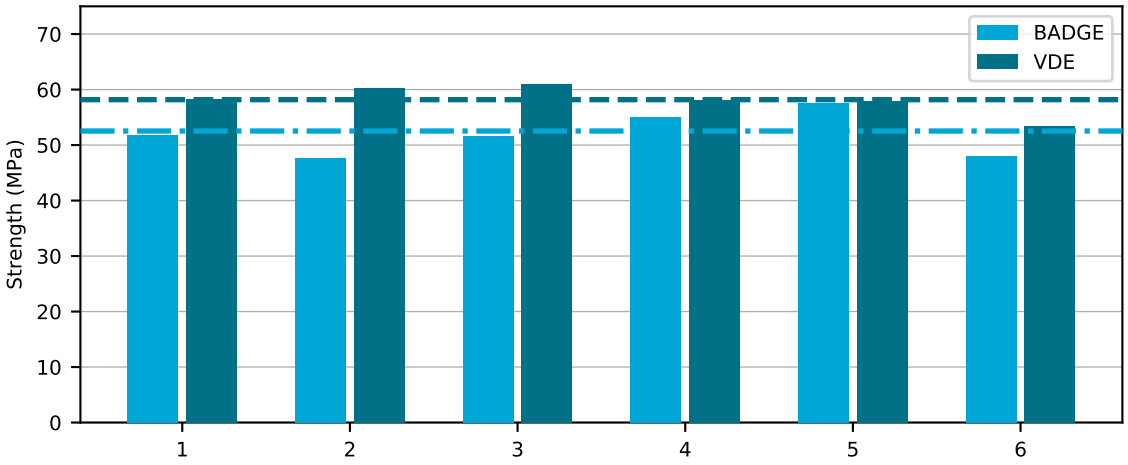

Figure 7.7: Short-Beam Strength Comparison of Different Specimens

ILSS test showed that VDE-DDS samples had consistently higher short-beam strength than its BADGE-DDS counterpart. Even though some of the specimens did have incorrect failure modes like tension as reported in Section 6.3, enough samples had the correct failure mode to draw conclusions about the material properties. Inter-laminar shear strength depends on the matrix and the interface region of a composite. A higher shear strength implies good a stronger interface region and a stronger matrix. Alternatively, some manufacturing defects could lead to premature failure within the laminate for this test. On average, VDE-DDS samples were stronger than BADGE-DDS samples by 10%.

7.3.4. Impact Test

For impact test, different plates were manufactured since they had a different layup to the other tests. Three plates were manufactured for each type of material and tested. Even though the impactor was dropped from the same height, the measured impact energy was different for two out of the three samples, making any comparisons between the absorbed energy across samples futile. A more appropriate way to compare them was to calculate the percentage of absorbed energy compared to the measured impact energy. This is shown in Figure 7.8 (left). The average percentage for BADGE-DDS samples is 94% and for VDE-DDS it is 95%, and if the standard deviation were to be included, the values are very similar. Therefore, the response of the materials can be considered to be quite similar. Comparing the absorbed energy of the test specimen of the two types of materials which had the same impact energy- VDE-DDS specimen absorbed more energy. However, this is not conclusive as that particular specimen could just be an outlier in the results due to manufacturing defects.

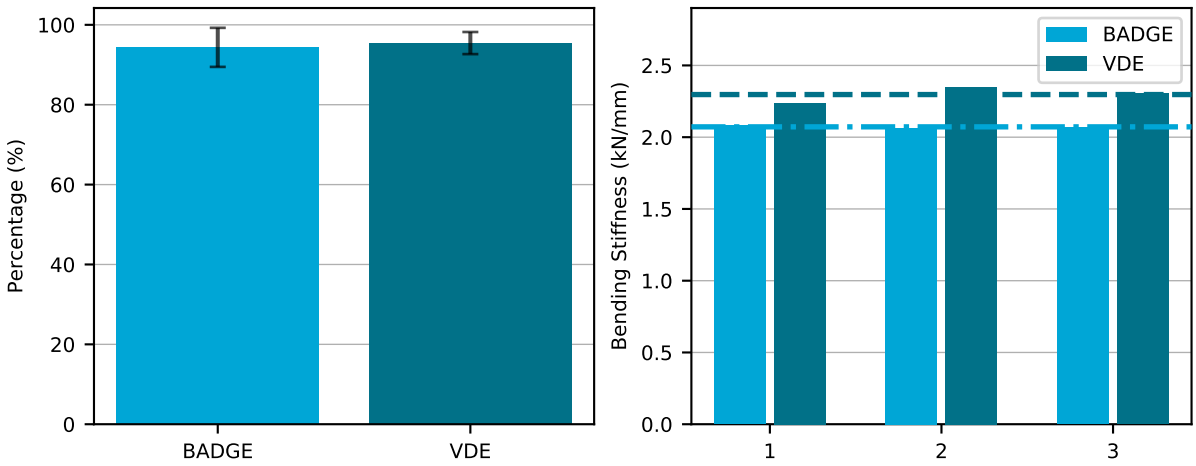

Figure 7.8: (Left) Percentage of Absorbed Energy to Impact Energy and (Right) Bending Stiffness

Based upon the slope generated by the force-deflection curve from the tests, the bending stiffness of the composite material could also be calculated. This is also shown in Figure 7.8 (right). The composite made with VDE-DDS showed a higher stiffness for all samples. This is another important property which demonstrates the ability to withstand deformation by the composite. On average the composite made of VDE-DDS had 10% higher bending stiffness.

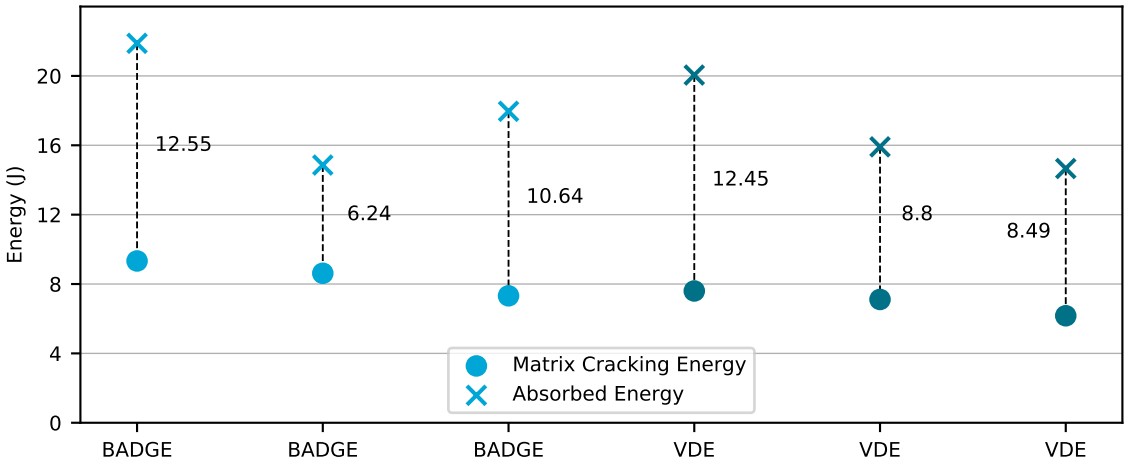

Figure 7.9: Absorbed and Matrix Cracking Energy

As discussed in Section 6.4, the energy at which the matrix starts to develop cracks can be found through the first peak of the measured force from the force-deflection graph, shown in Figure 6.17. The matrix-cracking energy is plotted in Figure 7.9 for all test specimens. Composite samples made of BADGE-DDS showed a higher matrix-cracking energy, meaning that the material started to crack after a higher amount of energy was deposited to it. The average energy required for damage initiation was 21% higher for BADGE-DDS compared to VDE-DDS. To ensure that this was not related to the higher absorbed energy for some of the samples, the values were compared and plotted in Figure 7.9. It can be observed that there is very little correlation between the two as the cracking energy remains about the same while the absorbed energy varies for each specimen.

Overall, through these composite mechanical tests, a few observations can made:

- The stiffness of composites made of VDE-DDS was consistently higher in all of the tests performed compared to BADGE-DDS. This was an expected result for compression and ILSS given that the resin system of VDE-DDS showed higher flexural modulus. This would also explain why the bending

stiffness came out higher for VDE-DDS samples in the impact test. However, since IPSS test is geared towards tensile properties, it was strange to observe BADGE-DDS samples having lesser modulus values.

- The strength of VDE-DDS resin was higher in both flexural and tensile tests and hence a higher value in terms of strength was expected in the tests as well. The difference in the strength of composites however was not as high as the resin tests. This could be due to different methodologies followed by the reference material and also that composites have more homogeneous values as the loads are distributed evenly across the fibers as well. In IPSS, compression and ILSS tests, VDE-DDS composites showed 4%, 6% and 10% higher strength respectively, compared to BADGE-DDS specimens.
- The impact test showed that composites made out of BADGE-DDS require more energy before damage initiates in a low-velocity impact event. The test also showed that VDE-DDS composites tend to absorb more energy relative to their impact energy, although more testing is required to conclusively comment on this property. These results are opposite when the resin properties are compared. VDE-DDS has a higher flexural modulus and strength, therefore it should be stronger in impact events and it has a higher fracture toughness as well. VDE-DDS composites also showed a higher inter-laminar strength. This is presented in Figure 7.10. It could be that BADGE-DDS provides more inter-facial strength to the fibers, or that the interface region of BADGE-DDS with CF is stronger compared to VDE-DDS. It could also be manufacturing errors within the composite, which weren't observed before testing. Another factor could be lesser number of specimens tested particularly as impact testing requires a high number of samples to be tested for conclusive results.

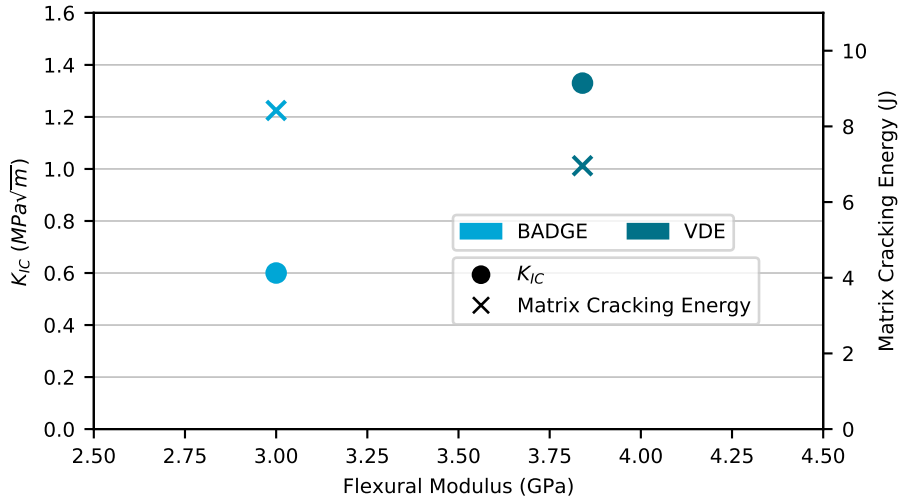

Figure 7.10: Comparison Between Fracture Toughness and Matrix Cracking Energy as a Function of Flexural Modulus

Through all these tests, it can be concluded that VDE-DDS performs equal to, if not better than, composites made out of BADGE-DDS, hence it represents incredible potential towards bio-based materials being used in primary structures.

8

Conclusion

An aircraft's life cycle continues to be emission-heavy in the present day. This stems from fuel consumption during flight and manufacturing of the aircraft using high-performance materials which require energy-intensive manufacturing processes. These high-performance materials include CFRP composites which offer incredible mechanical properties but are environmentally burdensome. For some of these structural composites, epoxy resins are used as matrix material, most commonly being based on BADGE, which is derived from petroleum-based products, adding to its environmental footprint. Research on alternative materials for BADGE-based epoxies is critical. Bio-based materials present a viable pathway toward reducing environmental impact.

Vanillin is a molecule which can be derived from lignin, a material which is makes up around 35% of woody biomass. Lignin is currently a by-product of the paper industry. Most of the supply of vanillin in the world is petroleum-based. A derivative of vanillin, diglycidyl ether of vanillyl alcohol (VDE), can be obtained by a chemical reaction between vanillyl alcohol and epichlorohydrin. The VDE monomer contains two epoxy functional groups and when mixed with a hardener can be used as matrix material in a composite. The hardener 4,4' diaminodiphenyl sulfone (DDS) was chosen in this project because of its usage in high-performance epoxies.

The objective of this thesis project was to investigate the efficacy of VDE-DDS resin system to be used in primary structural parts of aircrafts. A literature review showed studies that focused on vanillin-based molecules' chemical and thermal properties but few discussed mechanical properties and even fewer discussed composite characterization. Since VDE is bi-functional and has an aromatic structure similar to BADGE, it was hypothesized to have similar macro-properties. It was decided to investigate the properties of the resin system first, moving on further with composite manufacturing and testing. The properties of VDE-DDS were compared against the properties of other commercial epoxy systems and a direct comparison was provided by BADGE-DDS.

However, it should be acknowledged that usage of a bio-based material doesn't inherently guarantee greater sustainability, but rather indicates that the starting material is derived from a non-fossil fuel source. With further research more insights can be gained into how much emissions are reduced by employing these kind of materials. It is also worth reflecting more on the definition of environmental performance for bio-based materials. VDE-DDS is only 70% bio-based, with the hardener DDS still being sourced from petroleum-based products.

The cure cycle of VDE-DDS was established through DSC measurements and cure kinetics modelling. A further post-cure cycle was created following experiments done through DMA. The final cure cycle found was 160° C for 2 h followed by a post-cure at 220° C for 1 h. The glass transition temperature was 158° C which was found through DMA experiments. Further, the heat-deflection temperature was also found to be 149° C, which offers a more practical limit in terms of usage of the material. These properties were found to be in-line with other commercial aerospace epoxies used currently, as primary structural materials have a requirement of high temperature operability.

Due to the requirement of high operating temperature range of the material, its thermal expansion properties were also checked. VDE-DDS showed a lower coefficient of thermal expansion when compared to BADGE-DDS. Further research could be done on this aspect to improve the material even further. TGA was used

to find the degradation temperature, around 270° C there was a mass loss of 5%, which is probably when the side chains of the molecule break-off and further dramatic degradation occurred around 390° C which is probably when the epoxy chain itself most-likely started to break. Viscosity of the resin system was found to understand its processing parameters for composite manufacturing. The viscosity of the resin was lower than that of BADGE-DDS, however it still was high at room temperatures that it couldn't be used in processes like vacuum infusion. A more industrial process like RTM is suggested for this resin system.

Bio-based resins tend to be hydrophilic which can affect the thermal and mechanical properties of the resin when exposed to water. This was checked by measuring the water-contact angle of the surface which was found to be 71°, meaning that the surface is hydrophilic. A water absorption test was performed which showed higher levels of water absorbed by the material when compared to BADGE-DDS. The density and cure-shrinkage were also measured. Both of these were higher for VDE-DDS when compared to BADGE-DDS, however not by a large amount.

The thermal and physical characteristics of the resin showed a promising material that was comparable to the resin system made of BADGE, one the most widely used epoxy monomers in the world. Mechanical characterization of VDE-DDS showed promising results. The tensile and flexural strengths were very high when compared to other commercial epoxies (including BADGE-DDS) and the fracture toughness of the resin was also on the higher end. This was due to its more elastic nature represented by a lower tensile modulus value. Since the viscosity of the resin was low, it represented an opportunity to manufacture composites with the hand layup technique and curing in autoclave. Whilst hand layup is not without problems, its one of the easier composite manufacturing methods and can be done with little equipment. The void content for the final plates were checked and deemed to be appropriate.

A single composite plate offered three types of test specimens which was considered optimal since it would equate the amount of errors in manufacturing. Since composites have an increased amount of complexity in terms of load transfer, another plate was manufactured with BADGE-DDS to make a direct comparison, since other commercial epoxies use additives and are optimized only for certain manufacturing processes. The tests were also chosen to ensure matrix-dominant behaviour would be displayed.

The mechanical tests done on the composites revealed that the ones made of VDE-DDS consistently showed higher strength and stiffness compared to its BADGE-DDS counterpart. This was true for IPSS, ILSS and compression tests. Low-velocity impact test however presented different results. The energy required to initiate damage in the matrix was higher for BADGE-DDS composite specimens. VDE-DDS composite specimens did provide more bending stiffness.

Overall, VDE-DDS resin system offers excellent mechanical properties and is comparable to epoxy materials being used in the industry and offers similar thermal and physical characteristics including viscosity and curing kinetics, negating a potential effect of changing processes for manufacturing which would be a huge expense for industry and is a key factor in finding more sustainable, directly substitutional alternatives. VDE-DDS also behaves as good matrix material within composites as was demonstrated by the mechanical tests. VDE-DDS holds a lot of potential to be used within the aerospace industry as a starting point in the usage of bio-based materials.

9

Recommendations For Future Work

This chapter provides a brief overview of the primary recommendations for future work based on the VDE-DDS resin system. The recommendations are as follows:

1. **Prepreg Manufacturing**: As mentioned in Appendix A, isothermal DSC at 120° C showed that the degree of cure stopped after a certain point indicating that it might have reached B-staging. Prepregs are one of the most widely used form of composites in the industry today and manufacturing it using this resin would be beneficial in its applicability.
2. **Reducing Viscosity**: Although the viscosity for the resin is pretty low compared to BADGE-DDS, it is not low enough to be used in manufacturing processes like vacuum infusion. Therefore, adding reactive diluents to the resin system would be a good strategy to open the material for wider uses. How the mechanical and thermal properties get affected the the use of reactive diluents should also be checked.
3. **Hydrophobic Coatings**: Due to the higher water absorption and a lower water contact angle, VDE-DDS is hydrophilic and hence should be used with hydrophobic coatings in practical applications. Further research should also be performed on how water absorption would affect the thermal and physical properties of the resin system.
4. **Comprehensive Impact Testing**: Due to a smaller time left for the impact test, only a limited number of samples were created for the test. A more comprehensive test would show more uniform results and the material properties could be conclusively determined. A more rigorous test like compression after impact could also be done to understand the material's place in real-world applications.
5. **Vitrimeric Systems**: The resin system VDE-DDS is not recyclable or reusable as the chemical bonds formed during curing are irreversible. By researching on creating a vitrimeric system, true material circularity could be reached.
6. **Composite Manufacturing**: This project utilized the hand layup technique which is often unreliable and non-repeatable for consistent results. An appropriate method like RTM should be investigated.
7. **LCA Studies**: To fully understand whether VDE is performs better environmentally an LCA study should be performed. While LCA studies have their challenges, it would show where the benefits or drawbacks of using this resin system are compared to its BADGE counterpart.
8. **Flammability Tests**: Although bio-based resin systems tend to have poor flame retardancy, vanillin-based resins have been shown to have good flame characteristics. It is an important characteristic that should be studied for future use of the material.

References

[1] S Kangishwar et al. “A comprehensive review on polymer matrix composites: material selection, fabrication, and application”. In: *Polymer Bulletin* 80.1 (2023), pp. 47–87.

[2] Robert A. Witik et al. “Economic and environmental assessment of alternative production methods for composite aircraft components”. In: *Journal of Cleaner Production* 29-30.5 (2012), pp. 91–102. DOI: 10.1016/j.jclepro.2012.02.028.

[3] Silu Huang et al. “Characterization of interfacial properties between fibre and polymer matrix in composite materials–A critical review”. In: *journal of materials research and technology* 13 (2021), pp. 1441–1484.

[4] Modern Airliners. *Modern Airliners Boeing 787 Dreamliner*. Retrieved on 17/09/2024. URL: http://www.modernairliners.com/boeing-787.

[5] Júnior Sousa Ribeiro et al. “Proposed Framework for End-of-life Aircraft Recycling”. In: *Procedia CIRP* 26 (2015), pp. 311–316. DOI: 10.1016/j.procir.2014.07.048.

[6] Eylem Asmatulu et al. “Recycling of Aircraft: State of the Art in 2011”. In: *Journal of Industrial Engineering* 2013.2 (2013), pp. 1–8. DOI: 10.1155/2013/960581.

[7] Vincenzo Lunetto et al. “Sustainability in the manufacturing of composite materials: A literature review and directions for future research”. In: *Journal of Manufacturing Processes* 85 (2023), pp. 858–874. DOI: 10.1016/j.jmapro.2022.12.020.

[8] Eleonore Pierrat et al. “Global environmental mapping of the aeronautics manufacturing sector”. In: *Journal of Cleaner Production* 297.6 (2021), p. 126603. DOI: 10.1016/j.jclepro.2021.126603.

[9] S. Howe et al. “Environmental life cycle assessment of commercial passenger jet airliners”. In: *Transportation Research Part D: Transport and Environment* 19 (2013), pp. 34–41. DOI: 10.1016/j.trd.2012.12.004.

[10] William E Dyer et al. “Polymers as Aerospace Structural Components: How to Reach Sustainability?” In: *Macromolecular Chemistry and Physics* 224.24 (2023), p. 2300186.

[11] Jingkai Liu et al. “Advances in sustainable thermosetting resins: From renewable feedstock to high performance and recyclability”. In: *Progress in polymer science* 113 (2021), p. 101353.

[12] Ai-jun Li et al. “Effects of fiber and matrix properties on the compression strength of carbon fiber reinforced polymer composites”. In: *New Carbon Materials* 35.6 (2020), pp. 752–761.

[13] Ross F Minty et al. “The influence of hardener-to-epoxy ratio on the interfacial strength in glass fibre reinforced epoxy composites”. In: *Composites Part A: Applied Science and Manufacturing* 112 (2018), pp. 64–70.

[14] Wei Helen Li et al. “Advances in benzoxazine resins for aerospace applications”. In: *Proceedings of 2010 SAMPE international symposium, Seattle WA, SAMPE Covina CA*. 2010.

[15] Bijender Kumar et al. “Effect of bio-based derived epoxy resin on interfacial adhesion of cellulose film and applicability towards natural jute fiber-reinforced composites”. In: *International Journal of Biological Macromolecules* 222 (2022), pp. 1304–1313.

[16] Dietmar Haba et al. “Correlation of epoxy material properties with the toughening effect of fullerene-like WS2 nanoparticles”. In: *European polymer journal* 84 (2016), pp. 125–136.

[17] Aratz Genua et al. “Build-to-specification vanillin and phloroglucinol derived biobased epoxy-amine vitrimers”. In: *Polymers* 12.11 (2020), p. 2645.

[18] Dietmar Haba et al. “Observation of elastic modulus inhomogeneities in thermosetting epoxies using AFM–Discerning facts and artifacts”. In: *Polymer* 55.16 (2014), pp. 4032–4040.

[19] Qi Li et al. “Curing of DGEBA epoxy using a phenol-terminated hyperbranched curing agent: Cure kinetics, gelation, and the TTT cure diagram”. In: *Thermochimica acta* 549 (2012), pp. 69–80.

[20] Dimitrios Apostolidis et al. “An algae-derived partially renewable epoxy resin formulation for glass fibre-reinforced sustainable polymer composites”. In: *RSC Applied Polymers* 2.2 (2024), pp. 149–154.

[21] Yu Qi et al. “Magnolol-based bio-epoxy resin with acceptable glass transition temperature, processability and flame retardancy”. In: *Chemical Engineering Journal* 387 (2020), p. 124115.

[22] Hiroyuki Okada et al. “Direct evidence revealing structural elements essential for the high binding ability of bisphenol A to human estrogen-related receptor-γ”. In: *Environmental health perspectives* 116.1 (2008), pp. 32–38.

[23] Pranshul Gupta. “Naturally sourced epoxies for High-performance composite applications: A feasibility study of renewable algae-derived epoxy resin system”. Master’s Dissertation. Delft, The Netherlands: TU Delft, 2024.

[24] Jens Bachmann et al. “Outlook on ecologically improved composites for aviation interior and secondary structures”. In: *CEAS Aeronautical Journal* 9.3 (2018), pp. 533–543. DOI: 10.1007/s13272-018-0298-z.

[25] Jens Bachmann et al. “Environmental analysis of innovative sustainable composites with potential use in aviation sector—A life cycle assessment review”. In: *Science China Technological Sciences* 60.9 (2017), pp. 1301–1317. DOI: 10.1007/s11431-016-9094-y.

[26] Fatemeh Ferdosian et al. “Curing kinetics and mechanical properties of bio-based epoxy composites comprising lignin-based epoxy resins”. In: *European Polymer Journal* 82 (2016), pp. 153–165.

[27] Rosario Vidal et al. “Life Cycle Assessment of Novel Aircraft Interior Panels Made from Renewable or Recyclable Polymers with Natural Fiber Reinforcements and Non–Halogenated Flame Retardants”. In: *Journal of Industrial Ecology* 22.1 (2018), pp. 132–144. DOI: 10.1111/jiec.12544.

[28] Maxence Fache et al. “Vanillin, a key-intermediate of biobased polymers”. In: *European polymer journal* 68 (2015), pp. 488–502.

[29] Gudbrand Rødsrud et al. “History and future of world’s most advanced biorefinery in operation”. In: *Biomass and bioenergy* 46 (2012), pp. 46–59.

[30] Maxence Fache et al. “Vanillin production from lignin and its use as a renewable chemical”. In: *ACS sustainable chemistry & engineering* 4.1 (2016), pp. 35–46.

[31] Jintao Wan et al. “Ultrastiff biobased epoxy resin with high T g and low permittivity: from synthesis to properties”. In: *ACS Sustainable Chemistry & Engineering* 4.5 (2016), pp. 2869–2880.

[32] Maxence Fache et al. “Vanillin, a promising biobased building-block for monomer synthesis”. In: *Green Chemistry* 16.4 (2014), pp. 1987–1998.

[33] Diane Kukich. “MIL-HDBK-17”. In: *AMPTIAC Newsletter* 1.3 (), p. 2.

[34] Chang Woon Jang et al. “Mechanical Properties and Failure of Aerospace-Grade Epoxy Resins from Reactive Molecular Dynamics Simulations with Nanoscale Defects”. In: *ACS Applied Polymer Materials* 4.8 (2022), pp. 5269–5274.

[35] Radhika Wazalwar et al. “Mechanical properties of aerospace epoxy composites reinforced with 2D nano-fillers: current status and road to industrialization”. In: *Nanoscale Advances* 3.10 (2021), pp. 2741–2776.

[36] Specific Polymers. *DGEVA- Technical Data Sheet*. Retrieved on 04/07/2024. URL: https://specificpolymers.com/product/dgeva/.

[37] Mike Reading et al. *Modulated temperature differential scanning calorimetry: theoretical and practical applications in polymer characterisation*. Vol. 6. Springer Science & Business Media, 2006.

[38] Chenglin Zhang et al. “Curing kinetics, mechanical properties and thermomechanical analysis of carbon fiber/epoxy resin laminates with different ply orientations”. In: *Iranian Polymer Journal* 30 (2021), pp. 1297–1308.

[39] Guyonne Alleman. “The effects of different cure cycles on the mechanical performance of thick-walled composites”. Master’s Dissertation. Delft, The Netherlands: TU Delft, 2018.

[40] Alfréd Kállay-Menyhárd. “Joseph D. Menczel and R. Bruce Prime (eds): Thermal analysis of polymers fundamental and applications: Published by John Wiley and Sons Inc.(688 pp)”. In: *Journal of Thermal Analysis and Calorimetry* 102.3 (2010), pp. 1183–1184.

[41] ASTM International. *ASTM D648-18*. Standard. Standard Test Method for Deflection Temperature of Plastics Under Flexural Load in the Edgewise Position. United States, 2018. URL: `https://www.astm.org/d0648-18.html`.

[42] Sujan E Bid Wadud et al. “Using the DMA Q800 for ASTM International D 648 Deflection Temperature Under Load”. In: *no. d* (2019), pp. 1–4.

[43] Benjamin J Anderson. “Thermal stability of high temperature epoxy adhesives by thermogravimetric and adhesive strength measurements”. In: *Polymer degradation and stability* 96.10 (2011), pp. 1874–1881.

[44] Ming-xin Xu et al. “Insights into the pyrolysis mechanisms of epoxy resin polymers based on the combination of experiments and ReaxFF-MD simulation”. In: *Chemical Engineering Journal* 473 (2023), p. 145404.

[45] Guo Li et al. “Simulation of pyrolysis of crosslinked epoxy resin using ReaxFF molecular dynamics”. In: *Computational and Theoretical Chemistry* 1200 (2021), p. 113240.

[46] Daniel Angel Bellido-Aguilar et al. “Hydrophobization of fully bio-based epoxy polymers using water as solvent: effect of additives”. In: *European Polymer Journal* 140 (2020), p. 110043.

[47] ASTM International. *ASTM D792-20*. Standard. Standard Test Methods for Density and Specific Gravity (Relative Density) of Plastics by Displacement. United States, 2020. URL: `https://www.astm.org/standards/d792`.

[48] Eric Leroy et al. “Evolution of the coefficient of thermal expansion of a thermosetting polymer during cure reaction”. In: *Polymer* 46.23 (2005), pp. 9919–9927.

[49] ASTM International. *ASTM D638-14*. Standard. Standard Test Method for Tensile Properties of Plastics. United States, 2014. URL: `https://www.astm.org/d0638-14.html`.

[50] José R Lerma Valero. *Plastics injection molding: scientific molding, recommendations, and best practices*. Carl Hanser Verlag GmbH Co KG, 2020.

[51] ASTM International. *ASTM D790-17*. Standard. Standard Test Methods for Flexural Properties of Unreinforced and Reinforced Plastics and Electrical Insulating Materials. United States, 2017. URL: `https://www.astm.org/standards/d790`.

[52] Seul-Yi Lee et al. “Roles of small polyetherimide moieties on thermal stability and fracture toughness of epoxy blends”. In: *Polymers* 13.19 (2021), p. 3310.

[53] Xiaoran Zhao et al. “Improved fracture toughness of epoxy resin reinforced with polyamide 6/graphene oxide nanocomposites prepared via in situ polymerization”. In: *Composites Science and Technology* 171 (2019), pp. 180–189.

[54] Wakako Araki et al. “Fracture toughness of bisphenol A-type epoxy resin”. In: *Journal of applied polymer science* 86.9 (2002), pp. 2266–2271.

[55] Seyed Rasoul Mousavi et al. “A review of recent progress in improving the fracture toughness of epoxy-based composites using carbonaceous nanofillers”. In: *Polymer Composites* 43.4 (2022), pp. 1871–1886.

[56] ASTM International. *ASTM D5045-14 (Reapproved 2022)*. Standard. Standard Test Methods for Plane-Strain Fracture Toughness and Strain Energy Release Rate of Plastic Materials. United States, 2022. URL: https://www.astm.org/d5045-14r22.html.

[57] R&G Faserverbundwerkstoffe GmbH. *CF Roving- Technical Details*. Retrieved on 16/07/2024. URL: https://www.r-g.de/en/art/205024-1600.

[58] ASTM International. *ASTM D3171-22*. Standard. Standard Test Methods for Constituent Content of Composite Materials. United States, 2022. URL: https://www.astm.org/d3171-22.html.

[59] Essam Totry et al. “Effect of fiber, matrix and interface properties on the in-plane shear deformation of carbon-fiber reinforced composites”. In: *Composites Science and Technology* 70.6 (2010), pp. 970–980.

[60] ASTM International. *ASTM D3518-18*. Standard. Standard Test Method for In-Plane Shear Response of Polymer Matrix Composite Materials by Tensile Test of a ±45° Laminate. United States, 2018. URL: https://www.astm.org/d3518_d3518m-18.html.

[61] ASTM International. *ASTM D6641-09*. Standard. Standard Test Method for Compressive Properties of Polymer Matrix Composite Materials Using a Combined Loading Compression (CLC) Test Fixture. United States, 2009. URL: https://www.astm.org/d6641_d6641m-16e02.html.

[62] CV Opelt et al. “Compressive failure of fiber reinforced polymer composites–A fractographic study of the compression failure modes”. In: *Materials Today Communications* 15 (2018), pp. 218–227.

[63] ASTM International. *ASTM D2344-22*. Standard. Standard Test Method for Short-Beam Strength of Polymer Matrix Composite Materials and Their Laminates. United States, 2022. URL: https://www.astm.org/d2344_d2344m-22.html.

[64] ASTM International. *ASTM D7136-20*. Standard. Standard Test Method for Measuring the Damage Resistance of a Fiber-Reinforced Polymer Matrix Composite to a Drop-Weight Impact Event. United States, 2020. URL: https://www.astm.org/d7136_d7136m-20.html.

[65] MFSF De Moura et al. “Modelling the interaction between matrix cracking and delamination in carbon–epoxy laminates under low velocity impact”. In: *Composites Science and Technology* 64.7-8 (2004), pp. 1021–1027.

[66] Eric Ramon et al. “A review of recent research on bio-based epoxy systems for engineering applications and potentialities in the aviation sector”. In: *Aerospace* 5.4 (2018), p. 110.

[67] Sudarisman Sudarisman et al. “Tensile, compressive, and flexural characterization of CFRP laminates related to water absorption”. In: *Journal of Composites Science* 7.5 (2023), p. 184.

[68] Huntsman Advanced Materials. *Araldite® LY 8605 / Aradur® 8605 System- Technical Data Sheet*.

[69] Huntsman Advanced Materials. *Araldite® LY 1556 / Aradur® 34055- Technical Data Sheet*.

[70] Huntsman Advanced Materials. *Araldite® LY 1568 / Aradur® 3492- Technical Data Sheet*.

[71] Westlake Epoxy. *EPIKOTE™ Resin 862 / EPIKURE™ Curing Agent W System- Technical Data Sheet*.

[72] DIC Corporation. *EPICLON® 850-S / DDS- Technical Data Sheet*.

[73] DIC Corporation. *TGDDM / DDS*. Retrieved on 17/09/2024. URL: https://www.dic-global.com/pdf/products/catalog/dic_epoxy_for_composite_en.pdf.

A

Appendix

A.1. DSC & Prepreg Manufacturing

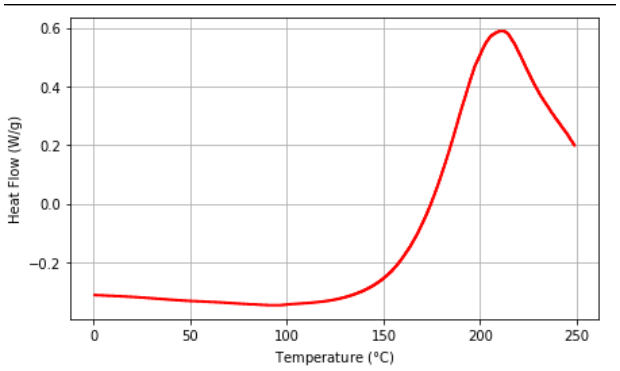

Figure A.1: Dynamic DSC for Heating Rate of 10 K/min

Since the aim of the project was to ultimately develop a resin system to be used in composites, its benefits for composite manufacturing were studied. A widely used form of composite used today is in the form of prepregs. Prepreg stands for pre-impregnated in that the resin is already impregnated with the fibers before it reaches its final consumers. This helps in reducing manufacturing errors and controlling the fiber volume fraction which is difficult to control if not done with the help of industrial facilities or manufacturing methods like vacuum infusion. To manufacture prepregs, epoxies are cured till they reach a certain process called ”b-staging” which is when the epoxy reaches a tacky stage before it starts its final cure.

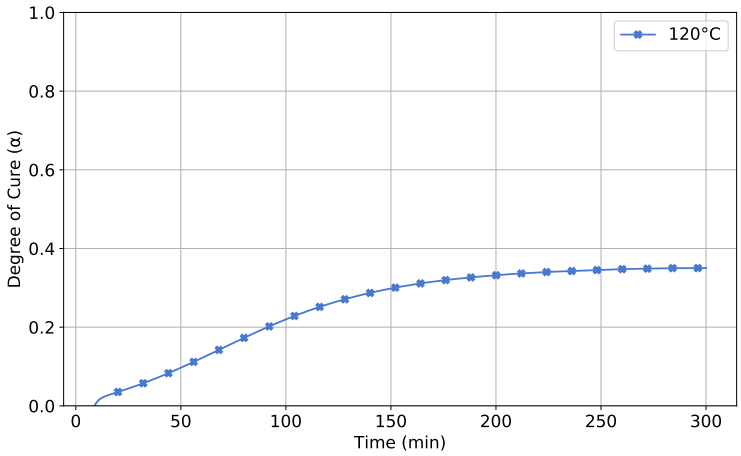

Figure A.2: Isothermal DSC at 120° C

As can be seen in Figure A.2, when trying to cure the resin mixture at 120° C, its α never goes above 0.38, even after 5 hours. This could indicate that the epoxy has reached its final stages of cure at this temperature and requires more energy to cure further. Potentially, manufacturers could do first dwell cycle of curing with the prepreg at 120° C and then consumers could do the remaining cure for a lesser time. This would reduce the residual stresses within the material as discussed earlier. However, this data is not conclusive enough to actually prove that b-staging occurs within this resin mixture, more rheological experiments would have to be done to understand whether it is possible at all.

A.2. Additional Post-Curing Temperatures

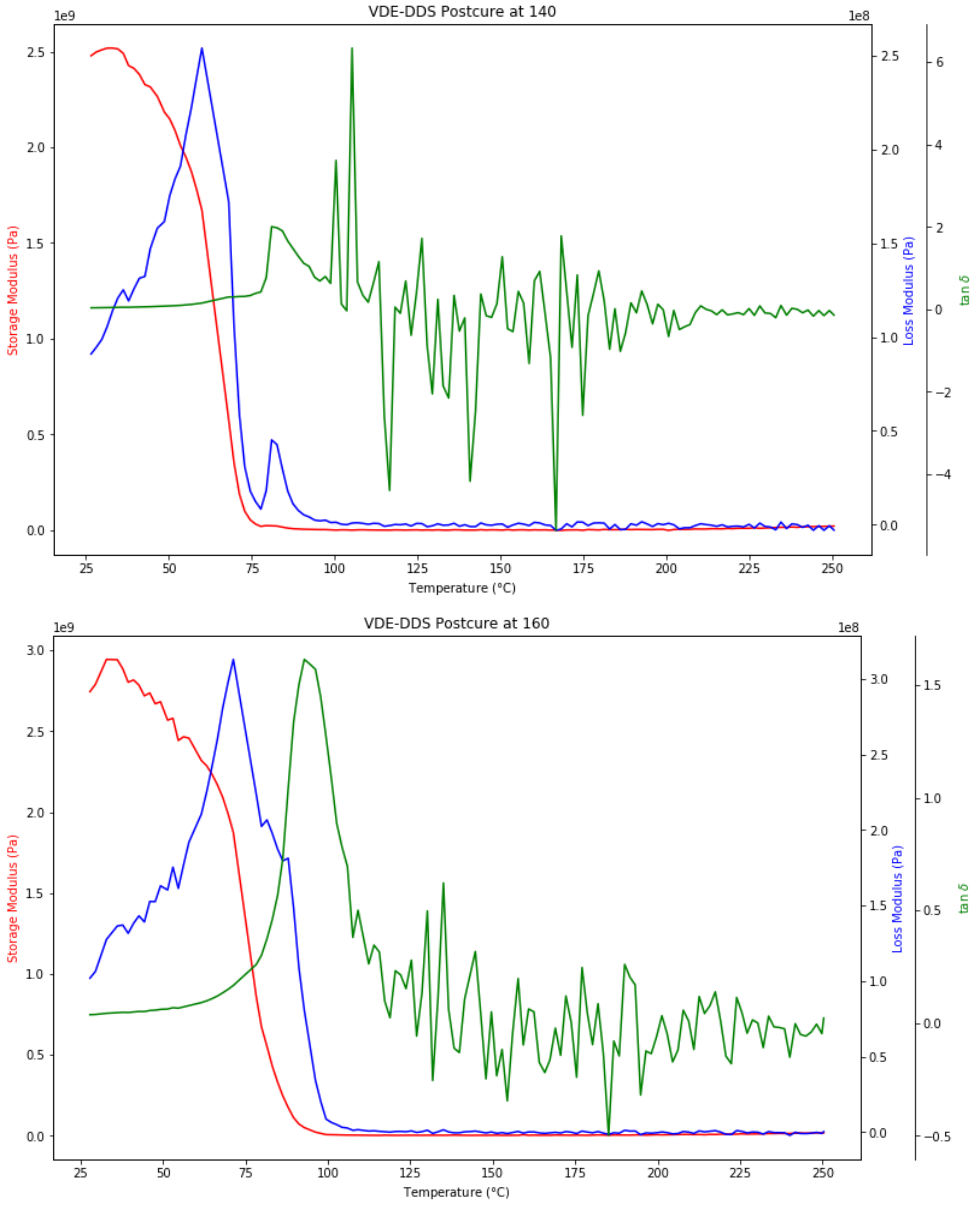

Figure A.3: DMA for Post Cure at 140° C and 160° C

A.3. Composite Test Specimen Dimensions

Table A.1: Specimen Dimensions for IPSS Test

Specimen Number	BADGE		VDE	
	Length (mm)	Cross Sectional Area (mm^2)	Length (mm)	Cross Sectional Area (mm^2)
1	250.10	61.09	250.06	58.93
2	250.09	61.82	250.12	58.06
3	250.10	62.67	250.09	58.70
4	250.06	57.82	250.07	57.88
5	250.09	61.27	250.16	59.04
6	250.15	60.66	250.10	58.22

Table A.2: Specimen Dimensions for Compression Test

Specimen Number	BADGE		VDE	
	Length (mm)	Cross Sectional Area (mm^2)	Length (mm)	Cross Sectional Area (mm^2)
1	140.12	32.88	139.98	29.13
2	140.02	31.89	139.89	30.14
3	140.01	32.42	139.89	32.57
4	139.95	33.77	139.98	28.68
5	139.90	31.69	139.88	30.51
6	140.02	33.40	140.04	30.06
7	139.94	32.49	139.95	28.49
8	139.90	32.40	139.98	30.91
9	140.04	33.27	139.94	30.79

Table A.3: Specimen Dimensions for ILSS Test

Specimen Number	BADGE		VDE	
	Length (mm)	Cross Sectional Area (mm^2)	Length (mm)	Cross Sectional Area (mm^2)
1	16.04	17.05	14.99	10.02
2	15.75	15.18	15.02	11.00
3	14.32	14.21	15.05	10.57
4	15.76	14.45	14.97	10.35
5	15.81	16.50	15.01	10.60
6	15.87	14.02	14.92	10.36
7	15.75	13.18	15.00	10.18
8	15.15	16.90	15.01	9.61
9	14.88	14.06	15.03	11.04
10	-	-	14.99	11.20